University of Nottingham
UK | CHINA | MALAYSIA

UPGRADING OF BIO-OIL FROM PALM EMPTY FRUIT BUNCH FIBRE WITH NON-ACIDIC OXIDES VIA CATALYTIC INTERMEDIATE PYROLYSIS

YEN YEE CHONG, MEng.

Department of Chemical and Environmental Engineering

Thesis submitted to the University of Nottingham

for the degree of Doctor of Philosophy

2019

ABSTRACT

In response to the concerns regarding environmental pollution and energy security, renewable energy has been perceived as a solution. As liquid fuel is the most consumed form of energy in the world, much attention has been paid to pyrolysis for the production of bio-oil. Bio-oil may be derived from biomass and is a potential fuel supplement and source of chemicals. However, lignocellulosic biomass-derived bio-oil is generally highly acidic and highly oxygenated than crude oil. Consequently, the bio-oil is unstable and has a comparatively low energy density. Hence, bio-oil has to be upgraded in order to use directly as fuel and other applications. One of the upgrading methods is catalytic pyrolysis using non-acidic oxides.

The current project investigated the effects of calcium oxide (CaO), magnesium oxide (MgO), and zinc oxide (ZnO) on the upgrading of palm empty fruit bunch fibre (EFBF)-derived bio-oil. Apart from that, cellulose was used as feed to study the effects of the oxides on lignocellulosic biomass at its simplest form upon intermediate pyrolysis. The possible reaction pathways involved upon the utilization of the oxides were also summarized.

Thermogravimetric studies revealed that the addition of MgO and ZnO did not affect the degradation behaviour of both cellulose and EFBF. However, because CaO is prone to adsorb moisture and carbon dioxide (CO_2), an additional weight loss stage was observed. Even though the oxides did not affect the activation energy and mechanism of EFBF devolatilization, the amount of volatiles released reduced due to the restriction posed by the oxides. Despite the catalytic

effects posed by the oxides, the reaction of the oxides with CO_2 and water categorizes CaO, MgO, and ZnO as catalytic additives, rather than catalysts.

Based on the results obtained when cellulose was used as feed, the reaction pathways involved in the catalytic upgrading of bio-oil were compiled. Nevertheless, upon comparing the results of the results with literature, it was concluded that the results may be used as a reference of the reactions involved during catalytic pyrolysis of biomass but it may not exactly reflect the absolute effects of the oxides on the physical properties of all bio-oils.

All three oxides showed evidence in enhancing the physical properties of cellulose and EFBF-derived bio-oil, in terms of reducing the amounts of acids and oxygenated compounds. However, the oxides reacted with carbon dioxide (CO_2) and water. Hence, the oxides may be considered as catalytic additives rather than as catalysts. Among the three oxides, CaO exhibited the best performance in the matter of reducing the acidity for both cellulose and EFBF-derived bio-oils, without affecting the bio-oil yield substantially. CaO also showed potential in stabilizing the EFBF-derived bio-oil without influencing the surface structure of the bio-oil.

LIST OF PUBLICATIONS

Refereed journals

- Chong, Y.Y., Thangalazhy-Gopakumar, S., Ng, H.K., Gan, S., et al., 2019. Catalytic pyrolysis of cellulose with oxides: effects on physical properties and reaction pathways. Clean Technologies and Environmental Policy. (IF: 2.277)

- Chong, Y.Y., Thangalazhy-Gopakumar, S., Ng, H.K., Lee, L.Y., et al., 2019. Effect of oxide catalysts on the properties of bio-oil from in-situ catalytic pyrolysis of palm empty fruit bunch fiber. Journal of Environmental Management, 247, pp.38–45. (IF: 4.175)

- Chong, Y.Y., Thangalazhy-Gopakumar, S., Gan, S., Ng, H.K., Lee, L.Y., et al., 2017. Kinetics and Mechanisms for Copyrolysis of Palm Empty Fruit Bunch Fiber (EFBF) with Palm Oil Mill Effluent (POME) Sludge. Energy and Fuels, 31(8), pp.8217–8227. (IF: 3.091)

- Chow, L.W., Tio, S. A., Teoh, J.Y., Lim, C. G., Chong, Y. Y., et al., 2018. Sludge as a Relinquishing Catalyst in Co-Pyrolysis with Palm Empty Fruit Bunch Fiber. Journal of Analytical and Applied Pyrolysis. (IF: 3.470)

Under review

- Book chapter: Chong, Y. Y., Thangalazhy-Gopakumar, S., Gan, S., Ng, H. K. and Lee, L. Y. 'Effect of Oxide Catalysts on the Properties of Bio-oil from In-situ Catalytic Pyrolysis of Palm Empty Fruit Bunch Fiber', Handbook of Biofuels

Conference presentations

Presented by Chong:

- Oral presentation at 4th International Conference on Alternative Fuels, Energy and Environmental (ICAFEE) 2019, Taiwan
  - Date: 18th – 21st October 2019
  - Title: Kinetics on Catalytic Pyrolysis of Cellulose with Oxides

- Oral presentation at 5th Postgraduate Colloquium for Environmental Research (POCER) 2019, Malaysia
  - Date: 8th and 9th August 2019
  - Title: Kinetics on Catalytic Pyrolysis of Palm Empty Fruit Bunch Fibre with Oxides

- Oral presentation at LINK'18, student-led interdisciplinary research conference, Malaysia
  - Date: 26th July 2018
  - Title: Catalytic Pyrolysis of Lignocellulosic Biomass with Metal Oxides

- Oral presentation at 4th Postgraduate Colloquium for Environmental Research (POCER) 2017, Malaysia
  - Date: 25th and 26th July 2017
  - Title: In-Situ Catalytic Pyrolysis of Cellulose with Calcium Oxide

Presented by Dr Suchithra (supervisor):

- Oral presentation at 2nd International Conference on Bioresources, Energy, Environmental, and Materials Technology (BEEM), Korea
  - Date: 10th – 13th June 2018
  - Title: Catalytic Pyrolysis of Lignocellulosic Palm Empty Fruit Brunch with Metal Oxides

- Oral presentation at 30th Symposium of Malaysian Chemical Engineers (SOMChE), Malaysia
  - Date: 6th – 7th December 2017
  - Title: In-situ catalytic pyrolysis of cellulose with basic metal oxides

Awards

- Oral presentation at LINK'18, student-led interdisciplinary research conference; First prize
  - Date: 26th July 2018
  - Title: Catalytic Pyrolysis of Lignocellulosic Biomass with Metal Oxides

- The Institution of Engineers, Malaysia (IEM) research paper competition 2017; First prize
  - Date: 14th April 2017
  - Title: Synergic effects and kinetic mechanisms for co-pyrolysis of empty fruit bunch and palm oil sludge

- Faculty of Engineering (FOE) Postgraduate (PGR) Research Showcase; Third prize
  - Date: 27th September 2017
  - Title: Synergic effects and kinetic mechanisms for co-pyrolysis of empty fruit bunch and palm oil sludge

ACKNOWLEDGEMENT

First, I would like to express my sincere gratitude to my supervisors, Dr Suchithra Thangalazhy Gopakumar and Prof. Ng Hoon Kiat for their continuous guidance and support. Their patience, optimism, encouragement, and immense knowledge helped tremendously throughout my research. I would also like to offer my sincere thanks to Prof. Gan Suyin and Dr Lee Lai Yee for their input and support on my work.

Besides that, my sincere gratitude to Ministry of Higher Education, Malaysia and The University of Nottingham Malaysia for the realization of this research project. I would also like to thank the laboratory technicians for providing the required support and assistance for my experiments and analyses.

I am deeply grateful to my family, Lik Yin, and his parents for their love and support throughout my studies. Thank you all so much for loving me, motivating me, listening to my frustrations, praying for me, and being there for me all the time.

Last but definitely not the least, praise be to God in the highest, who made all things possible. All glory to Him, now and forevermore.

TABLE OF CONTENTS

LIST OF FIGURES

LIST OF TABLES

LIST OF NOMENCLATURE

α	Conversion degree
A	Apparent frequency factor
CaO	Calcium oxide
CR method	Coats-Redfern method
DAEM	Distributed activation energy model
DTG	Derivative thermogravimetric
E	Apparent activation energy
EFB	Empty fruit bunches
EFBF	Empty fruit bunch fibre
f(α)	Function of conversion
FTIR	Fourier transform infrared spectrum
g(α)	Integrated function of conversion
GC-FID	Gas chromatography – flame ionization detector
GC-MS	Gas chromatography – mass spectrometry instrument
HHV	Higher heating value
MgO	Magnesium oxide
POME	Palm oil mill effluent
TAN	Total acid number
TG	Thermogravimetric
TGA	Thermogravimetric analysis
ZnO	Zinc oxide

CHAPTER 1

1 INTRODUCTION

1.1 Background

With the development of industries, innovation of technologies, and increment in world population, global energy demand has been on the rise. The world energy consumption is estimated to grow from 549 quadrillion British thermal units (Btu) in 2012 to 815 quadrillion Btu in 2040, an alarming 48 % increment (U.S. Energy Information Agency, 2017). Figure 1 depicts the primary energy consumption by energy source and projections. As observed, petroleum and other liquids will remain as the world's dominant fuel for the next decades. Since carbon dioxide (CO_2) emission is commonly associated with energy production and is a major global greenhouse gas that contributes to climate change, concerns on the effects of fossil fuel emissions to the environment have been raised. Since fossil fuels are defined as non-renewable energy sources, energy security is of concern as well.

Malaysia is a rapidly developing country and is one of the largest energy consumers in Southeast Asia. From year 1995 to year 2015, the total energy consumption of Malaysia increased by 136.7 % (Suruhanjaya Tenaga (Energy Commission), 2018). In the effort to encourage the utilization of renewable resources, Malaysian government announced renewable energy as the 5^{th} fuel in the energy supply mix (Chong *et al.*, 2015)

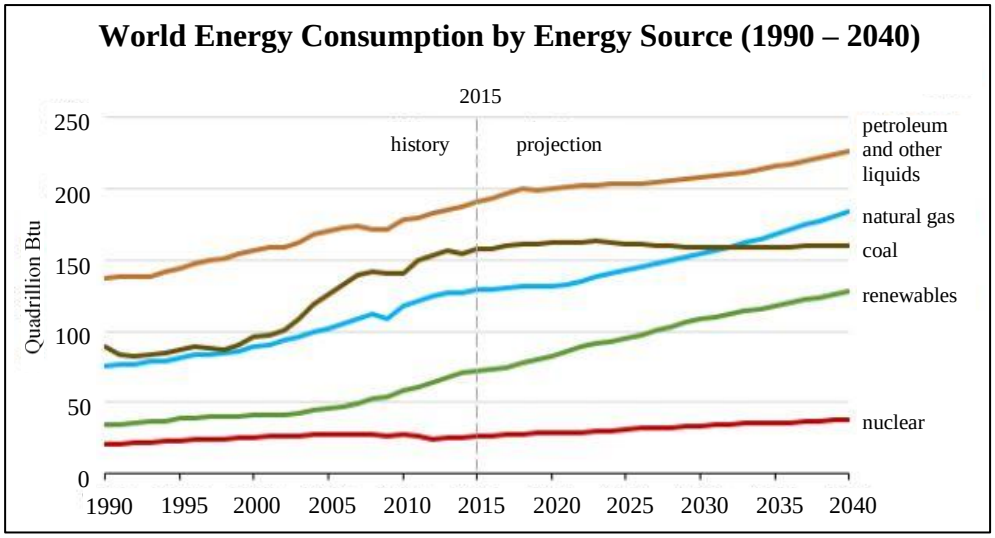

Figure 1: World energy consumption by energy source, 1990 - 2040 (Source: U.S. Energy Information Agency, 2017)

Major renewable energy sources are wind power, tidal power, wave power, solar power, hydroelectricity, and biomass. Among renewable energy sources, biomass is the only carbon-based source for energy production. Nitrogen (N_2) and sulphur (S) emissions are also negligible as compared to that of fossil fuels. Biomass are biological materials derived from living organisms and can be categorized broadly as woody, non-woody, and animal wastes. Studies are conducted to exploit the different biomasses as sources of energy depending on their local abundance. Biomass can be converted to different forms of energy such as solid biochar, liquid bio-oil and syngas. The flexibility of biomass not only overcomes environmental pollution and mitigate waste disposal issues, but also provides local energy security.

Different types of biomasses are available in Malaysia, for example, rice husk, palm waste, manure, sawdust, and so on. Being one of the world's largest palm oil exporter, Malaysia is estimated to account for 27 % of world palm oil production and 34 % of world exports in year 2019 (Index Mundi, 2019). Thus,

the amount of biomass waste produced concurrently with the production of palm oil would be tremendous. Annually, palm waste accounts up to 94 % of the total biomass feedstock available in Malaysia (BE-Sustainable, 2012). Palm biomass wastes include oil palm fronds, oil palm trunk, palm kernel cake, palm kernel shell, empty fruit bunch (EFB), mesocarp fibre, and palm oil mill effluent (POME).

Palm biomass have been studied on their recyclability as an energy source, feedstock, fertilizer, adsorbent, and biodiesel (Faridah *et al.*, 2018). Some examples are the utilization of POME as a medium for microalgae cultivation, EFB as feedstock for bio-ethanol production, treated oil palm fronds for co-firing in coal power plants, and biochar production from palm kernel shell (Cheah *et al.*, 2018; Derman *et al.*, 2018; Haryati *et al.*, 2018; Lau *et al.*, 2018). Researchers from A*STAR are in the effort of converting palm biomass to bioethanol and biodegradable plastic by developing a fungal culture (Wu, 2015). In addition, EFB, mesocarp fibre, and palm kernel shell may be used directly as fuel by producing steam for the generation of electricity. However, pre-treatment is required before being burnt in the boiler. The study is still ongoing and has been deemed a success. Many projects on using biomass for power generation have been launched in Malaysia (Shuit *et al.*, 2009). More than decade ago, Lafarge Malaysia Berhad, a construction materials manufacturer, uses pulverized palm kernel shell as an alternative biomass fuel to partially replace fossil fuel (Dit, 2007). Besides that, with the high cellulose content, palm biomass has the potential to be converted to a promising bio-polymer that has a wide application in different industries (Yahya *et al.*, 2015).

Unlike other renewable energy sources, biomass may be converted directly to liquid fuels. In Malaysia, the highest consumed fuel type is petroleum products (55.4 %) and the transportation sector currently contributes 45.2 % to Malaysia's energy consumption (Suruhanjaya Tenaga (Energy Commission), 2018). Hence, the study on producing a supplement or substitute for liquid fuel from biomass would decrease the dependency on fossil fuels.

Fast pyrolysis and intermediate pyrolysis are considered as potential thermochemical processes to convert biomasses to liquid fuel, involving the rapid heating of biomass and then quenching the vapour produced. The condensed liquid is known as bio-oil. One of the major parameters of differentiating the two types of pyrolysis processes is the heating rate: while fast pyrolysis requires high heating rates (up to 1000 °C/s), intermediate pyrolysis requires a comparatively lower heating rate (up to 300 °C/s). Depending on the feedstock used, fast pyrolysis typically produces approximately 75 wt.% of liquid bio-oil whereas intermediate pyrolysis usually produces about 55 wt.% of bio-oil (Hornung, 2013). Despite the lower liquid yield, the bio-oil from intermediate pyrolysis contains lower quantity of reactive tar and is more suitable for direct application in boilers and engines (Mohammed *et al.*, 2016).

Generally, bio-oil that is derived from lignocellulosic biomass is acidic in nature. Abdulla et al. (2011) characterized the bio-oil derived from EFB and obtained a low pH of between 2 and 3, which was contributed by the presence of organic acids, mostly acetic acid and formic acids (Abdullah, Sulaiman and Gerhauser, 2011). Having a high acidity causes the bio-oil to be corrosive. Aside from that, bio-oil is highly oxygenated, which contributes to the low heating value of the bio-oil (average of 21.0 MJ/kg) as compared to that of crude oil (average of 43.4

MJ/kg). Hence, bio-oil may not be suitable to be used directly as fuel yet and would have to be upgraded to widen its applications by improving the properties in terms of reducing the acidity and oxygenated compounds, which would in turn increase both the heating value and stability of the bio-oil. Despite the available technologies, a high cost is required (e.g. hydrodeoxygenation requires high pressure hydrogen) for bio-oil upgrading and altering of the available equipment (e.g. boiler and furnace).

One of the *in-situ* bio-oil upgrading methods is catalytic pyrolysis and studies have been taking interest in utilizing acidic zeolites catalysts due to their acidic properties and shape selectivity. Despite the advantages that acidic catalysts demonstrate with regard to the reduction in acids, the low production of bio-oil prompted interests in employing less acidic materials as catalysts (Pütün, 2010). In addition, the employment of acidic zeolite catalysts showed increment in coke formation, which then deactivates the catalysts. Hence, investigating the potential of non-acidic catalysts or additive on bio-oil upgrading is a worthy avenue of research.

1.2 Problem statement

Co-pyrolysis of lignocellulosic biomass with high ash content solid waste is getting attention as the alkaline and alkali earth metals (AAEMs) in ash behaves as catalyst (Samolada and Zabaniotou, 2014; Chow *et al.*, 2018). However, none of the studies have investigated the effect of AAEMs on lignocellulosic bio-oil. As a confirmation for literature, preliminary work involving the analysis on kinetic mechanisms of co-pyrolysis of POME sludge with EFB was carried out (presented in Section 2.4). The activation energy of co-pyrolysis decreased as the ratio of POME sludge increase, which suggested that AAEMs such as

calcium oxide (CaO) and magnesium oxide (MgO) that were present in the POME sludge may have exhibited catalytic activity on the pyrolysis reaction.

Many researchers focused on the utilization of oxides in the upgrading of bio-oil recently. While CaO was found to be an excellent catalyst for deacidification of biomass-derived bio-oil, MgO showed great potential in deoxygenation of bio-oils (Pütün, 2010; Wang *et al.*, 2010; Chen, Chen, *et al.*, 2017). On the other hand, zinc oxide (ZnO) was deduced to be a mild deoxygenating catalyst that can improve the qualities of the bio-oil without compromising the bio-oil yield evidently (Nokkosmäki *et al.*, 2000; Zhou *et al.*, 2013). Due to the multivalent nature and/or certain acid-base properties, oxides hold either redox properties. In the case of alkaline earth metal oxides such as CaO and MgO, oxide ions behave as bases whereas metal cations functions as Lewis acids (Wachs, 2005; Liu *et al.*, 2014). ZnO is an amphoteric oxide, reacting with both acid and base.

Despite the available studies on the utilization of these oxides on biomass pyrolysis, there were no studies that relates the catalytic intermediate pyrolysis of palm waste with the oxides. The differences in pyrolysis conditions and feedstock groups may contribute to a difference in bio-oil properties as dissimilar feedstocks have different lignocellulosic content and may exhibit distinction in heat transfer characteristics.

In general, most studies focused on the effects of catalysts or additives on the properties of the biomass-derived bio-oil produced but scarcely on the kinetics and mechanisms involved. The kinetics and mechanisms of biomass degradation are usually studied by subjecting the biomass to thermogravimetric

analysis (TGA). Based on TGA results, the pyrolytic behaviour of the biomass may be observed and by using appropriate models, the kinetic triplets (apparent reaction activation energy (E), apparent frequency factor (A), and kinetic model, $f(\alpha)$) may be obtained. Such information is essential in assisting in the design, optimization, and scaling up of the operation.

Besides that, the possible reaction pathways upon the addition of the oxides have not been summarized, to be used as a guide in understanding the effects of the catalysts or additives on lignocellulosic biomass-derived bio-oils. Having an understanding on the reaction pathways provide more opportunities for studies to identify and to produce any targeted products.

Apart from that, currently available studies focused little on the stability of the bio-oil, which is crucial for long-term storage and transportation. The stability of the bio-oil is commonly evaluated based on the change in viscosity with time, where a smaller change in viscosity indicates a more stable bio-oil. Upon aging, any change in the water content and acidity of the bio-oil would have to be monitored, also because these properties contribute to the stability of the bio-oil.

1.3 Research objectives

The study on catalytic upgrading of empty fruit bunch fibre (EFBF)-derived bio-oil with non-acidic oxides is scarce. The aim of this project is to comprehensively investigate the effects of oxides (CaO, MgO, and ZnO) on the upgrading of EFBF-derived bio-oil, concerning the kinetics, mechanisms, and bio-oil properties. Studies were also carried out using cellulose to understand

the influence of the oxides on lignocellulosic biomass at its simplest form and to provide an understanding on the possible reaction pathways.

The objectives of this work are as follows:

1. Investigate the change in thermal behaviour and obtain the kinetics and mechanisms for catalytic pyrolysis of cellulose and EFBF in the presence of CaO, MgO, and ZnO. (Chapter 4)
2. Examine the effects of oxides (CaO, MgO, and ZnO) on the catalytic pyrolysis of cellulose and EFBF. (Chapter 5)

Upon identifying the disadvantages of acidic catalysts for bio-oil upgrading and lack of information regarding the upgrading of EFBF-derived bio-oil using oxides, the novelty of the current work resides in gaining an in-depth understanding on the influences and potential of the selected oxides (CaO, MgO, and ZnO) for catalytic intermediate pyrolysis of palm waste.

1.4 Outline of thesis

This thesis comprises of six chapters, where Chapter 1 presents the introduction and background study to the problem statement. The aim and objectives of this study were specified as well. Chapter 2 presents a literature review on the pyrolysis of biomass to produce bio-oil and on the upgrading methods, specifically co-pyrolysis, catalytic pyrolysis, esterification, and hydrodeoxygenation (HDO). The review includes the current findings and knowledge that are related to this study. In addition, results from preliminary studies that were conducted to develop the objectives were presented. The preliminary experiment involves the co-pyrolysis of EFBF with palm oil mill

effluent (POME) sludge. Subsequently, the materials and methodology used in this study are outlined in Chapter 3.

Chapter 4 discusses the changes in thermal behaviour and kinetics of the biomass feedstock when the non-acidic oxides were added for bio-oil upgrading, using thermogravimetric analysis (TGA). The objectives strive to gain an understanding of the interactions and influences between EFBF and the oxides for upgrading. This chapter includes the findings on the kinetics and mechanisms for catalytic pyrolysis of cellulose and EFBF with oxides (CaO, MgO, and ZnO) as well.

Next, Chapter 5 discusses the changes in the physical properties of bio-oil upon catalytic intermediate pyrolysis at laboratory scale, using CaO, MgO, and ZnO as catalytic additives. The physical properties of the bio-oils include product yield, acidity, water content, surface structure, and major compounds in the bio-oil. The current chapter is divided into two sections: 1) cellulose is used as the feedstock, with the main aim to understand the influences of the catalysts on bio-oil at the lignocellulosic biomass' simplest form and to summarize possible reaction pathways based on the obtained results and literature; 2) EFBF is utilized as feed to investigate the effects of the oxides (CaO, MgO, and ZnO) on the physical properties and stability of the EFBF-derived bio-oil.

Chapter 6 discusses the overall findings and contributions of the research. Apart from that, potential future work that may be done to extend the scope of study were highlighted in this chapter.

CHAPTER 2

2 LITERATURE REVIEW

2.1 Introduction

This chapter provides an overview to the pyrolysis of lignocellulosic biomass, the influence of other feedstock and catalyst in pyrolysis. Firstly, an introduction was given for palm empty fruit bunch (EFB), one of the major biomass available in Malaysia. Subsequently, the parameters and conditions for the pyrolysis of the biomass were compiled and discussed. Besides, the properties of bio-oil were compared and reviewed, providing an insight to the problem that was to be addressed in this project. The final section of this chapter reviews selected upgrading methods, which may be loosely categorized as chemical upgrading or physical upgrading methods, where the former was emphasised. The chemical upgrading methods include co-pyrolysis, catalytic pyrolysis, esterification, and hydrodeoxygenation (HDO). Moreover, preliminary studies were conducted to evaluate the kinetic and mechanism of co-pyrolysis, which was added at the end of this chapter.

2.2 Biomass

Lignocellulosic biomass has been the focus in biofuel production because they are inexpensive, abundant, and environmentally friendly, as compared to edible oil and sugar crops. Lignocellulosic biomass consist mainly of three polymers: cellulose (35 – 50 wt%), hemicellulose (15 – 30%), and lignin (12 – 35%), associated with each other in a hetero-matrix (Bajpai, 2016). Cellulose is the main constituent of plant cell walls, which provides structural support and chemical stability to plants. This common organic compound has a chemical

formula of $(C_6H_{10}O_5)_n$, and is considered as a polymer of glucose, linked via β - 1,4 glycosidic bonds (Pérez *et al.*, 2002). In contrast to cellulose, hemicellulose has a lower molecular weight and has branches with short lateral chains that consist of monosaccharides. The sugars are linked together by β - 1,4 - and sometimes β - 1,3 glycosidic bonds (Pérez *et al.*, 2002). The highly branched sugar polymers of the hemicellulose contributes to the lack of crystalline structure (Harmsen and Huijgen, 2010). Next, lignin is known to be the most complex natural polymer of aromatic compounds. As lignin acts as a binder between cells, it creates a composite material that is resistant to impact, compression, and bending. Thus, providing the cell wall with structural support and resistance to microbial attacks and oxidative stress.

Lignocellulosic biomasses also contain water, a small amount of proteins, and some mineral extractives in addition to cellulose, hemicellulose, and lignin. The compositions of biomass vary depending on the source (Harmsen and Huijgen, 2010).

2.2.1 Palm biomass

Malaysia is one of the world largest palm oil producers and according to the statistics provided by Malaysia Palm Oil Board (MPOB), the fresh fruit bunch (FFB) yield in year 2018 was reported to be 25.1 tonnes per hectare, over a land area of 5.8 million hectares (Malaysian Palm Oil Board, 2018). Simultaneously, a great amount of palm biomass such as mesocarp fibre, palm kernel shells, empty fruit bunches (EFB), oil palm fronds, oil palm trunks, and palm oil mill effluent (POME) are being generated. Therefore, palm based lignocellulosic biomasses have been the focus in many bioenergy studies in Malaysia.

Table 1: Composition of EFB on dry basis

References	(Yoo *et al.*, 2014)	(Abdullah and Gerhauser, 2008)	(Khor *et al.*, 2009)	(Mohammed *et al.*, 2012)	(Bensidhom *et al.*, 2018)
Component analysis (wt%)					
Cellulose	40.5	59.7	38.52	22.24	38.44
Hemicellulose	17.6	22.1	33.52	20.58	24.65
Lignin	28.7	18.1	20.36	30.45	25.08
Proximate analysis (wt %)					
Moisture	7.57	7.95	8.65	5.18	7.68
Volatile	66.78	83.86	75.09	82.58	81.2
Fixed carbon	18.32	10.78	12.34	8.97	6.92
Ash	7.35	5.36	3.92	3.45	4.2
HHV (MJ/kg)	16.25	19.35	18.66	17.02	19.21
Elemental analysis (wt %)					
C	43.63	49.07	43.21	46.62	43.49
H	5.75	6.48	7.42	6.45	7.51
N	0.77	0.7	0.86	1.21	0.188
O	38.1	38.29	47.76	45.66	52.73
S	-	< 0.1	0.75	0.035	-

"-" unavailable

EFB accounts for 22 % of the FFB and upon utilizing a fraction of the palm biomass for combined heat and power generation, excess EFB would be considered devoid of value. The remaining biomass is approximately 40 % of the produced EFB, or 9.2 % of the FFB harvested (Abdullah and Sulaim, 2013; Reeb, Hays and Venditti, 2014). Simple calculations would then give an estimation on the production of EFB from oil palm mills throughout Malaysia

to be 8.7 million tonnes in year 2018 (Malaysian Palm Oil Board, 2018). Table 1 shows the composition of EFB as presented in other studies.

As observed, the compositions of EFB vary for all the selected studies and has a high moisture content of 67 % as received (Salman, 2015). Thus, pre-processing is required to reduce the moisture content of EFB for further utilization and to improve handling properties. EFB is commonly incinerated to produce steam for power generation and the ash is used as fertilizer. However, due to the 'white smoke' problem, incineration of EFB was discouraged (Yusoff, 2006). EFB has been studied to produce bio-based value added products such as bioplastic and bio-ethanol as well (Shuit *et al.*, 2009; Sudiyani *et al.*, 2013).

2.3 Pyrolysis of lignocellulosic biomass

With the aim to produce a supplement or substitute for fuel, fast pyrolysis and intermediate pyrolysis are considered as potential processes in the conversion of biomass. Pyrolysis process produces high liquid yield by rapidly heating the biomass and then quenching the vapour produced in the absence of oxygen (O_2). The condensate is known as bio-oil. As compared to other conversion processes such as gasification and other biological approaches, the pyrolysis of biomass requires lower cost for liquid fuel production, has the ability to process wider range of feedstock, requires shorter residence time, and needs simpler feedstock pre-treatment (Routray, Barnett and Huber, 2017).

The criteria and product distribution for both fast and intermediate pyrolysis are as follows:

Fast pyrolysis (Adhikari, Thangalazhy-Gopakumar and Taylor, 2012; Hornung, 2013)

(i) very high heating and heat transfer rates, which are dependent on the particle sizes of biomass feed (up to 1000 °C/s),
(ii) well-controlled reaction temperature (400 – 600 °C),
(iii) short vapour residence time (< 2 s),
(iv) rapid removal of char to keep the cracking of vapours to a minimum,
(v) rapid cooling of vapours to obtain bio-oil
(vi) product distribution: 80 wt.% bio-oil, 12 wt.% biochar, and 13 wt.% gas

Intermediate pyrolysis (Hornung, 2013; Mohammed *et al.*, 2016)

(i) moderate heating rates, up to 200 – 300 °C/min
(ii) typical reaction temperatures from 350 – 550 °C
(iii) short vapour residence time (2 – 4 s)
(iv) rapid removal of char to keep the cracking of vapours to a minimum,
(v) rapid cooling of vapours to obtain bio-oil
(vi) product distribution: 40 – 60 wt.% bio-oil, 15 – 25 wt.% biochar, and 20 – 30 wt.% gas

Despite the lower liquid yield, the bio-oil from intermediate pyrolysis contains lower quantity of reactive tar and is more suitable for direct application in boilers and engines (Mohammed *et al.*, 2016).

2.3.1 Parameters

The operating parameters that contribute to the varying of product yields are temperature, vapour residence time, feed particle size, heating rates, sweeping

gas flowrate, initial moisture content of feed, and mineral matters. Among all, operating temperature and heating rates are classified as two of the most influencing parameters in terms of maximizing the bio-oil yield. Generally, higher heating rates and pyrolysis temperatures that ranges from 400 to 550 °C would produce the highest bio-oil yield (Akhtar and Saidina Amin, 2012; Strezov *et al.*, 2015).

The optimization studies on operating conditions of EFB in producing bio-oil were performed and are presented in Table 2. As can be deduced, the biomasses are recommended to have a moisture content of less than or about 10 wt.%, with particle sizes of less than 2 mm in order to produce homogenous bio-oil from palm waste of the highest yield. In addition, the pyrolysis conditions are suggested to be at 500 °C, ramped between 10 to 100 °C/min with sweeping gas flow rates of 2 L/min. Nevertheless, the technical limitations posed by the experiment setup have to be taken into consideration as well.

Table 2: Optimized pyrolysis conditions for bio-oil production

Biomass	Moisture content* (wt %)	Particle size (mm)	Reactor	Temperature (°C)	Heating rate (°C/min)	Gas, flowrates	Product			References
							Bio-oil	Char	Gas	
EFB	2.4	0.091 – 0.106	Fluidized fixed bed	500	100	Ar, 1.5 L/min	42.3	~ 36.0	~ 22.0	(Sukiran *et al.*, 2009)
EFB	6.4	0.21	Fluidized bed	500	-	N_2	27.0	50.0	23.0	(Sembiring, Rinaldi and Simanungkalit, 2015)
EFB	-	0.87	Fixed bed	442	50	N_2, 0.15 L/min at 2 bars	46.2	25.4	28.3	(Mohamed, Hamzah and Daud, 2014)
EFB	18.8	0.1 – 0.15	Fixed bed	500	-	-	30.0	27.2	42.8	(Ogunsina *et al.*, 2014)
EFB	6.9	1 – 2	Tubular	500	10	N_2, 2.0 L/min	45.8	29.1	25.2	(Abnisa *et al.*, 2013)

"-" not mentioned; "*"dry basis

2.3.2 Properties of bio-oil

The bio-oil produced is a deep brown, free-flowing organic liquid that has a distinct odour. Table 3 compares the properties of EFB-derived bio-oil, crude oil, and ASTM D7544-09.

Table 3: Comparison between properties of crude oil, and ASTM standards

Properties		Crude oil (Ahmed, 2013; Jukić, 2013; Speight, 2014)	EFB (Sukiran, Chin and Bakar, 2009; Abdullah, Sulaiman and Gerhauser, 2011; Abnisa *et al.*, 2013; Sembiring, Rinaldi and Simanungkalit, 2015; Yakub *et al.*, 2015)	ASTM D7544
Specific gravity		0.65 – 1.02	1.0 – 1.2	1.1 – 1.3
Typical composition	% C	82.4 – 87.5	11.5 – 49.8	-
	% H	10.4 – 15.4	6.1 – 9.6	-
	% O	0.05 – 1.5	33.9 – 78.8	-
	% S	0.05 – 6.0	0 – 0.2	0.05 max
	% N	0.1 – 2.0	0.04 – 1.9	-
	Ash, wt%	0.1 – 0.2	0.7	0.25 max
Viscosity	cP @ 25 °C	-	2.3 – 46.3	-
Water	% wt	-	18.7 – 65.0	30 max
HHV	MJ/kg	39.82 – 46.89	20.3 – 21.6	15 min
Acidity	pH	-	2.7 – 3.2	Report*

* Detailed information is required in reporting the results of the standard

As seen from Table 3, compositions of bio-oil show that bio-oil is environmental-friendly as the nitrogen (N) and sulphur (S) contents are negligible. However, bio-oil cannot be used directly as fuel currently. One of the concerns is that bio-oil has a higher viscosity. With a high viscosity, the bio-oil may tend to polymerize and plug the engines upon combustion. This will then prevent sufficient atomization of the bio-oil for good air/fuel mixing, reducing the performance of the engines (Martin and Boateng, 2014). Besides that, high percentage of oxygenated compounds and water content in the bio-oil, as compared to crude oil, reduces the energy density, which is reflected from the comparatively low higher heating value (HHV) of the bio-oil. As reported by Czernik & Bridgewater (2004), water in bio-oils was a product of dehydration reaction that occur during pyrolysis. Water poses both negative and positive effects on the storage and utilization of bio-oils (Lu, Li and Zhu, 2009). Relatively high-water content would decrease the HHV and encourage the stratification of the bio-oils. On the contrary, the presence of water aids in lowering of bio-oil viscosity for good pumping and atomization prior to combustion (Diebold and Czernik, 1997). Water in bio-oil is also able to reduce the emission of pollutants (NO_x) upon combustion (Czernik and Bridgwater, 2004).

Another main concern is low pH of bio-oil. Having a low pH indicates the strong acidity of the bio-oil, which was contributed by the presence of organic acids, mostly acetic acid and formic acids (Abdullah, Sulaiman and Gerhauser, 2011). Apart from the mentioned volatile acids, the acidity of bio-oils were also influenced by compounds such as phenolics, fatty and resin acids and hydoxy

acids (Oasmaa, Elliott and Korhonen, 2010). This property causes the instability of the bio-oil and the corrosion of equipment (Czernik and Bridgwater, 2004).

2.3.3 Upgrading techniques

Two of the main challenges faced in utilizing the bio-oil are the high amounts of acids and oxygenated compounds in the bio-oil. Therefore, the upgrading of bio-oil would have to be carried out to widen the applications of the bio-oil. The upgrading of bio-oil may be carried out via chemical, physical, or a combination of both methods. The chemical methods include co-pyrolysis, catalytic pyrolysis, esterification, hydrodeoxygenation (HDO) whereas physical methods include emulsification, filtration, and water or solvent addition. The current study focuses mainly on the chemical upgrading methods of bio-oil.

The upgrading of bio-oil may not be sustainable unless a bio-oil with better quality is produced, which can be done through upstream upgrading. Two of the upstream upgrading techniques are co-pyrolysis and catalytic pyrolysis of biomasses. On the other hand, esterification and HDO of bio-oil are two of the ex-situ upgrading methods.

2.3.3.1 Co-pyrolysis

Co-pyrolysis of biomass is one of the potential options to improve the quality of biofuel produced and is being widely explored. Co-pyrolysis involves the blending of two or more materials as feedstock. This upgrading technique does not require extensive changes to the pyrolysis system but requires knowledge on the ratio of feedstock. According to a literature review completed by Abnisa et al. (2014), many studies have been revolving around co-pyrolysis and discovered that co-pyrolysis is able to improve the quality of bio-oil in terms of

increase in oil yield, reduction in water content, and increase in higher heating value (HHV). Besides, this technique reduces the dependency on specifically one feedstock, where waste management problems may be mitigated (Abnisa, Mohd and Daud, 2014). The key to successfully upgrade the characteristic of bio-oil via co-pyrolysis is the synergistic effect, which is generated from the reaction of feedstocks during the process. This is due to the difference in the chemical and physical properties of different biomass, which may show different thermal reactivities upon co-pyrolysis (Mu *et al.*, 2016).

Positive synergistic effect was observed when Krerkkaiwan et al. (2013) conducted a study on co-pyrolysis/ gasification of biomass (rice straw and Leucaena leucocepha wood) and sub-bituminous coal in a drop tube fixed-bed reactor. A higher gas yield and a lower char yield were obtained in experiments as compared to theoretically calculated yields. Due to the fact that hydrogen/carbon (H/C) and oxygen/carbon (O/C) molar ratios of both biomasses are higher than those of coal, a larger amount of H and OH radicals might be generated. The radicals then acted as H donor species that encouraged the cracking of aromatic compounds in the coal. Apart from that, the presence of alkali and alkaline earth metallic species, especially potassium (K) played a catalytic role, interacting with the produced char during the co-pyrolysis of coal and biomass (Krerkkaiwan *et al.*, 2013).

Synergistic effects during co-pyrolysis may differ at different analysis scales as well. Mu et al. (2016) studied the synergistic effects for the co-pyrolysis of petrochemical wastewater sludge (PWS) with Huolinhe lignite (HL). The study was initially carried out using TGA. It was observed that the weight loss (TG) and derivative weight loss (DTG) curves of the blends laid between those of the

individuals during pyrolysis. By comparing the weight loss values, experimental values were evidently lower than that of theoretical values, signifying an inhibitive synergistic effect between PWS and HL. At a lower temperature, the weight loss of the blends was contributed by the releasing of volatile matter from PWS. However, the HL particles with a higher heat stability would play a role in hindering and restraining the release of the volatiles. As the temperature increased, PWS components in the blends decomposed and formed char. The char formed would then accumulate on the surface of HL particles, hindering the pyrolysis of HL. Mu et.al. (2016) then acknowledged the limitation of TGA analysis for the small initial weight loading and therefore, carried out co-pyrolysis of the blends in a vertical packed-bed reactor. In contrast to the inhibiting effects observed in TGA, positive synergistic effects in the packed-bed reactor promoted the release of gas products and left less tars and chars than those calculated by additive manner. The main reason of this phenomena was that a relatively huge amount of sample was used in the packed-bed reactor. This in turn strengthened the contact between fuels and their volatiles, leading to a series of secondary reactions. Since TGA utilized a small amount of sample with a higher flow rate of nitrogen (N_2) sweep, possible gas-solid interactions were excluded. Besides, it was mentioned that PWS and HL decomposed at different temperature ranges in TGA. However, in the packed-bed reactor, PWS and HL in the blends decomposed simultaneously, intensifying the secondary reactions between chars and volatiles. In result, more volatiles were yielded (Mu *et al.*, 2016).

While studying the co-pyrolysis behaviours of sewage sludge and pine sawdust blends, Zhu et al. (2015) prepared several proportions (pine sawdust/sewage

sludge weight percentage ratio of 25:75, 50:50, and 75:25) and conducted the behavioural study using thermogravimetric analysis (TGA). Upon analysing the data, there were no significant differences between the experimental and theoretical weight loss. Hence, it was stated that there was no obvious presence of synergistic activities during the co-pyrolysis of sewage sludge and pine sawdust. This may be caused by the inhomogeneity of the blends. Besides that, one of the possible reasons given was that the flow of N_2 sweep prevented the volatile products to remain close to the solid residue, and thus inhibiting secondary reactions (Zhu *et al.*, 2015).

The co-pyrolysis of EFB was carried out by both Salman et al. (2019) and Zullaikah et al. (2018) recently. While the former utilized plastic wastes and co-feed, the latter used low rank coal. Both co-pyrolysis studies produced bio-oil in a reactor and studied the composition of the bio-oils. Salman et al. (2019) concluded that co-pyrolysis of EFB with plastic wastes showed potential to produce phenol-rich bio-oil whereas Zullaikah et al. (2018) observed an increase in methyl ester (Zullaikah *et al.*, 2018; Salman, Nomanbhay and Salema, 2019).

2.3.3.2 Catalytic pyrolysis

Catalytic pyrolysis is one of the upgrading methods to improve the properties of bio-oil via the cracking of oxygenates in bio-oil. During catalytic pyrolysis, multiple complex reactions occur simultaneously, including cracking, aromatization, ketonization/aldol condensation and hydrotreating of the bio-oil (Liu *et al.*, 2014). A list of selected catalysts used and their effects on the properties of the bio-oil are presented in Table 4. On the other hand, Table 5

presents the effects of a selection of catalysts on targeted compounds in the bio-oil during catalytic pyrolysis.

Studies have been taking interest in utilizing acidic zeolites catalysts in catalytic pyrolysis due to their acidic properties and shape selectivity. Acidic sites of catalysts are critical in the cracking of oxygenates in pyrolysis vapour, which in turns helps in the lowering of O content in the bio-oil and increase the hydrocarbon yield in the bio-oil (Liu *et al.*, 2014). One of the examples of acidic zeolite catalysts is HZSM-5, a microporous catalyst. HZSM-5 has been studied extensively due to its thermal and hydrothermal stability. Among zeolites and zeolite-supported transition metals, HZSM-5 zeolite was the best catalyst for producing deoxygenated organics (Ma, Troussard and van Bokhoven, 2012; Ma *et al.*, 2014).

Literature studies showed that the catalytic activity increased with the increased in HZSM-5 acidity. As observed from Table 4, the application of different acidic zeolite catalysts generally produced low bio-oil yield of the pyrolysis products and increased the water content in the bio-oil. With reference to Table 5, the effects of zeolite catalysts on the production of anhydrosugars, furan compounds, and phenolic compounds varies. However, the aliphatic and aromatic hydrocarbons proportions increased undoubtedly. Despite the advantages that acidic catalysts demonstrate, the low production of bio-oil prompted interests in employing less acidic materials as catalysts (Pütün, 2010).

Many researchers have focused on the utilization of alkali and alkaline earth metals (AAEMs) and their compounds as catalysts for catalytic pyrolysis. One of the earliest works to utilize AAEMs in the oxide form as catalysts was carried

out by Nokkosmäki et al. (1998), where, magnesium oxide (MgO), dolomite, and limestone were used as catalysts. The study used sawdust as feed and was carried out in a microscale pyrolysis and vapour-phase catalyst reactor. While zeolite HZSM-5 catalyst produced mainly gases and aromatic hydrocarbons, MgO, dolomite, and limestone promoted mainly degradation products of polysaccharides and lignin (Nokkosmäki *et al.*, 1998). Recently, a detailed study on the use of MgO as a catalyst was done by Stefanidis et al. (2016). The study compared the bio-oil produced from basic MgO metal and acidic ZSM-5 catalysts and the results obtained were comparable to each other, signifying that there is indeed a potential of substituting acidic catalysts with basic ones. However, contrary to what was observed with ZSM-5 catalyst, there was no significant increase of aromatic hydrocarbons due to the absence of acid sites in MgO. Besides, more ketones were observed with MgO, which led to a higher carbon dioxide (CO_2) yield. There was no obvious trend in the organic fraction yield and oxygen content with the strength of catalyst basicity and the yield of catalytic coke (Stefanidis *et al.*, 2016).

Calcium oxide (CaO) is found to be an excellent catalyst for deacidification of biomass-derived bio-oil and at the same time promoting the formation of hydrocarbons (Wang *et al.*, 2010; Chen, Chen, *et al.*, 2017). Wang et al. (2010) compared the performances of both MCM-41 and CaO on the pyrolysis of corncob using TGA-FTIR analysis. Comparatively, CaO showed significant change in product distribution. The study showed a decrease in molality of acids by 75.9 % and an increase in molality of hydrocarbons by 19.8 %. On the other hand, Chen et al. (2017) subjected cotton stalk biomass to pyrolysis with the addition of CaO. The study presented the roles of CaO during pyrolysis in a

comprehensive manner, which depends on the pyrolysis conditions. The three distinct roles of CaO were CO_2 absorbent, reactant, and catalyst (Chen, Yang, *et al.*, 2017).

Besides, Zabeti et al. (2012) used amorphous silica alumina (ASA) containing AAEMs like sodium (Na), potassium (K), caesium (Cs), magnesium (Mg), and calcium (Ca) for catalytic pyrolysis of Canadian pinewood. All the alkali/ASA catalysts were effective in deoxygenation of pyrolysis vapours. While K/ASA and Na/ASA were most active in eliminating oxygen via decarboxylation, Cs/ASA was most active in doing so via decarbonylation. Cs/ASA also selectively converted undesired phenols to hydrocarbons and maximized the amount of required furans (Zabeti *et al.*, 2012).

Both Shimada et al. (2008) and Patwardhan et al. (2010) investigated the influence of AAEMs on cellulose. While Shimada et al. (2008) utilized sodium (Na), K, Mg, and Ca in their chloride forms, Patwardhan et al. (2010) employed inorganic salts such as sodium chloride (NaCl), potassium chloride (KCl), magnesium chloride ($MgCl_2$), calcium chloride ($CaCl_2$), calcium hydroxide ($Ca(OH)_2$), calcium nitrate ($Ca(NO_3)_2$), calcium carbonate ($CaCO_3$) and dicalcium phosphate ($CaHPO_4$). Both studies observed a decrease in levoglucosan yield and a substantial increase in lower molecular weight products such as glycoaldehyde, formic acid, and acetol, even at a very low level of addition (Shimada, Kawamoto and Saka, 2008; Patwardhan *et al.*, 2010).

Apart from AAEMs, transition metals were used in catalytic pyrolysis studies. Transition metals were mostly used in the form of oxides or supported on zeolites. Ma et al. utilized the metal oxides of cobalt (Co), molybdenum (Mo),

nickel (Ni), iron (Fe), manganese (Mn), and copper (Cu), as well as those metal loaded zeolites on the pyrolysis of lignin. The study concluded that by supporting Co and Ni onto zeolites, more aromatic hydrocarbons were obtained as compared to blank zeolite. It was also concluded that the variation of catalyst and reaction conditions has potential for obtaining targeted compounds such as vanillin and guaiacol (Ma *et al.*, 2014). Besides that, nano titanium dioxide (TiO_2), iron (III) oxide (Fe_2O_3), nickel oxide (NiO), and zinc oxide (ZnO) were used as catalysts in pyrolysis of poplar wood. These oxides reduced bio-oil yield and increased gas, water, and solid yields. The study concluded that the oxides have the potential to improve the bio-oil qualities in terms of stability, calorific value, and phenol content (Lu *et al.*, 2010). ZnO was also used as catalyst in the catalytic pyrolysis of sawdust and gave a highest liquid yield among other catalyst such as MgO, dolomite, and limestone (Nokkosmäki *et al.*, 1998). In the next work, the stability of oils produced from ZnO was studied. Nokkosmäki et al. (2000) discovered that ZnO is a mild catalyst that did not reduce the bio-oil liquid yield significantly. In addition, the stability of the catalytically treated bio-oil improved (Nokkosmäki *et al.*, 2000).

The catalytic upgrading of EFB has also been carried out previously. Auta et al. (2014) introduced potassium carbonate (K_2CO_3), $Ca(OH)_2$, and MgO to the pyrolysis system of EFB whereas Ahmad et al. (2014) utilized CaO from eggshell waste. Both studies aimed to optimize the operating conditions of catalytic pyrolysis of EFB for bio-oil production. Auta et al. (2014) concluded that $Ca(OH)_2$ gave the maximum bio-oil yield and also decreased the acidic content of the bio-oil (Ahmad, Rohim and Ibrahim, 2014; Auta, Ern and Hameed, 2014).

Table 4: Effects of catalysts on the properties of bio-oil

Biomass	Reactor	Gas	Temperature (°C)	Catalyst	Findings with respect to bio-oil					References
					Yield (wt.%)	Moisture content	Acidity	HHV (MJ/kg)	Viscosity	
Zeolite catalysts										
Eucalyptus woodchips	Fixed bed	N_2, 100 mL/min	500	HZSM-5	-	Increased from 15.0 to 19.0 wt%	-	-	-	(Fermoso *et al.*, 2017)
Oak						Increased from 16.0 to 19.0 wt%				
Miscanthus						Increased from 13.0 to 16.0 wt%				
Straw from wheat						Increased from 15.0 to 17.0 wt%				
Palm kernel shell	Fixed bed	N_2	500	Meso-HZSM-5 (10.35)	Decreased from 49.8 to 32.6 wt%	Increased from 49.3 to 63.3 wt%	-	-	-	(Asadieraghi and Wan Daud, 2015)
Corncob	Fluidized bed	N_2, 3.4 L/min	550	HZSM-5 (24)	-	Increased from 22.9 to 25.6 %	pH increased from 2.8 to 5.2	Increased from 18.8 to 34.6 MJ/kg	Specific gravity decreased from 1.2 to 1.0	(Zhang *et al.*, 2009)

Table 4: Effects of catalysts on the properties of bio-oil (continue)

Rice husk	Close-coupled reactor	N_2	500	ZSM-5	Decreased from 39.61 wt% to 38.29 wt%	Increased from 52.6 to 55.56 wt%	pH decreased from 3 to 2.74 Acid number decreased from 55.54 to 39 mg KOH/g	Wet basis: Insignificant Dry basis: Increased from 28.71to 30.01 MJ/kg	Decreased from 1.68 to 1.55 cSt	(Abu Bakar and Titiloye, 2013)
Beech wood	Fixed bed tubular	N_2, 100 and 50 mL/min	500	ZSM-5 (80)	Decreased from 58.7 to 34.3 wt%	-	-	-	-	(Iliopoulou *et al.*, 2012)
Oxides										
Cotton stalk	Fixed bed	N_2, 100 mL/min	500	CaO (50 wt%)	Decreased when from approx. 50.0 to 48.0 wt%	Increased from approx. 27.0 to 33.0 wt%	-	-	-	(Chen, Chen, *et al.*, 2017)
White pine powder	Fluidized bed	N_2, 50 L/min	520	CaO (50 wt%)	Insignificant (from approx. 56.0 to 57.0 %)	Increased from approx. 18.0 to 20.0 %	-	-	-	(Lin *et al.*, 2010)

Table 4: Effects of catalysts on the properties of bio-oil (continue)

Cotton seed	Fixed bed	N_2, 200 mL/min	550	MgO (10 wt%)	Decreased from 46.0 to approx. 36.0 %	-	-	Increased from 39.8 to 42.9 MJ/kg	-	(Pütün, 2010)
Rice husk	Fixed bed	N_2, 150 mL/min	550	ZnO (10 wt%)	Decreased from 47.0 to approx. 45.0 wt%	Decreased from 15.3 to 14.6 wt%	pH insignificant (from 4.2 to 4.4)	HHV increased from 24.7 to 26.5 MJ/kg	-	(Zhou *et al.*, 2013)
Loblolly pinewood tree stem	Auger and PBR (ex-situ)	N_2, 4 L/min	450	TiO_2 (rutile)	Increased from 36.3 to 43.0 wt%	Decreased from 15.6 to 13.3 wt%	Acid value increased from 30.1 to 62.9 mg NaOH/g oil	Insignificant (from 32.5 to 32.1 MJ/kg)	-	(Guda and Toghiani, 2017)
				TiO_2 (anatase)	Increased from 36.3 to 45.2 wt%	Decreased from 15.6 to 11.5 wt%	Acid value increased from 30.1 to 64.6 mg NaOH/g oil	Insignificant (from 32.5 to 32.8 MJ/kg)	-	
Pine sawdust (Finnmehl)	Fluidized bed	N_2, 27 L/min	525	ZnO	-	Increased from 20.8 to 24.8 wt%	-	HHV insignificant (remained at 18.0 MJ/kg)	Decreased from 9.5 to 5.7 cSt	(Nokkosmäki *et al.*, 2000)

Table 5: Effects of catalysts on the targeted compounds in bio-oil

Biomass	Reactor	Gas	Temperature (°C)	Catalyst	Findings				References
					Anhydrosugars	Furan compounds	Phenolic compounds	Aromatics and hydrocarbons	
Zeolite catalysts									
Corncob (vapour)	TGA-FTIR	N_2, 65 mL/min	From room temperature to 1000	MCM-41 (38)	-	-	Molality increased by 10.2 %	Molality increased by 15.3 %	(Wang *et al.*, 2010)
Waste pepper stems	Py-GC/MS	He	550	HZSM-5 (23)	-	Distribution area: Furans increased from approx. 3.5 to 9.2 % Furanones decreased from approx. 1.1 to 0.6 %	Distribution area: Decreased from approx. 30.0 to 17.0 %	Distribution area: Aliphatics increased from approx. 0 to 2.0 % Aromatics increased from approx. 1.0 to 15.0 % PAHs increased from approx. 0 to 6.0 %	(Park *et al.*, 2015)

Table 5: Effects of catalysts on the targeted compounds in bio-oil (continue)

Waste pepper stems	Py-GC/MS	He	550	HZSM-5 (280)		Distribution area: Furans increased from approx. 3.5 to 9.4 % Furanones increased from approx. 1.1 to 1.4 %	Distribution area: Decreased from approx. 30.0 to 21.0 %	Distribution area: Aliphatics increased from approx. 0 % to <1 % Aromatics increased from approx. 1.0 to 4.0 % PAHs increased from approx. 0 to 1.0 %	(Park *et al.*, 2015)
Sawdust	CDS Pyroprobe 5200HP pyrolyser	He	600	ZSM-5 (17.3)	-	Peak area: Furans decreased to seemingly 0	Peak area: Decreased from 3.5×10^8 to 0.5×10^8	Peak area: Aromatics increased from seemingly 0 to approx. 1.6×10^9	(Sun *et al.*, 2016)

Table 5: Effects of catalysts on the targeted compounds in bio-oil (continue)

Eucalyptus woodchips	Fixed bed	N_2, 100 Nml/min	500	H-ZSM-5 (58)	Relative area: Decreased from approx. 18.0 to 0 %	Relative area: Furans decreased from approx. 7.5 to 4.0 %	-	Relative area: Aromatics increased from approx. 2.0 to 13 %	(Hernando *et al.*, 2017)
				H-Beta (24)	Relative area: Decreased from approx. 18.0 to 6 %	Relative area: Furans decreased from approx. 7.5 to 6.5 %		Relative area: Aromatics increased from approx. 2.0 to 4 %	
Rice husk	Close-coupled reactor	N_2	500	ZSM-5	Peak areas: Decreased from 3.7 to 2.0 %	Peak areas: Increased from 9.0 to 9.6 %	Peak areas: Light phenols increased from 12.8 to 14.4 % Heavy phenols insignificant (13.6 to 13.5 %)	Peak areas: Aromatics increased from 1.5 to 2.2 %	(Abu Bakar and Titiloye, 2013)
Pine (*Pinus sylvestris*)	Fluidized bed	N_2, 2.5 L/min feeder and 1.25 L/min through reactor	450	H-Beta	Increased from 20.9 to 23.8 wt%	-	Increased from 4.8 to 5.6 wt%	PAHs increased from 0 wt% to 2.1 wt%	(Aho *et al.*, 2008)

Table 5: Effects of catalysts on the targeted compounds in bio-oil (continue)

				H-Y	Increased from 20.9 to 21.3 wt%		Increased from 4.8 to 6.2 wt%	PAHs increased from 0 wt% to 1.3 wt%	
				H-ZSM-5	Increased from 20.9 to 24.4 wt%		Increased from 4.8 to 5.4 wt%	PAHs increased from 0 to 3.1 wt%	
				H-Mordenite	Insignificant (20.9 to 20.3 wt%)		Increased from 4.8 to 5.8 wt%	PAHs increased from 0 to 0.1 wt%	
Eucalyptus woodchips	Fixed bed	N_2, 100 mL/min	500	HZSM-5	Relative area: Decreased from approx. 18.0 to seemingly 0 %	Relative area: Decreased from approx. 6.0 to 2.0 %	-	Relative area: Increased from approx. 1.0 to 10.0 %	(Fermoso *et al.*, 2017)
Oak					Relative area: Decreased from approx. 26.0 to 2.0 %	Relative area: Decreased from approx. 10.0 to 5.0 %		Relative area: Increased from seemingly 0 to approx. 17.0 %	
Miscanthus					Relative area: Decreased from approx. 5.0 to seemingly 0 %	Relative area: Insignificant (Remained at approx. 7.0 %)		Relative area: Increased from seemingly 0 to approx. 14.0 %	

Table 5: Effects of catalysts on the targeted compounds in bio-oil (continue)

Straw from wheat	Fixed bed	N_2, 100 mL/min	500	HZSM-5	Relative area: Decreased from approx. 5.0 to seemingly 0 %	Relative area: Insignificant (Remained at approx. 8.0 %)	-	Relative area: Increased from seemingly 0 to approx. 10.0 %	(Fermoso *et al.*, 2017)
Beech wood	Fixed bed	N_2, 100 mL/min for 15mins and 50 mL/min for 10 mins	500	ZSM-5 (80)	-	Chromatogram area: Increased from approx. 1.0 to 2.0 %	Chromatogram area: Increased from approx. 29.0 to 35.0 %	Chromatogram area: Aromatics increased from seemingly 0 to approx. 6.0 % Aliphatics decreased from approx. 1.0 to 0 %	(Iliopoulou *et al.*, 2012)
Oxides									
Poplar wood	CDS Pyroprobe 5250 pyrolyser	-	500	Nano MgO	Peak area: Decreased from 10.1 to 8.4 %	Peak area: Insignificant (from 7.0 to 7.4 %)	Peak area: Increased from 26.5 to 30.2 %	Peak area: Insignificant (from 0.2 to 0.8 %)	(Lu *et al.*, 2010)
Corncob	TGA-FTIR	N_2, 65 mL/min	From room temperature to 1000 °C	CaO	-	-	Molality decreased by 42.6 %	Molality increased by 19.8 %	(Wang *et al.*, 2010)

Table 5: Effects of catalysts on the targeted compounds in bio-oil (continue)

Poplar wood	CDS Pyroprobe 5250 pyrolyser	-	500	Nano CaO	Peak area: Decreased from 10.1 to 1.2 %	Peak area: Decreased from 7.0 to 5.2 %	Peak area: Decreased from 26.5 to 13.0 %	Peak area: Hydrocarbons increased from 0.2 to 4.2 %	(Lu *et al.*, 2010)
				Nano Fe_2O_3	Peak area: Decreased from 10.1 to 7.5 %	Peak area: Insignificant (from 7.0 to 6.8 %)	Peak area: Increased from 26.5 to 28.1 %	Peak area: Hydrocarbons increased from 0.2 to 3.1 %	
				Nano NiO	Peak area: Increased from 10.1 to 13.6 %	Peak area: Insignificant (from 7.0 to 6.4 %)	Peak area: Increased from 26.5 to 32.6 %	Peak area: Insignificant (from 0.2 to 0.3 %)	
				Nano TiO_2	Peak area: Decreased from 10.1 to 4.0 %	Peak area: Increased from 7.0 to 9.2 %	Peak area: Increased from 26.5 to 27.3 %	Peak area: Insignificant (from 0.2 to 0.9 %)	
Loblolly pinewood tree stem	Auger and PBR (ex-situ)	N_2, 4L/min	450	TiO_2 (rutile)	Anhydrosugars increased from approx. 0.001 to 0.042 g/g oil LGO increased from approx. 0 to approx. 0.002 g/g oil	Furfural increased from approx. 0.008 to 0.011 g/g oil 5-methyl-furfural increased from approx. 0.003 to 0.011 g/g oil	Phenols increased from 15.1 to 21.8 g/g bio-oil	Decreased from 183.5 to 169.1 µg/mL bio-oil	(Guda and Toghiani, 2017)

Table 5: Effects of catalysts on the targeted compounds in bio-oil (continue)

Loblolly pinewood tree stem	Auger and PBR (ex-situ)	N_2, 4L/min	450	TiO_2 (anatase)	Anhydrosugars increased from approx. 0.001 to 0.022 g/g oil LGO increased from seemingly 0 to approx. 0.001 g/g oil	Furfural increased from approx. 0.008 to 0.009 g/g oil 5-methyl-furfural increased from approx. 0.003 to 0.018 g/g oil	Phenols increased from 15.1 to 25.0 g/g bio-oil	Increased from 183.5 to 249.0 µg/mL bio-oil	
Cotton stalk	Fixed bed	N_2, 100 mL/min	500	CaO (50 wt%)	Peak area: Anhydrosugar insignificant (remained at approx. 1.0 %)	Peak area: Increased from approx. 9.0 to 11.0 %	Peak area Decreased from approx. 20.0 to 15.0 %	Peak area Increased from seemingly 0 to approx. 3.0 %	(Chen, Chen, *et al.*, 2017)
White pine powder	Fluidized bed	N_2, 50 L/min	520	CaO (50 wt%)	Relative abundance: Decreased from approx. 13.0 to 11.0 %	-	Relative abundance: Insignificant (remained at approx. 0.5 %)	-	(Lin *et al.*, 2010)
Poplar wood	CDS Pyroprobe 5250 pyrolyser	-	500	Nano ZnO	Peak area: Decreased from 10.1 to 7.2 %	Peak area: Increased from 7.0 to 8.2 %	Peak area: Increased from 26.5 to 28.3 %	Peak area: Insignificant (from 0.2 to 0.3 %)	(Lu *et al.*, 2010)

2.3.3.3 Esterification

The esterification of bio-oils involves the converting of acids in the bio-oil to esters in the presence of alcohol and catalyst. The esterification degree of bio-oil may be evaluated based on the change in the acid number of the bio-oil (Wang, Chang and Fan, 2010).

To ease the separation of catalysts after reaction, a variety of heterogeneous catalysts have been studied for esterification of bio-oil. Two of the catalysts studied were solid acid catalyst ($40SiO_2/TiO_2$-SO_4^{2-}) and solid base catalyst ($30K_2CO_3/Al_2O_3$-NaOH). Zhang et al. (2006) observed that solid acid catalyst showed higher esterification activity as compared to solid base catalyst in terms of acetic acid conversion over ethanol. Upon analysing the upgraded bio-oil by gas chromatography mass spectrometry (GC-MS), evidence showed the both solid catalysts were able to convert organic acids in the bio-oil to their respective esters: formic acid to ethane,1,1′,1-[methylidynetris(oxy)]tris, butanedioic acid to butanedioic acid, diethyl ester, and 1,2-benzenedicarboxylic acid to 1,2-benzenedicarboxylic acid, diethyl ester (Zhang, Wang and Wu, 2007).

Besides, ionic liquid resins (732- and NKC-9) were also employed as catalysts for esterification over methanol by Wang et al. (2010). Esterification experiments were carried out in reactors over wood chips-derived bio-oil and methanol. In a batch reactor, both 732 and NKC-9 resins were able to decrease the acid number of the bio-oil by more than 85 %, representing a large conversion of organic acids to neutral esters. Moreover, good recyclability was also presented by the resins without significantly affecting efficiency (Wang, Chang and Fan, 2010).

Zeolites such as H-ZSM-5 and H-Beta were also investigated for their esterification activities over cyclohexanol and acetic acid by Viswanadham et al. (2010) as a model reaction. H-Beta showed higher activity due to the larger diameter in pore channels than that of H-ZSM-5, indicating the significance of pore channel in relation to esterification activity. Therefore, the study also revealed the positive influences of a larger surface area, larger pore volume, and a higher density of acid sites in the zeolites on the esterification activity of the catalysts. In comparison, nanosized H-ZSM-5 showed higher catalytic activity than that of commercial H-ZSM-5 (Viswanadham *et al.*, 2010).

2.3.3.4 Hydrodeoxygenation (HDO)

Hydrodeoxygenation (HDO) contribute to the improving of bio-oil quality by removing oxygen as water, at the same time retaining all carbon atoms in the bio-oil in the presence of pressurized hydrogen (H_2) (Ruddy *et al.*, 2014). A range of supported metal catalyst has been utilized in HDO studies such as transition metals, noble metals, and noble metal-like catalysts.

Transition metal catalysts that are commonly used for HDO are Ni, Co, and Mo. Mortensen et al. (2013) screened 23 types of catalysts for HDO of phenol and among the catalysts tested, Ni was found to be the only active non-noble metal catalyst. The study also concluded that Ni-based catalysts require a metal oxide as a carrier for the hydrogenation of phenol (Mortensen *et al.*, 2013).

Co is known as one of the promoter metals and has been studied for the promoting effect on Mo-based catalysts. Bui et al. (2011) compared the performances of unsupported and alumina supported MoS_2 and CoMoS catalysts on the HDO of guaiacol. With the addition of Co, the conversion of

guaiacol strongly increased via direct deoxygenation pathway (Bui *et al.*, 2011). Co was also used for enhancing the stability of molybdenum carbide (Mo_2C) catalyst in the HDO of furfural to produce 2-methylfuran, a promising fuel additive. The addition of Co was able to improve the stability by reducing the O_2 and furfural binding energies on the Mo_2C catalyst (Lin *et al.*, 2018).

Noble metals are metallic chemical elements that are extremely resistant to oxidation, even at elevated temperatures. Zanuttini et al. (2013) observed that at higher platinum (Pt) metal loadings, high selectivity to toluene was obtained; at lower metal loadings, high yields of light hydrocarbons were obtained (Zanuttini *et al.*, 2013). On the other hand, a study by Griffin et al. (2016) showed that the employment of TiO_2 as support showed higher activity on a metal site basis and exhibited higher selectivity to toluene as compared to that of C support (Griffin *et al.*, 2016).

De Souza et al. (2017) investigated the effect of various types of supports on the HDO performance of palladium (Pd)-based catalyst on phenol in a fixed bed reactor at 300 °C. The study showed that the types of support significantly affected the product distribution (de Souza *et al.*, 2017). Apart from that, Barrios et al. (2018) concluded that between Pd supported on niobium (V) oxide (Nb_2O_5) and silicon dioxide (SiO_2), the former exhibited higher activity and selectivity to deoxygenated products for HDO of phenol (Barrios *et al.*, 2018).

Ruthenium (Ru) was also supported onto TiO_2, zirconium dioxide (ZrO_2), and TiO_2-ZrO composite oxides with varying Ti/Zr ratios by Lu et al. (2017). In the study of guaiacol conversion, the selectivity of benzene varied according to the active surface of Ru and as compared to the other supports, TiO_2-ZrO_2 showed

to be the most promising support for Ru catalyst in HDO reaction (Lu *et al.*, 2017).

Rhodium (Rh)-containing catalysts exhibit good HDO and hydrogenation performances at high and low temperatures. Gutiérrez (2013) had even reported that in hydrotreatment and autothermal reforming, Rh-containing catalysts were the most active, selective, and stable (Gutiérrez, 2013). The main product obtained was benzene, along with small amounts of cyclohexanol (Gutierrez *et al.*, 2009). Besides that, Nan et al. (2014) had also compared the performances of both Ru and Rh metals that were supported on C. The catalysts were used in the HDO of switchgrass-derived bio-oil at the temperature range of 200 – 280 °C at H_2 pressure of 20 – 70 bar. While Rh/C was more effective in CO_2 formation, Ru/C had high H_2 consumption (Nan *et al.*, 2014).

Despite the many advantages of utilizing noble metals for bio-oil upgrading, the high cost associated with noble metals employment led to the production and studying of noble metal-like catalysts. Noble metal-like catalysts are produced from base metal catalysts (e.g. tungsten carbide) and other transition metal carbides and nitrides (e.g. W_2N, Mo_2C, and Mo_2N). These catalysts are expected to exhibit similar catalytic performances as Pt, Ru and Ir-based catalysts (Lu *et al.*, 2018).

2.3.3.5 Emulsification

Emulsification is one of the most convenient physical upgrading techniques for bio-oil, where immiscible bio-oil and diesel are blended into a homogenous stable system, with or without surfactants. The presence of polar compounds (e.g. phenol and carboxylic acid) in bio-oil may cause undesirable stratification

of bio-oil and diesel emulsion. Hence, surfactants and agitation techniques have to be used (Majhi, Sharma and Naik, 2012). Since the bio-oil is acidic in nature, only non-ionic surfactants can be used. Upon emulsification, the bio-oil would be diluted by diesel and hence, would have properties more similar to that of diesel than those of bio-oil itself (Yang *et al.*, 2014). Bio-oil that was upgraded via catalytic pyrolysis in the presence of HZSM-5 was found to be miscible with diesel without surfactant (Martin, Mullen and Boateng, 2014).

One of the limitations of emulsifying bio-oil with diesel is the emulsion stability and Martin et al. (2014) attributed the instability of the emulsion to the presence of levoglucosan (LG) in bio-oil. To address this limitation, studies were carried out by manipulating the surfactant type and amount, agitation mechanism, concentration of bio-oil, and other factors. Chiaramonti et al. (2003) tested on approximately 100 surfactants and found that Atlox group surfactants are most effective in stabilizing bio-oil/diesel emulsion (Chiaramonti *et al.*, 2003). In another study, Guo et al. (2014) concluded that smaller droplet sizes would increase the stability of the emulsion (Guo, Wang and Wang, 2014).

2.3.3.6 Hot vapour filtration

Hot vapour filtration is studied to improve the bio-oil quality by reducing the amounts of metals, solids, and biochar in the bio-oil. The presence of these solids affects the storage stability of the bio-oil negatively and would cause fouling in downstream upgrading equipment (Baldwin and Feik, 2013). However, the application of hot vapour filtration might affect the yield and properties of the bio-oil.

Upon utilizing hot vapour filtration system on the pyrolysis of rice husk, the bio-oil obtained decreased by 2 wt.% in yield, had higher water content, higher pH, and lower alkali metal content (Chen *et al.*, 2011). In a study was carried out by Baldwin and Feik (2013), ceramic filter element for the filtration of bio-oil vapour was employed. Favourable results were obtained, where bio-oil with very little amount of solids was produced. Nevertheless, mass loss due to filtration was 10 – 30 wt.% (Baldwin and Feik, 2013). A study was also carried out by Paenpong et al. (2013) to study the effects of pour granular filtration unit on the pyrolysis of cassava rhizome. Even though the bio-oil yield decreased, the solid content, ash content, viscosity, and ageing rate of the bio-oil decreased upon filtration, which are deemed to be positive effects. Nevertheless, the filtration unit showed no significant effects in improving the properties of the bio-oil such as water content and acidity (Paenpong, Inthidech and Pattiya, 2013).

2.3.3.7 Water or solvent addition

Solvents or water are added to the bio-oil with the aim of separating or extracting different chemical groups from the bio-oil via liquid-liquid extraction, which would then enhance the bio-oil quality. As the solvents are selective to different compounds, unfavourable compounds in the bio-oil may be identified and extracted. Park et al. (2016) separated switchgrass-derived bio-oil into aqueous and organic phases by adding water, organic solvents (hexadecane and octane), and sodium hydroxide (NaOH) for pH adjustment. While acetic acid was extracted in the aqueous phase, phenolic compounds were extracted in the organic phase. Upon neutralization, the oxygen content in the organic bio-oil decreased by 37 % whereas the HHV increased by 100 %, signifying an

improvement in bio-oil quality (Park *et al.*, 2016). Besides, upon identifying 1, 6-anhydro-b-D-glucose and other sugar derivatives as one of the main contributors to the high viscosity in poultry litter-derived bio-oil, the compound was extracted using methanol and later by water to lower the viscosity of the bio-oil (Ma and Agblevor, 2014).

Aside from the selection of solvent, the amount of solvent used would significantly affect the extraction efficiency of compounds. With the increase in solvent, the organic mass in the solvent phase increased as well: the organic matter in chloroform solvent increased from 50 to 67 wt.% when solvent/bio-oil volume ratio increased from 0.5 to 1. As for solvent/water phase, volume ratio of 1 was regarded as the optimum extraction condition (Wei *et al.*, 2014).

2.4 Preliminary experiments (Co-pyrolysis of empty fruit bunch fibre (EFBF) with palm oil mill effluent (POME) sludge)

In contrast to the bio-oil derived from lignocellulosic biomass, bio-oil derived from palm oil mill effluent (POME) sludge showed a high pH of about 9.4, signifying that the bio-oil was alkaline in nature. Hence, co-pyrolysis of lignocellulosic biomass and sludge to produce a neutralized bio-oil was suggested (Thangalazhy-Gopakumar *et al.*, 2015). Though many studies have reported on co-pyrolysis of lignocellulosic biomass with solid waste, there are no much studies on kinetics and mechanisms. Therefore, preliminary experiment to this project involves the study on kinetics and mechanisms for co-pyrolysis of empty fruit bunch fibre (EFBF) with POME sludge and to observe the change in pyrolytic behaviour of EFBF, if any, upon the addition of POME sludge. The study was carried out via thermogravimetric analysis

(TGA), adopting both Vyazovkin and Coats-Redfern method to formulate the kinetics and to determine the mechanisms involved.

2.4.1 Biomass characterization

Table 6 presents the proximate analysis and values of higher heating values (HHV) of both EFBF and POME sludge.

Table 6: Ultimate and proximate analyses and HHV of EFBF and POME sludge

	EFBF	POME sludge
Proximate analysis		
Moisture content (wt.%)	5.3 ± 0.3	8.5 ± 1.6
Volatile matter (wt.%)	74.0 ± 1.0	47.7 ± 0.8
Ash content (wt.%)	1.3 ± 0.2	23.8 ± 0.5
Fixed carbon (wt.%)	19.4 ± 0.8	20.0 ± 1.4
HHV (MJ/kg)	17.6 ± 0.9	13.8 ± 0.9

As observed from Table 6, the volatile matter of sludge was very low as compared to that of EFBF, which was expected. On the other hand, the fixed carbon available in sludge was about the same as that of EFBF, which showed the potential application of sludge biochar from pyrolysis. As sludge has high ash content, POME sludge was further examined by X-ray microanalysis, using Energy Dispersive X-ray Spectroscopy (EDX) in order to understand its inorganic content, where three points were taken for each microscopic analysis. Table 7 shows the elements detected in POME sludge and the standards used. The elements detected such as calcium (Ca), magnesium (Mg), and potassium (K) have been studied for their catalytic activities for the thermal degradation

of biomass (Refaat, 2011; Ninduangdee and Kuprianov, 2015; Lee *et al.*, 2016; Jiang, Liu and Liu, 2017). The presence of alkaline earth metals were able to enhance the breakdown of biomass components, where the effect was increasing in the order of Mg, Ca, K, sodium (Na) (Mahadevan *et al.*, 2016). The high oxygen content together with the presence of the mentioned elements in POME sludge suggested the presence of the metal oxides in the sludge, which may pose catalytic effects on EFBF upon co-pyrolysis with sludge.

Table 7: Elements detected and the standard used in POME sludge from EDX analysis

Element	Standard	Weight %
C	$CaCO_3$	50.4 ± 4.0
O	SiO_2	38.0 ± 3.8
Mg	MgO	1.3 ± 0.8
Al	Al_2O_3	0.7 ± 0.1
Si	SiO_2	1.2 ± 0.3
P	GaP	2.1 ± 0.8
S	FeS_2	1.3 ± 0.2
K	MAD-10 Feldspar	1.7 ± 0.5
Ca	Wollastonite ($CaSiO_3$)	1.3 ± 0.2
Mn	Mn	1.7 ± 0.9

2.4.2 Thermogravimetric analysis (TGA)

Figure 2 shows the thermogravimetry weight loss (TG) and derivative thermogravimetry weight loss (DTG) curves of EFBF and POME sludge at a heating rate of 20 °C/min in nitrogen (N_2) atmosphere. As observed, the pyrolysis of EFBF may be distinguished into three stages: 1) evaporation of

moisture (50 – 160 °C); 2) devolatilization of mainly cellulose and hemicellulose (160 – 420 °C); 3) decomposition of lignin and other stronger chemical bonds (420 – 660 °C).

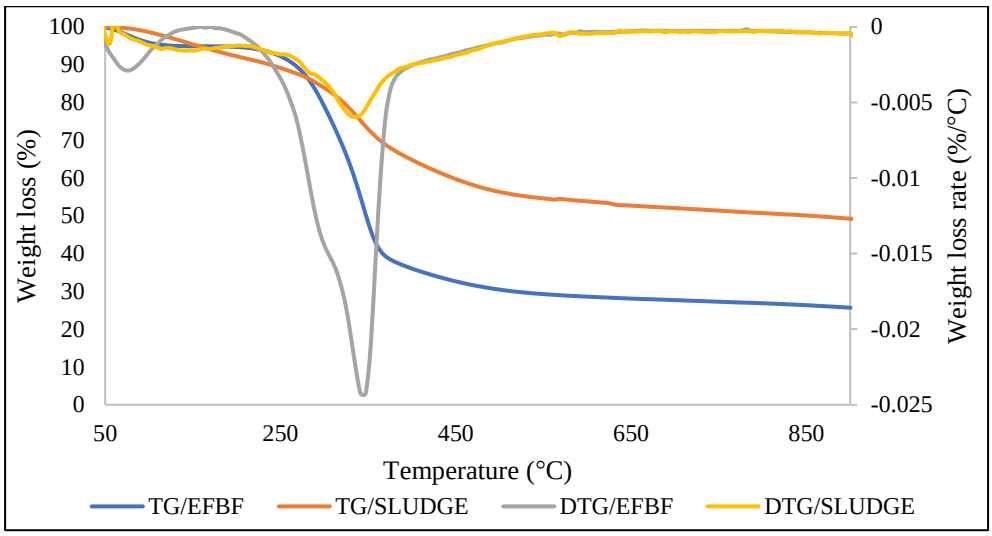

Figure 2: TG and DTG curves of EFBF and POME at a heating rate of 20 °C/min

With regards to the decomposition of POME sludge, three stages were observed and was similar to the results obtained by Thangalazhy-Gopakumar et.al. (2015) (Thangalazhy-Gopakumar *et al.*, 2015). The first stage mainly corresponds to the dewatering of the samples at a temperature below 210 °C. Subsequently, the second stage at 210 °C to 440 °C involves the main decomposition of the POME sludge. Decomposition of major organic compounds present in sludge would occur in this temperature range as well. Beyond 440 °C, the decomposition rate of POME sludge reduced greatly as carbonaceous materials formed from the pyrolysis of the sample in the second stage such as tar and coke go through secondary cracking. In addition, other inorganic materials present in the POME sludge were being decomposed (Liu *et al.*, 2009). As compared to organic compounds, the structure of inorganic compounds is more complex and their

chemical bonds are more difficult to break, contributing to the slower decomposition rate in stage three.

The weight loss rate of EFBF is higher than that of POME sludge, signifying that EFBF has a higher reactivity than POME sludge. This is because EFBF has higher organic volatiles content than POME sludge (Mu *et al.*, 2016). Moreover, as the percentages of POME sludge increased in the sample, the temperature at which stage (Stage 2) decomposition starts increased, which again indicates that POME sludge has a lower reactivity than EFBF.

2.4.3 Synergic effect

Figure 3 depicts the TG and DTG curves of EFBF – POME sludge blends at various POME sludge percentages, at a heating rate of 20 °C/min with N_2 flow. From the peak position and height of DTG curves, the combustion reactivity of the samples can be studied, where the DTG peak height is directly proportional to the reactivity, whereas the temperature in correspondence to the peak height is inversely proportional to the reactivity (Ghetti, Ricca and Angelini, 1996). The curves labelled as "10%" refers to samples with 10 wt.% of POME sludge, "25%" to samples with 25 wt.% of POME sludge, and so on so forth for the other samples. With the increase of sludge percentages in the blends, the profiles of both the TG and DTG curves shifted from those of EFBF to sludge where combustion reactivity gradually decreased.

The understanding of synergic effect in the production of bio-oil via co-pyrolysis is important as it is one of the main factors responsible in the measuring or determining improvements in oil quality and quantity (Abnisa, Mohd and Daud, 2014). Positive or negative synergic effects rely on the type

and contact between the components, duration of pyrolysis, temperature and heating rate, removal or equilibrium of volatiles formed, and addition of solvents, catalysts, and hydrogen donors (Johannes, Tiikma and Luik, 2013; Abnisa, Mohd and Daud, 2014). Since the effect is dependent on the type of feedstock, the synergistic effects of different co-pyrolysis feedstock would vary according to their composition and pyrolytic behaviour. Operating conditions contribute to the varying of synergic effect during co-pyrolysis as well.

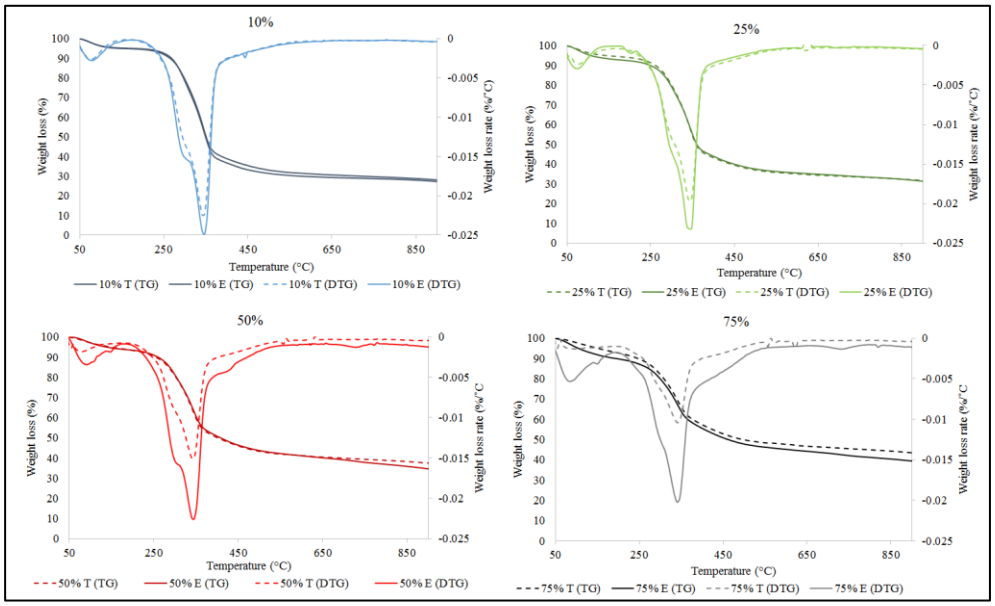

T indicates the theoretical values (dotted lines) whereas E indicates the experimental values (solid lines).

Figure 3: TG and DTG curves of: (a) 10 % sludge, (b) 25 % sludge, (c) 50 % sludge, and (d) 75 % sludge at heating rate of 20 °C/min and N2 flow of 20 mL/min

In order to investigate the synergistic interaction between EFBF and POME sludge, the theoretical and experimental values of blends during co-pyrolysis are presented in Figure 3. Comparing theoretical and experimental values, TG curves for blends showed differences in terms of weight loss and could be clearly observed from the major peaks of DTG curves. The experimental values showed higher weight loss at the second stage as compared to theoretical values,

suggesting that more cellulose and hemicellulose were being degraded than expected. Since metal oxides in sludge ash have been proven to act as heterogeneous catalyst in the recent years, metal oxides such as CaO and MgO that are present in the POME sludge might have posed catalytic effect on the pyrolysis of EFBF (Cheng, Li and Yoshikawa, 2015; Nam *et al.*, 2016).

A difference between experimental and theoretical values hinted the existence of interactions between EFBF and POME sludge, known as the synergistic effect (Quan *et al.*, 2014). Fei et al. (2012) mentioned that synergistic effect was greater when the contact between particles improves (Fei *et al.*, 2012). However, a close contact between particles may pose an inhibitive effect as they will fill in the interspaces of each other (Quan *et al.*, 2014). This contradicting theory further confirms the fact that synergistic effect varies with the type of feedstock upon co-pyrolysis.

2.4.4 Kinetics of co-pyrolysis by Vyazokin method

Vyazovkin method is a non-linear method that uses integration technique. As compared to other integral model-free methods, i.e. Ozawa, Vyazovkin method provides a more accurate value of activation energy. This is because Vyazovkin method acknowledges the strong variation of activation energy with the degree of conversion, whereas the other methods do not (Vyazovkin, 2001; Criado, Sánchez-Jiménez and Pérez-Maqueda, 2008). Despite its accuracy, the application of Vyazovkin method remains limited due to mass transfer at high conversions (above 80 wt.%) (Pérez-Maqueda and Criado, 2000; Cortés and Bridgwater, 2015).

Figure 4 shows the activation energies of different samples with respect to the degree of conversion (α). The activation energies for EFBF and other blends with different sludge percentages showed significant increase from α = 0.1 to 0.3, and hereafter a slight increase until α equals to 0.7. On the other hand, the activation energy of sludge increased with the increasing of conversion until a maximum of 232.61 kJ/mol when α = 0.6.

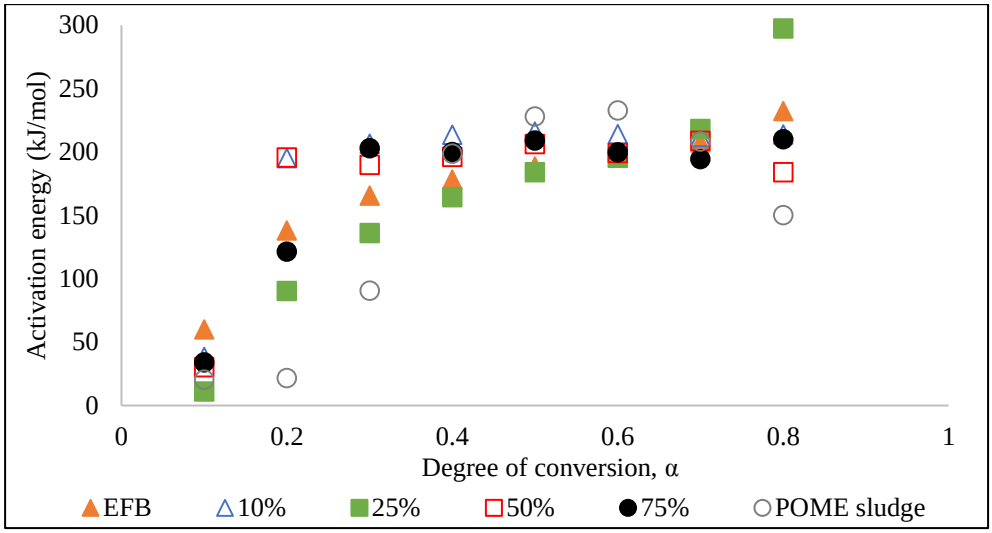

Figure 4: Activation energies of EFBF, POME sludge, and sludge percentages in the blends with respect to degree of conversion

As seen from the TG curves in Figure 2 and Figure 3, hemicellulose and cellulose in the biomasses devolatilized below 70% conversion, which corresponds to the average activation energy of 192.25 ±11.63 kJ/mol. Typical activation energies obtained for the devolatilization of both hemicellulose and cellulose are 100 – 111 kJ/mol and 195 – 236 kJ/mol, respectively, which is comparable to the results obtained in this study (Varhegyi *et al.*, 1989; Várhegyi *et al.*, 1997; Grønli, Várhegyi and Di Blasi, 2002). From Vyazovkin analysis, insignificant variations in activation energies were observed for conversion 0.4 to 0.7, which may be accounted for the liquid production in fast pyrolysis.

2.4.5 Kinetics and mechanisms of co-pyrolysis at individual stages by Coats-Redfern (CR) method

The solid-state mechanisms involved in the pyrolysis of EFBF, POME sludge, and their blends were determined using Coats-Redfern (CR) method. The highest correlations obtained ranged between 0.9753 – 0.9992, indicating the reliability of the kinetic parameters obtained. The kinetic parameters are presented in Table 8.

Table 8: Kinetic parameters for EFBF, POME sludge, and their respective blends at a heating rate of 20 °C/min

Stages	Samples (Weight ratio of EFBF : POME sludge)	Activation energy, E (kJ/mol)	Frequency factor, A (1/s)	Kinetic model	Correlation coefficient, R^2
1	100 : 0	116.47	1.40×10^{18}	F3	0.9910
	90 : 10	96.49	7.21×10^{14}	F3	0.9968
	75 : 25	91.95	1.44×10^{14}	F3	0.9948
	50 : 50	80.96	1.02×10^{12}	F3	0.9882
	25 : 75	70.73	2.32×10^{10}	F3	0.9795*
		49.17	4.47×10^{6}	F2	0.9831
	0 : 100	66.63	1.51×10^{9}	F3	0.9467*
		38.34	1.81×10^{4}	F3/2	0.9853
2	100 : 0	89.33	2.77×10^{7}	F1	0.9986
		79.41	9.29×10^{5}	R3	0.9972
		168.49	2.41×10^{13}	D3	0.9976
	90 : 10	81.20	4.25×10^{6}	F1	0.9914
		71.67	1.55×10^{5}	R3	0.9768
		194.16	7.63×10^{15}	D5	0.9972
	75 : 25	81.27	4.43×10^{6}	F1	0.9970
		71.92	1.68×10^{5}	R3	0.9880

Table 8: Kinetic parameters for EFBF, POME sludge, and their respective blends at a heating rate of 20 °C/min (continue)

		193.80	7.50×10^{15}	D5	0.9971
	50 : 50	74.11	1.03×10^{6}	F1	0.9992
		65.68	4.65×10^{4}	R3	0.9961
		141.01	7.36×10^{10}	D3	0.9968
	25 : 75	68.97	3.25×10^{5}	F1	0.9990
		61.00	1.62×10^{4}	R3	0.9940
		131.69	9.77×10^{9}	D3	0.9952
	0 : 100	63.47	8.39×10^{4}	F1	0.9967
		27.05	1.94×10^{2}	R3	0.9385#
		154.20	1.53×10^{12}	D5	0.9987
3	100 : 0	167.91	1.55×10^{12}	F3	0.9836
	90 : 10	202.13	1.32×10^{14}	F3	0.9785
	75 : 25	176.80	2.64×10^{12}	F3	0.9753
	50 : 50	173.55	3.46×10^{12}	F3	0.9774
	25 : 75	169.51	1.25×10^{12}	F3	0.9971
	0 : 100	211.31	1.39×10^{15}	F3	0.9790

* Even though the highest correlation values were not obtained for F3 model, this model was identified as the dominant kinetic model. # Even though R3 model was not dominant for sludge, this model was selected in order to compare with EFBF and other blends at stage 2 decomposition.

Stage 1 mainly involves the dewatering of samples, where the third order chemical reaction model (F3) was in dominion. The exceptions to this model were samples with EFBF: POME sludge weight ratio of 25 : 75 and 0 : 100, which have higher correlation coefficients attributed to second order (F2) and one and a half order (F3/2), respectively. The different reaction orders reflect the different rates of reaction, where higher reaction order signifies higher rate

of reaction. A lower rate of reaction for the two exceptions might be caused by inorganic materials (ash content) present in POME sludge. At this stage, the rate determining step was the chemical reaction.

Hemicellulose and cellulose devolatilize at Stage 2, where the samples experienced a major weight loss. At this stage, the solid-state reaction was not only controlled by chemical reaction, but also by diffusion and phase boundary resistance. The major mechanisms involved in stage 2 were first order kinetic (F1), power law in phase boundary reaction (R3), and diffusion mechanisms, either Jander equation (D3) or Zhuravlev-Lasokin-Tempelman equation (D5). The rate determining mechanism for F1 is the chemical reaction, where there was an equal probability of nucleation at each active site (Alshehri *et al.*, 2000). R3 is a reaction controlled by movement of an interface at constant velocity and at which nucleation occurs virtually immediately, so that the surface of each particle is covered with a layer of the product (Mahfouz *et al.*, 2012). This function relates α and t for a sphere reacting from the surface inward and is usually assumed to be the governing conversion model in the combustion of certain carbonaceous materials (Alshehri *et al.*, 2000; López-Fonseca *et al.*, 2007). Both D3 and D5 are both three-dimensional diffusion mechanisms (Parker, 1968). D3 is for reactions in a sphere, where diffusion in all three directions is equally important (Alshehri *et al.*, 2000). In contrast, Zhuravlev-D5 does not reveal the shape of the particle.

At this stage, some of the samples showed high correlation coefficients for kinetic models R3 and D3, which involve reaction for spherical symmetries, suggesting the presence of spherical particles in EFBF or POME sludge. Since both kinetic models are attributed to EFBF but not POME sludge, it may be

concluded that the sphere particles were contributed by EFBF, and that the shape of POME sludge particle is unknown. Similar to other heterogeneous reactions, three major mechanisms that control pyrolysis were interphase reaction, diffusion, and chemical reaction. The solid-state mechanisms for decomposition of lignocellulosic materials had been studied by other researchers. Liu et al. (2002) discovered that decomposition of the wood and leaf of fir plant obtained good linearity for F1, D3, and R3 as well, which is similar to that obtained for EFBF in this study (Liu *et al.*, 2002). Three-dimensional diffusion mechanism is common in the pyrolysis of lignocellulosic biomass. Guo and Lua (2000) found that for the pyrolysis of extracted oil palm fibres at low temperature regimes, D3 is the effective mechanism (Guo and Lua, 2000); Yorulmaz and Atimtay (2009) studied the effective mechanisms for untreated pine samples and discovered that for two mass loss regions, the three-dimensional diffusion mechanisms Valensi equation (D2) and Ginstling-Brounstein equation (D4) were in dominion (Yorulmaz and Atimtay, 2009).

For stage 3, devolatilization of lignin occurs for all samples and the unanimous model obtained was third order kinetic model (F3). Similar study on the pyrolysis kinetics of lignin was carried out by Xie et al. (2013) and determined that pine cone lignin fitted F3 best for Horowitz-Metzger method and F2 for Coats-Redfern method (Xie *et al.*, 2013). Employing Coats-Redfern method, Bu et al. (2016), too, concluded that F2 fits well for raw alkali lignin pyrolysis with R^2 of 0.9970 (Bu *et al.*, 2016). However, F3 also showed a good R^2 of 0.9960.

As observed from Table 8, activation energies for the Stage 1 decreased with the increase of POME sludge percentages. The increase in water content in the

sample with the increase in sludge percentages may have been the cause of this finding. Besides that, as the percentages of POME sludge increases, the amount of volatiles decreases, which in turns lower the activation energy of the sample.

With reference to Section 2.4.2, the degradation temperature of EFBF was lower than that of POME sludge, which indicated that EFBF has higher reactivity than that of POME sludge. It may also be interpreted that the energy barrier that needs to be overcome for reaction should be lower for EFBF than for POME sludge. However, as seen from Table 8, the activation energy for EFBF was higher and decreased with the increase in POME sludge percentage, which is contradictory. This finding had been obtained by Mu et al. (2016) as well as Du et al. (2014) (Du *et al.*, 2014; Mu *et al.*, 2016). It was explained that the percentage of volatiles in the samples played a role in contributing to the activation energy, where with the increase in volatile percentage, activation energy increases. As observed in Figure 2, both TG and DTG curves showed that the devolatilization stage of EFBF is indeed much steeper than that of POME sludge, indicating the much higher volatile percentage in EFBF. This explains the higher values of activation energy for EFBF, despite the observed lower decomposition temperatures.

As compared to other stages, Stage 3 that mainly involves the devolatilization of lignin showed the highest activation energy. The activation energy obtained was 183.5 ± 18.5 kJ/mol. Decomposition of lignin required higher activation energy as compared to that of other components as lignin has a more complicated structure and higher molecular weight. Besides that, char that formed in Stage 2 might have contributed to the higher activation energy due to secondary cracking.

2.5 Concluding remarks

The utilization of lignocellulosic biomass as a renewable source of liquid fuel via pyrolysis has been gaining great attention. Studies have also recognized the challenges faced in the application of the bio-oil due to the high acidity and high amounts of oxygenated compounds. Co-pyrolysis and catalytic pyrolysis of biomasses were acknowledged as promising methods to enhance the qualities of the bio-oil and to widen the applications of the bio-oil. Besides, the esterification of the bio-oil also showed potential in lowering the amounts of acid in the bio-oil by converting them to esters. For hydrodeoxygenation (HDO), though promising results were obtained, the cost of utilizing pressurized hydrogen (H_2) as carrier gas is considerably higher than the other methods. Aside from that, literature showed that the metals used as catalysts for HDO would require support, which plays a significant role in the catalyst activity.

Calcium oxide (CaO), magnesium oxide (MgO), and zinc oxide (ZnO) are classic oxides that have showed potential in improving the qualities of bio-oils via catalytic pyrolysis. Even though the oxides have been employed repetitively for various lignocellulosic biomass, no specific trend were observed, owing to the difference in biomass compositions and thermal degradation behaviour.

In addition, based on the results from preliminary experiments on the kinetics and mechanisms of co-pyrolysis of EFBF and POME sludge, a positive synergic effect was observed. With regards to the results obtained from Coats-Redfern (CR) method, as the percentages of POME sludge increased in the blends, activation energy for the major weight loss stage decreased as well. This implied a catalytic effect of sludge in main degradation stage of EFBF, possibly owing

to the presence of oxides (e.g. CaO, MgO, and ZnO) in the sludge that posed catalytic effects on the pyrolysis of EFBF.

In Malaysia, even though the pyrolysis on EFB has been carried out previously, the studies focused mainly on the optimization of operating conditions for bio-oil production. Information on the effects of oxides on the physical properties and composition of the bio-oil were lacking. Hence, the current project aims to narrow down the research gap between EFB and oxides for bio-oil upgrading via catalytic intermediate pyrolysis. As bio-oil components are mainly from cellulose, the effects of the oxides on cellulose is important as well.

CHAPTER 3

3 MATERIALS AND METHODOLOGY

3.1 Introduction

This chapter presents the materials and methodology used in this study, describing the characterization of the feedstock and oxides used initially, followed by the methodology for kinetics and mechanisms studies. Then, a description on the methodology of catalytic intermediate pyrolysis is presented. Lastly, the characterization of the bio-oil produced was presented. The outline of the research is shown in Figure 5.

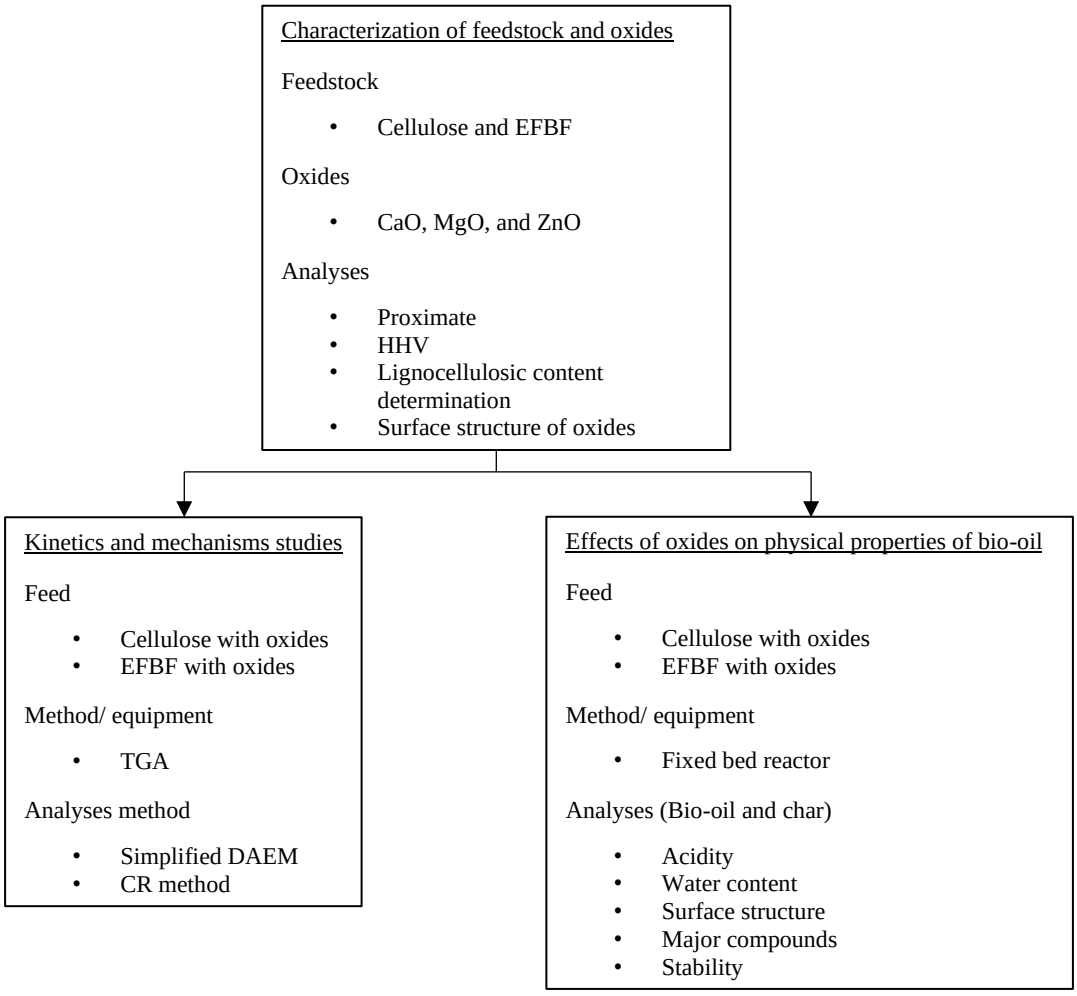

Figure 5: Outline of methodology used in the current project

3.2 Feedstock

The feedstocks used in this project were palm empty fruit bunch fibre (EFBF) and cellulose. EFBF was collected from Seri Ulu Langat Palm Oil Mill Sdn. Bhd, Dengkil, Selangor (Malaysia). Upon collection, the EFBF was pre-dried in the oven at 75 °C for 16 h and then grounded to less than 2 mm in particle size prior to analyses and experiments. Cellulose (CAS number 9004-34-6), in the form of microcrystalline powder with an average particle size of 50 µm, was purchased from Sigma–Aldrich (Kuala Lumpur, Malaysia).

3.3 Biomass characterization

Analyses were carried out to understand the characteristics and pyrolysis behaviour of the biomass. In general, the solid fuel combustion reactions are complex and thus, in order to effectively utilize biomass for fuel production, the characterization of the biomass is essential (Bushnell, 1989).

3.3.1 Proximate analysis

Proximate analysis gives the percentages of moisture, ash, volatile matter contents, and fixed carbon of the biomass.

3.3.1.1 Moisture content

The moisture content of the biomass can be explained as the quantity of water per unit mass of the solid. Initially, the biomass was placed in the oven for 16 h at 105 °C. The moisture content of the biomass was calculated as the biomass weight before and after drying. The maximum moisture content in the dried biomass should be 10 %, with a particle size of less than 2 – 3 mm to achieve high biomass heating rates (Bridgwater, 2012).

3.3.1.2 Ash content and analysis

Ash content is the incombustible solid matter in the fuel and was determined by placing 1 g of sample (dry basis) in the furnace at 600 °C for 4 h. The ash content of the sample was calculated from the weight difference before (dry basis) and after ashing, taking into consideration the weight difference of the crucible used as well.

3.3.1.3 Volatile content and fixed carbon

Volatile matter of biomass depends highly on the amount of cellulose and hemicellulose present in the biomass, where the higher the volatile matter, the higher the bio-oil yield (Chouhan and Sarma, 2013). Based on thermogravimetric analysis (TGA) results, the volatile matter percentages of samples were determined from the weight difference in the temperature range of 150 – 900 °C. The TGA programme used is presented later in Section 3.5.1

On the other hand, fixed carbon is that portion of fuel not pyrolyzed, and was calculated by subtracting the weight percentages of moisture content, volatile matter, and ash content from 100 %.

3.3.2 Higher heating value (HHV)

Higher heating value (HHV) is the quantity of heat released by a unit mass or volume of fuel (initially at 25 °C) upon complete combustion, and that the products cooled to a temperature 25 °C. HHV takes into consideration the latent heat of vaporization of water. In current study, the HHV of cellulose, EFBF, and POME sludge were determined using Parr 6100 bomb calorimeter.

3.3.3 Lignocellulosic content determination of EFBF

Lignocellulosic content and extractives amount of EFBF were determined with reference to the procedure described in literature (Lee *et al.*, 2017). Initially, 4 g of EFBF was refluxed with 250 mL of acetone using a Soxhlet extractor at 60 °C for 6 h. Then, the sample was dried in the oven at 105 °C for 16 h. The weight difference before and after treatment was taken as the amount of extractives in EFBF.

Next, 1 g of extractive-free EFBF was mixed with 150 mL of 0.5 mol/L sodium hydroxide (NaOH). The mixture was then placed in a water bath shaker (Protech, Malaysia) at 80 °C for 3.5 h, with shaking speed of 150 rev/min. Later, the contents were filtered through a filter paper and rinsed with distilled water until the filtrate reaches pH 7. After that, the sample was dried in the oven at 105 °C for 16 h. The weight difference before and after treatment was taken as amount of hemicellulose in EFBF.

Using a two-step acid hydrolysis process, the lignin content of EFBF was determined. Firstly, 3 mL of 14 mol/L sulphuric acid was added to 300 mg of extractive-free EFBF and then placed in a water bath shaker at 30 °C for 2 h, with shaking speed of 150 rev/min. Subsequently, the acid mixture was diluted with 84 mL of distilled water and autoclaved at 121 °C, 2 bar for 1 h. Upon cooling, the contents were filtered through a filter paper and rinsed with distilled water until the filtrate reaches pH 7. Then, the sample was dried in the oven at 105 °C for 16 h. The weight difference before and after treatment was taken as weight of lignin in EFBF.

Based on the assumption that extractive-free EFBF consists of only cellulose, hemicellulose, and lignin, cellulose content of EFBF was calculated by subtracting weight percentages of hemicellulose and lignin from 100 wt.%. All analyses were triplicated.

3.4 Oxides characterization and treatment

Calcium oxide (CaO), magnesium oxide (MgO), and zinc oxide (ZnO) used in this project were obtained from R&M Chemicals (M) Sdn. Bhd. (Kuala Lumpur, Malaysia) and calcined in a chamber furnace (Carbolite ELF 11/68, UK) for 5 h at 600 °C to remove volatile impurities and kept in a desiccator. Nitrogen (N_2) adsorption was carried out using an accelerated surface area porosimeter (ASAP) that was equipped with degassing ports (Micromeritics ASAP 2020, USA). The catalyst samples were degassed at 300 °C for 4 h and the N_2 isotherms were measured at 77 K with the relative pressure (P/P_0) ranging up to 0.99. Based on the N_2 adsorption-desorption data, the specific surface areas of the catalysts were determined by Brunauer-Emmett-Teller (BET) method whereas the pore volumes were determined by the Barrett-Joyner-Halenda (BJH) method.

3.5 Kinetics and mechanism studies (Objective 1)

Prior to the production of bio-oil in fixed bed reactors, the pyrolytic behaviour of the feedstocks in the presence of POME sludge and oxides were studied using thermogravimetric analysis (TGA). The kinetics and mechanisms of the samples involved during pyrolysis can be determined from thermogravimetric (TG) and derivative of thermogravimetric (DTG) data.

3.5.1 Thermogravimetric analysis (TGA)

TGA was carried out in programmable TGA DSC 1 Mettler Toledo (M) Sdn. Bhd. (Malaysia) to examine the decomposition behaviour of biomass upon pyrolysis. In each experimental run, approximately 10 mg of sample was subjected to heating from room temperature to 900 °C, and then held at that temperature for 10 min. The heating rate was varied at 10, 20, 30, and 40 °C/min and the N_2 purge was fixed at 20 mL/min to prevent loss of volatiles and to stimulate pyrolysis conditions. All experiments were duplicated.

Initially, the oxides (CaO, MgO, and ZnO) were subjected to TGA as a blank test to exclude the behaviour change in the catalysts during experiments, if any. Then, TGA was carried out to study the pyrolytic behaviour of both cellulose and EFBF, with and without the presence of the oxides. The oxides were added to both feedstock at various weight percentages of 0, 5, and 10 wt%.

3.5.2 Kinetic methods

Having known the kinetic triplets (apparent reaction activation energy (E), apparent frequency factor (A), and kinetic model, $f(\alpha)$), the degradation behaviour of the blends, kinetics, and their mechanisms may be further understood, which may assist in the design, optimization, and scaling up of the operation (Mu *et al.*, 2016).

The methods used to predict the kinetic parameters and mechanisms were simplified distributed activation energy model (DAEM), and Coat-Redfern (CR) method. These two methods are commonly used to formulate the kinetics and mechanisms by utilizing the data obtained from TGA.

DAEM has been comprehensively reviewed by Cai et al. (2014). Simplification of DAEM was carried out to facilitate the prediction of devolatilization curves and to obtain the kinetic triplets in a more straightforward manner. One of the commonly used simplified DAEM was proposed by Miura and Maki (1998), where the reactions were assumed to be first-order reactions (Miura and Maki, 1998). On the other hand, CR method is an integral method that requires an assumption to be made regarding the value of the reaction order for $f(\alpha)$ (Coats and Redfern, 1964; White, Catallo and Legendre, 2011).

3.5.2.1 Simplified distributed activation energy model (DAEM)

The brief derivation of simplified DAEM is presented in the current section whereas the detailed derivation can be obtained elsewhere (Miura and Maki, 1998).

Based on the DAEM model, the total conversion degree of biomass to volatiles over time for non-isothermal processes may be expressed as:

$$1 - \frac{V}{V^*} = \int_0^\infty exp\left[-A\int_0^t \exp\left(-\frac{E}{RT}\right)dt\right].f(E).dE \qquad (1)$$

where A is the frequency factor $(1/s)$ and is assumed to be the same for all reactions. E is the activation energy (kJ/mol); R is the gas constant of 8.314 J/mol K; T is the absolute temperature (K); $f(E)$ is the normalized distribution curve of the activation energy.

Upon a series of approximation and simplification by Miura and Maki (1998), Eqn. (2) is obtained:

$$ln\frac{\beta}{T^2} = \ln\left(\frac{AR}{E}\right) - 0.6075 - \frac{E}{R}\left(\frac{1}{T}\right) \qquad (2)$$

where β is the heating rate (K/min).

By plotting of $ln\frac{\beta}{T^2}$ against $\frac{1}{T}$ at a certain conversion degree, E and A values may be calculated as follows:

$$E = -m.R \tag{3}$$

$$A = -m.\exp(c - 0.6075) \tag{4}$$

where, m is the slope and c is the intercept.

3.5.2.2 Coats-Redfern (CR) method

The detailed mathematical background of the CR method may be obtained elsewhere whereas the current section presents a simplified version (Vlaev *et al.*, 2008).

In non-isothermal experiments, the rate of solid degradation may be written as:

$$\frac{d\alpha}{dt} = kf(\alpha) \tag{5}$$

where k is the temperature-dependant rate constant and $f(\alpha)$ is a function of conversion that varies according to the reaction model.

By expressing k as Arrhenius equation and considering constant heating rate of $\beta = \frac{dT}{dt}$, the following equation is obtained:

$$\frac{d\alpha}{dT} = \frac{A}{\beta}\exp\left(-\frac{E}{RT}\right).f(\alpha) \tag{6}$$

Upon integration, the logarithmic expression of Eqn. (12) may be written as

$$\ln\left[\frac{g(\alpha)}{T^2}\right] = \ln\left[\frac{AR}{\beta E}\left(1 - \frac{2RT}{E}\right)\right] - \frac{E}{RT} \tag{7}$$

where $g(\alpha)$ is the integrated form of the conversion dependence function $f(\alpha)$. As the value of $\frac{2RT}{E}$ was far less than one, the term was omitted and Eqn. (8) is obtained.

$$\ln\left[\frac{g(\alpha)}{T^2}\right] = \ln(\frac{AR}{\beta E}) - \frac{E}{RT} \quad (8)$$

where, $\ln(\frac{AR}{\beta E})$ is essentially a constant value.

A straight line should be obtained from the plotting of $\ln\left[\frac{g(\alpha)}{T^2}\right]$ against $\frac{1}{T}$ as they have a linear relationship. If the correct $g(\alpha)$ is used, the straight line should have a high correlation coefficient of linear regression analysis. Then, the values of E and A can be derived from the slope $-\frac{E}{R}$ and the intercept $\ln(\frac{AR}{\beta E})$, respectively.

By identifying $g(\alpha)$ that gives the highest correlation coefficient, the pyrolysis reaction of the samples may be associated with the appropriate mechanisms. $f(\alpha)$ that were used in this kinetic study of solid-state reactions include chemical processes or mechanisms, phase boundary reactions, and diffusion mechanisms (Vlaev *et al.*, 2008; Gil *et al.*, 2010). The employed f(α) are shown in Table 9.

Table 9: Expressions of functions $g(\alpha)$ and their corresponding mechanisms (Adapted from Vlaev et al. 2008; Gil et al. 2010))

No.	Symbol	Name of function	$f(\alpha)$	$g(\alpha)$	Rate-determining mechanism
Chemical process or mechanism non-invoking equations					
1.1	$F_{1/3}$	One-third order	$(3/2)(1-\alpha)^{1/3}$	$1-(1-\alpha)^{2/3}$	Chemical reaction
1.2	$F_{3/4}$	Three-quarters order	$4(1-\alpha)^{3/4}$	$1-(1-\alpha)^{1/4}$	Chemical reaction
1.3	F_1	First order	$1-\alpha$	$-\ln(1-\alpha)$	Chemical reaction
1.4	$F_{3/2}$	One and a half order	$2(1-\alpha)^{3/2}$	$(1-\alpha)^{-1/2}-1$	Chemical reaction
1.5	F_2	Second order	$2(1-\alpha)^2$	$(1-\alpha)^{-1}-1$	Chemical reaction
1.6	F_3	Third order	$(1/2)(1-\alpha)^3$	$(1-\alpha)^{-2}-1$	Chemical reaction
Phase boundary reaction					
2.1	R_1, F_0, P_1	Power law	$(1-\alpha)^0$	α	Contracting disk
2.2	$R_2, F_{1/2}$	Power law	$2(1-\alpha)^{1/2}$	$1-(1-\alpha)^{1/2}$	Contracting cylinder
2.3	$R_3, F_{2/3}$	Power law	$3(1-\alpha)^{2/3}$	$1-(1-\alpha)^{1/3}$	Contracting sphere
Based on the diffusion mechanism					
3.1	D_1	Parabola low	$1/2\alpha$	α^2	One-dimensional diffusion
3.2	D_2	Valensi equation	$[-\ln(1-\alpha)]^{-1}$	$\alpha+(1-\alpha)\ln(1-\alpha)$	Two-dimensional diffusion

Table 9: Expressions of functions $g(\alpha)$ and their corresponding mechanisms (Adapted from Vlaev et al. 2008; Gil et al. 2010)) continue

3.3	D_3	Jander equation	$(3/2)(1-\alpha)^{2/3}[1-(1-\alpha)^{1/3}]^{-1}$	$[1-(1-\alpha)^{1/3}]^2$	Three-dimensional diffusion, spherical symmetry
3.4	D_4	Ginstling-Brounstein equation	$(3/2)[(1-\alpha)^{-1/3}-1$	$1-2\alpha/3-(1-\alpha)^{2/3}$	Three-dimensional diffusion, cylindrical symmetry
3.5	D_5	Zhuravlev, Lasokin, Tempelman equation	$(3/2)(1-\alpha)^{4/3}[(1-$	$[(1-\alpha)^{-1/3}-1]^2$	Three-dimensional diffusion
3.6	D_6	anti-Jander equation	$(3/2)(1+\alpha)^{2/3}[(1$	$[(1+\alpha)^{1/3}-1]^2$	Three-dimensional diffusion
3.7	D_7	anti-Ginstling-Brounstein equation	$(3/2)[(1+\alpha)^{-1/3}-$	$1+2\alpha/3-(1+\alpha)^{2/3}$	Three-dimensional diffusion
3.8	D_8	anti-Zhuravlev, Lasokin, Tempelman equation	$(3/2)(1+\alpha)^{4/3}[(1$	$[(1+\alpha)^{-1/3}-1]^2$	Three-dimensional diffusion

3.6 Production of bio-oil via pyrolysis in fixed bed reactor (Objective 2)

The fixed-bed pyrolysis experiments were conducted in a horizontally tubular stainless-steel reactor (28.4 mm O.D. and 600 mm length), that was heated in a

split-able mini tube furnace (BSO-1200 G, Malaysia). The experimental setup is presented in Figure 6.

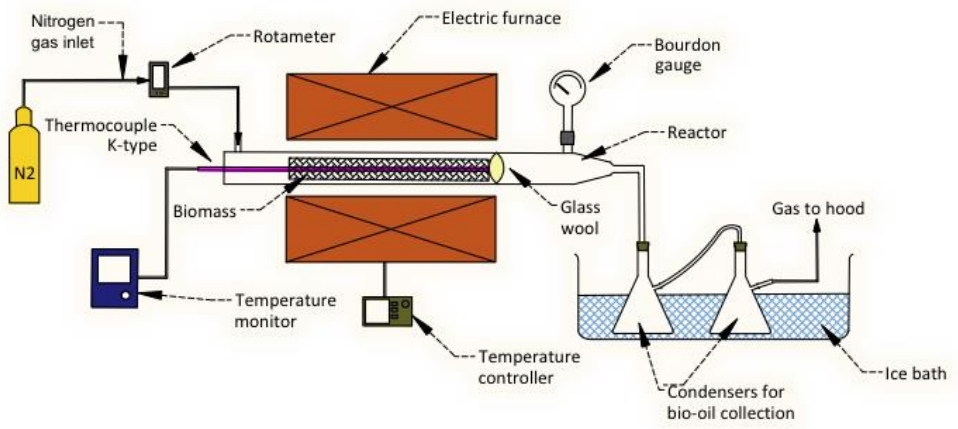

Figure 6: Experimental setup for pyrolysis experiments

For all the experiments, approximately 15 g of samples were loaded into the reactor. Glass wool was inserted at the effluent end of the reactor to prevent the solid particles from being entrained in the vapours. To create an inert atmosphere in the reactor, nitrogen (N_2) gas was purged at 20 – 40 mL/min through the bed. With reference to literature, the optimum pyrolysis temperature of EFBF was suggested to be 500 °C (Sukiran *et al.*, 2009; Sembiring, Rinaldi and Simanungkalit, 2015). To achieve a temperature of 500 ± 20 °C, the reactor was inserted into the furnace once it reaches 575 °C (for sufficient heat transfer). During the experiments, temperature in the reactor was measured using a K-type thermocouple. Two glass condensers were placed in an ice bath in series for bio-oil collection. The resulting bio-oil product was weighed to calculate the yield based on the amount of cellulose used whereas the char yield was obtained by calculating the difference between the weight of the solid residue and the amount of catalysts added. Next, the gas yield was determined from the

percentage weight difference. Each pyrolysis experiment was triplicated to ensure reproducibility of result. All the data presented were average values with standard deviation of < ±5 %.

3.6.1 Catalytic pyrolysis of cellulose and EFBF

In the catalytic pyrolysis of cellulose and EFBF, the three oxides (CaO, MgO, and ZnO) were used in both 5 wt.% and 10 wt.%. The pyrolysis of both cellulose and EFBF were carried out initially without any catalysts as control. For cellulose, the heating rate reached inside the reactor was 20.5 ± 2.9 °C/min and white fumes were observed within 6 – 7 min of reactor insertion when the reactor reached approximately 300 °C. Similarly, in the catalytic pyrolysis of EFBF, the heating rate inside the reactor was recorded to be 25.8 ± 4.7 °C/min. Within 4–5 min of reactor insertion, white fumes were observed when the reactor was at a temperature of approximately 300 °C. For both experiments, intermediate pyrolysis was achieved.

3.6.2 Bio-oil characterization

3.6.2.1 pH and total acid number (TAN)

The pH of bio-oil samples were measured using a digital pH meter (Eutech Instruments pH 700, Singapore), which was calibrated with buffer solutions of pH 4 and 7. Current study adopted a method proposed by Shao & Agblevor was adjusted and employed for total acid number (TAN) determination (Shao and Agblevor, 2015). This is a simple method and gives results that are in good agreement with those obtained by ASTM method. Aqueous potassium hydroxide (0.001 M KOH) was used as a standard titrant and acetone (50 mL) was used as titration solvent with 0.1 g of bio-oil sample. Each sample was

titrated in triplicate. While pH measurements represent only the concentration of hydrogen ions, TAN can quantify the acidic components in bio-oil samples.

3.6.2.2 Water content

Measurements of water content in bio-oil samples were conducted with a volumetric Karl-Fisher titrator (Mettler Toledo V20, Canada). Approximately 7 mg of sample was injected into the titration solvent (Combisolvent Keto) and titrated against the titration reagent (Combisolvent 5 Keto). By calculating the water equivalence of titration reagent (5 mg of H_2O/mL of titration reagent), the water content of the bio-oil was obtained.

3.6.2.3 Fourier transform infrared spectrum (FTIR)

FTIR (Perkin Elmer Frontier, USA) were used to analyse all the bio-oil and solid samples. The FTIR spectra were recorded within a wavenumber range of 400 – 4000 cm^{-1}, with 16 scans at resolution of 8 cm^{-1}.

3.6.2.4 Gas chromatography-mass spectrometry instrument (GC-MS)

0.75 g of bio-oil samples were diluted in 50 mL of methanol, where 3 mL of each sample was withdrawn and filtered (syringe filter, Agilent PTFE 0.45 µm) into Agilent vials. GC-MS (Perkin Elmer 680 GC/ SQ8S MS, USA) was used to analyse the volatile matters in the bio-oil. GC conditions: chromatographic column: DB1075 column; column temperature: 40 °C (initial) for 2 min and 250 °C (final) for 8 min with ramping rate of 10 °C /min; injector temperature: 280 °C; split of 50:1; volume injected: 1 µL; carrier gas: helium (1.35 mL/min). MS conditions: scan range: 50 – 550 Da; solvent delay: 2 min; threshold: 100; source temperature 250 °C; transfer temperature: 250 °C. The compounds were

identified by comparing mass spectra with National Institute of Standards and Technology (NIST) mass spectra library.

3.6.2.5 Statistical analysis

Experimental data that was obtained for product yield, water content, and TAN were statistically analysed using the one-way analysis of variance (ANOVA) technique, generated from MATLAB (Version R2013a). The probability values (p-values) were determined at a confidence interval of 95 %. If the p-value is less than or equals to 0.05, the null hypothesis would be rejected; having a p-value that is more than 0.05 shows that the sample means are all equal, and the null hypothesis would not be rejected.

3.6.2.6 Stability tests (Section 2)

Bio-oil produced by pyrolysis in the presence of CaO was taken for stability testing, which is based on the properties of bio-oils produced by the catalytic pyrolysis of EFBF. The weight percentages of the catalyst used in the production of bio-oil for stability testing were 0, 10, and 20 wt%. Thermal stability testing of bio-oils was carried out with reference to the method proposed by Anja (2013) (Anja, 2013). 5 mL of bio-oil samples were "aged" by being sealed and held for 16 h and 24 h at 80 °C using a water bath. The change in viscosity of raw and aged bio-oil was used to demonstrate the stability of the bio-oil, where a smaller change would indicate that the bio-oil has greater thermal stability during long-term storage (Rajamohan and Kasimani, 2018).

The viscosity of the bio-oil samples was measured using capillary viscometer (PM Tamson Instruments, Thailand; size: 75) at a fixed temperature of 25 °C whereas the solid content of the liquid samples was determined as ethanol

insoluble particulates. In addition to that, aged bio-oils were also subjected to TAN, water content, and FTIR analyses in similar manners as presented in Sections 3.6.2.1, 3.6.2.2, and 3.6.2.3, respectively.

3.7 Concluding remarks

This chapter presented the characterization of feedstocks, methodology, and equipment used in the current project to achieve to objectives presented in Chapter 1. Firstly, the feedstocks and oxides used were characterized. Then, methodology for experiments were explained and the results are presented and discussed in following chapters (Chapters 4 and 5). In general, the kinetics and mechanisms involved in the catalytic pyrolysis of cellulose and EFBF were investigated. Following that, the change in physical properties such as acidity, water content, surface structure, and major compounds of the bio-oils, before and after the experiments were studied using the methodology presented. Consequently, an insight on the upgradability of the bio-oils was gained.

CHAPTER 4

4 KINETICS AND MECHANISMS FOR CATALYTIC PYROLYSIS OF EMPTY FRUIT BUNCH FIBRE (EFBF)

4.1 Introduction

This chapter presents the study on kinetics and mechanisms involved in the upgrading of bio-oil. Both cellulose and empty fruit bunch fibre (EFBF) were used as feed and the catalytic additives employed were calcium oxide (CaO), magnesium oxide (MgO), and zinc oxide (ZnO) were used as catalytic additives. The kinetics and mechanisms were obtained by utilizing the simplified distributed activation energy model (DAEM) method and Coats-Redfern (CR) method.

4.2 Biomass characterization

Based on the characterization results presented in Table 10, both cellulose and hemicellulose content in EFBF were similar. As cellulose is generally the most abundant compound in lignocellulosic biomass, cellulose was opted as the model compound in current study.

For proximate analysis, as compared to cellulose, EFBF exhibited lower volatile matter, higher ash content, and higher fixed carbon due to the presence of hemicellulose and lignin. As for the ultimate analysis and HHV, the results of both cellulose and EFBF were comparable, except for nitrogen (N) content.

Table 10: Proximate and ultimate analysis and HHV of feedstock

	Cellulose	EFBF
Proximate analysis		
Moisture content (wt.%)	3.9 ± 0.2	9.3 ± 0.2
Volatile matter (wt.%)	88.7 ± 0.5	73.7 ± 1.0
Ash content (wt.%)	< 0.1	3.2 ± 0.4
Fixed carbon (wt.%)	9.7 ± 1.6	13.4 ± 1.2
HHV (MJ/kg)	17.3 ± 0.0	18.2 ± 0.0
Ultimate analysis		
C (wt.%)	41.2	43.3
H (wt.%)	6.7	6.1
N (wt.%)	0.1	0.6
O* (wt.%)	52.0	50.0
Lignocellulosic content		
Cellulose*	-	37.1 ± 3.5
Hemicellulose	-	37.3 ± 2.5
Lignin	-	25.6 ± 2.8
Extractives	-	18.8 ± 1.4

*from difference

4.3 Thermogravimetric analysis (TGA)

4.3.1 Metal oxides

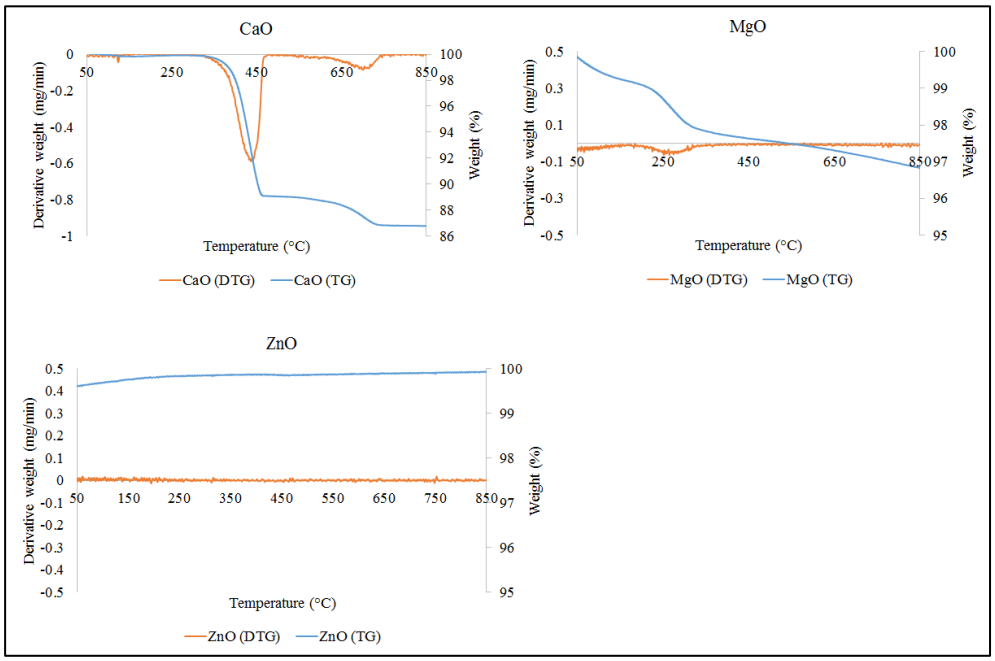

Figure 7: TG and DTG curves of (a) CaO, (b) MgO, and (c) ZnO used in current work at heating rate of 20 °C/min

Figure 7 presents the behaviour of the oxides (CaO, MgO, and ZnO) used in the current study when subjected to TGA with heating rate of 20 °C/min. The aim of the analysis was to differentiate the changes in behaviour of oxides and biomasses upon TGA. CaO showed two weight loss stages at 440 °C (10 % weight loss) and 700 °C (3 % weight loss), respectively. Wang et al. (2010), While the weight loss at 440 °C may be accredited to the decomposition of calcium hydroxide ($Ca(OH)_2$), the second weight loss stage may be attributed to decomposition of calcium carbonate ($CaCO_3$), which occurs at 700 °C (Wang *et al.*, 2010; Kwon *et al.*, 2018). $Ca(OH)_2$ is formed from the reaction of CaO with the moisture in the air prior to experiments whereas $CaCO_3$ is possibly

formed from the reaction of CaO before the experiment with carbon dioxide (CO_2) in air.

As for MgO, a weight loss stage (2 % weight loss) may be observed in the range of 190 °C to 350 °C. MgO is known to be a hygroscopic material and would adsorb moisture from air, forming magnesium hydroxide ($Mg(OH)_2$). The $Mg(OH)_2$ formed would then decompose in the temperature range of 200 °C to 450 °C (Aphane, 2009).

On the other hand, ZnO was stable throughout the analysis.

4.3.1.1 Cellulose and empty fruit bunch fibre (EFBF)

Figure 8 displays the TG and DTG curves for the thermal degradation of cellulose and EFBF at various heating rates (10, 20, 30, and 40 °C /min) at fixed N_2 flow of 20 mL/min. As the heating rates increased, the degradation behaviour of the biomasses remained almost the same whereas the degradation temperature increased. The delay in degradation of biomasses at higher heating rates was because of heat transfer limitations. At lower heating rates, the heating of biomass particles occurs more gradually and therefore, led to a more effective heat transfer within the particles. On the other hand, with the increase in heating rates, the mass loss rate of both biomasses increased. This is because at higher heating rates, biomass particles may have experienced stronger thermal shock and hence, exhibited higher activity (El-Sayed and Khairy, 2015).

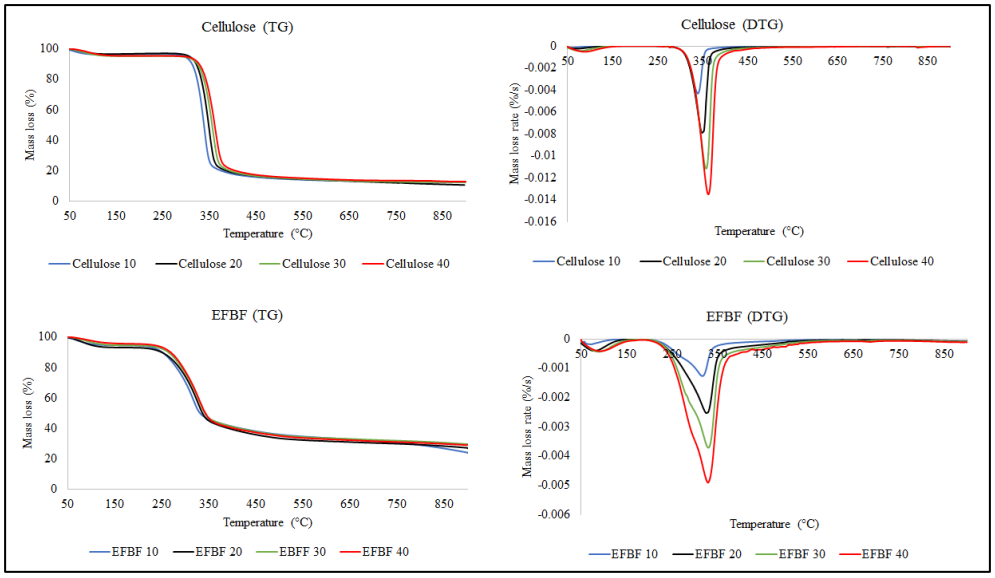

Figure 8: TG and DTG curves of cellulose and EFBF without oxides at various heating rates (10, 20, 30, and 40 °C/min) and fixed N_2 flow of 20 mL/min

For heating rate of 20 °C /min, the degradation of both cellulose and EFBF may be distinguished into three stages: (1) evaporation of moisture (50 – 160 °C); (2) devolatilization (160 – 420 °C); and (3) further decomposition of biomass to form gaseous products and residual char (and lignin for EFBF, above 420 °C). The first degradation stage may be attributed to the dehydration of biomass, which involved the drying of free and bound moistures on the raw material (Chen, Li and Zhu, 2012). Stage 2 of biomass degradation showed the most significant weight loss, where the weight loss rate for cellulose and EFBF was maximum at approximately 350 and 325 °C, respectively. At temperatures above 300 °C, glycosidic bonds in cellulose become very reactive and upon rupturing, depolymerization of cellulose occurs. In addition, volatilization is a endothermic reaction and at this stage, most of the released volatiles are condensable organic compounds (Yang *et al.*, 2007; Collard and Blin, 2014). Additionally, for EFBF, hemicellulose would devolatilize at this stage as well as cellulose. In order to justify this statement using TGA results, the weight loss

of EFBF in Stage 2 was recalculated by excluding the moisture (6.8 wt.%) and extractives content (18.8 wt.%) in EFBF. The recalculated weight loss from TGA results is 72.3 wt.%, which is close to the sum of cellulose and hemicellulose shown in Table 10 (74.4 wt.%). Subsequently, Stage 3 is an exothermic reaction, accredited to secondary cracking of char formed in the first two stages (Kilzer and Broido, 1965; Wang *et al.*, 2007). For EFBF, decomposition of lignin and other stronger chemical bonds occurred at this stage as well.

The pyrolytic behaviours of cellulose and EFBF were also studied under various heating rates (10, 20, 30, and 40 °C /min) with the addition of 5 wt.% and 10 wt.% of oxides. The sample labelled as "CCaO 5%" refers to cellulose with addition of 5 wt.% CaO, "CCaO 10 %" to cellulose with addition of 10 wt.% CaO, "ECaO 5%" refers to EFBF with 5 wt.% CaO added, "ECaO 10%" to that with 10 wt.% CaO added, and so on for the other samples.

The addition of MgO and ZnO did not alter the behaviour of both cellulose and EFBF degradation substantially and their respective curves at different heating rates are presented in Appendix 1 (Figure A.24 and Figure A.25). Alternatively, the weight losses experienced at each of the distinctive stages when heating rate was set to 20 °C/min are presented in Table 11.

Table 11: Weight loss of cellulose, with and without oxides at divided stages and the residual weight at the end of 850 °C at heating rate of 20 °C/min

Samples	Weight loss (wt.%)				Residual weight (wt.%)	Maximum weight loss rate (wt%/s)
	Stage 1	Stage 2	Stage 3	Stage 4		
Cellulose	3.3 ± 0.7	79.2 ± 0.2	5.2 ± 0.3	-	13.8 ± 1.1	0.0079 ± 0.0
CCaO 5%	2.8 ± 0.8	78.1 ± 2.4	5.8 ± 0.0	1.6 ± 0.0	13.2 ± 3.1	0.0078 ± 0.0
CCaO 10%	3.0 ± 0.2	78.1 ± 0.8	6.4 ± 0.3	1.8 ± 0.0	12.2 ± 1.3	0.0078 ± 0.0
CMgO 5%	2.8 ± 0.6	80.0 ± 1.4	3.9 ± 0.2	-	15.2 ± 0.8	0.0081 ± 0.0
CMgO 10%	2.5 ± 0.4	80.1 ± 4.6	3.6 ± 0.3	-	15.7 ± 4.2	0.0080 ± 0.0
CZnO 5%	2.7 ± 0.6	79.9 ± 2.1	4.2 ± 0.4	-	14.9 ± 1.7	0.0076 ± 0.0
CZnO 10%	3.5 ± 0.2	80.1 ± 2.0	4.3 ± 0.4	-	14.0 ± 2.1	0.0074 ± 0.0
EFBF	6.9 ± 0.1	53.8 ± 2.1	9.5 ± 0.3	-	30.2 ± 0.9	0.0024 ± 0.0
ECaO 5%	6.7 ± 0.2	41.2 ± 0.4	9.5 ± 1.0	8.6 ± 0.3	33.0 ± 0.1	0.0020 ± 0.0
ECaO 10%	5.4 ± 0.1	34.3 ± 2.5	10.8 ± 0.7	10.6 ± 1.7	37.2 ± 2.2	0.0015 ± 0.0
EMgO 5%	7.2 ± 0.6	46.5 ± 0.7	12.1 ± 1.6	-	33.8 ± 0.9	0.0018 ± 0.0
EMgO 10%	7.0 ± 1.1	46.1 ± 2.1	11.5 ± 2.0	-	33.3 ± 1.3	0.0018 ± 0.0
EZnO 5%	7.1 ± 0.8	48.7 ± 2.9	11.7 ± 0.3	-	33.2 ± 2.0	0.0020 ± 0.0
EZnO 10%	6.2 ± 0.7	47.6 ± 1.8	12.3 ± 2.3	-	34.1 ± 4.9	0.0015 ± 0.0

"-" not applicable

When compared to the weight loss of cellulose only, it may be interpreted as the addition of MgO and ZnO did not substantially affected the releasing of volatiles (Stages 1 and 2). Nevertheless, a slight decrement in maximum weight loss rate upon the incorporation of ZnO was observed, suggesting that ZnO decreased the activity of cellulose in thermal decomposition. For EFBF, both the amounts of volatiles and maximum weight loss rate decreased notably (difference of > 5 wt.%) when MgO and ZnO were added. Such observation indicates that both MgO and ZnO might have restrained the releasing of volatiles in EFBF due to the presence of other biomass components (e.g. hemicellulose and lignin) and impurities (e.g. dirt) instead of purely cellulose, whereby possible interaction might have occurred between the biomass components. Besides that, this may be contributed by the formation of coke on the oxides, which would block the diffusion pathways of volatiles (Balasundram *et al.*, 2018). Upon the addition of MgO and ZnO in cellulose and EFBF, the residual weight of both biomasses increased overall. This suggests that these oxides would increase the char yield during pyrolysis, possibly due to coke formation.

The incorporation of CaO showed visible change in the pyrolytic behaviour of both cellulose and EFBF, where two additional peaks were obtained. Since the addition of 5 wt.% CaO and 10 wt.% CaO showed similar TG and DTG curves, the former are presented in Appendix 1 (Figure A.24 and Figure A.25) whereas the latter are presented in Figure 9 in comparison with those of cellulose and EFBF only.

For both biomasses, an addition stage was noticed when CaO was added: Stage 1 (50 – 160 ˚C), 2 (160 – 380 ˚C), 3 (380 – 580 ˚C), and 4 (above 580 °C). The

stages may be accredited to moisture loss, devolatilization, decomposition of $Ca(OH)_2$, and secondary reactions together with decomposition of $CaCO_3$, respectively. For EFBF, lignin degrades in Stage 4 as well.

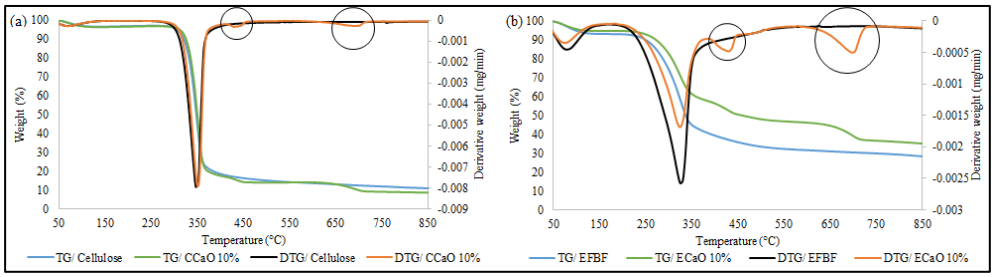

Figure 9: Comparison of TG and DTG curves between (a) cellulose and (b) EFBF, with and without 10 wt.% of CaO at heating rate of 20 °C/min

The formation and dissociation of $Ca(OH)_2$ and $CaCO_3$ have been explained earlier in Section 4.3.1. For the degradation of $CaCO_3$, a higher weight loss was observed for EFBF as compared to that of cellulose, indicating that $CaCO_3$ were formed not only prior to TGA but also during the degradation of EFBF with CaO. Upon pyrolysis of biomass, CO_2 is one of the main gas products and is mainly formed from the cracking and reforming of carboxyl groups at relatively low temperatures (Fu *et al.*, 2011). So, more $CaCO_3$ would be formed during pyrolysis of EFBF as compared to that of cellulose.

Besides, with reference to Table 11, the addition of CaO decreased the weight loss at Stage 2 and the maximum weight loss rate of volatiles for both cellulose and EFBF. This denotes that CaO caused a reduction in the releasing of volatiles from cellulose and more significantly in EFBF. Such observation was made when MgO and ZnO was employed as well.

4.4 Kinetics of catalytic pyrolysis by simplified distributed activation energy model (DAEM)

Simplified distributed activation energy model (DAEM) was used for determining the kinetics of cellulose and EFBF, with and without the presence of the oxides. Simplified DAEM assumes that complex reactions like the pyrolysis of biomass, as an infinite number of irreversible first-order parallel reactions occurring simultaneously, with their distinct rate parameters (Miura and Maki, 1998).

The ln $(\frac{\beta}{T^2})$ against $\frac{1000}{T}$ graphs that were used to determine the activation energy (E) and frequency factor (A) of the samples are presented in Appendix 2 (Figure A.26 and Figure A.27). The correlation coefficients of the plots were high with a minimum value of 0.97 for cellulose and an average of 0.95 for EFBF.

The activation energies (E_α) of cellulose, with and without oxides, against the degree of conversion (α) are presented in Figure 10 whereas the average values of E and range of A are presented in Table 12. The average E obtained is of 201.03 kJ/mol, for α in the range of 0.2 – 0.8, which corresponds to the temperature range of 320 – 380 °C. In this temperature range, cellulose was devolatilized and achieved maximum weight loss rate.

The E_α of cellulose decreased from α = 0.2 to 0.6, and hereafter slightly increased. The decrement and increment of E_α may be accredited to the competitive pathways in cellulose pyrolysis (Cooley and Antal, 1988; Rantuch and Balog, 2014).

The employment of the MgO and ZnO did not alter the trend of E_α with regards to α but did lower the average values of activation energy (E_{avg}). This suggests that the oxides elevated the reaction rate of cellulose. On the other hand, though the addition of CaO did lower E_{avg} slightly, E increased from α of 0.2 and 0.8. This may be attributed to the decomposition of $Ca(OH)_2$ and $CaCO_3$, where the formation of the compounds have been explained in Sections 4.3.1.

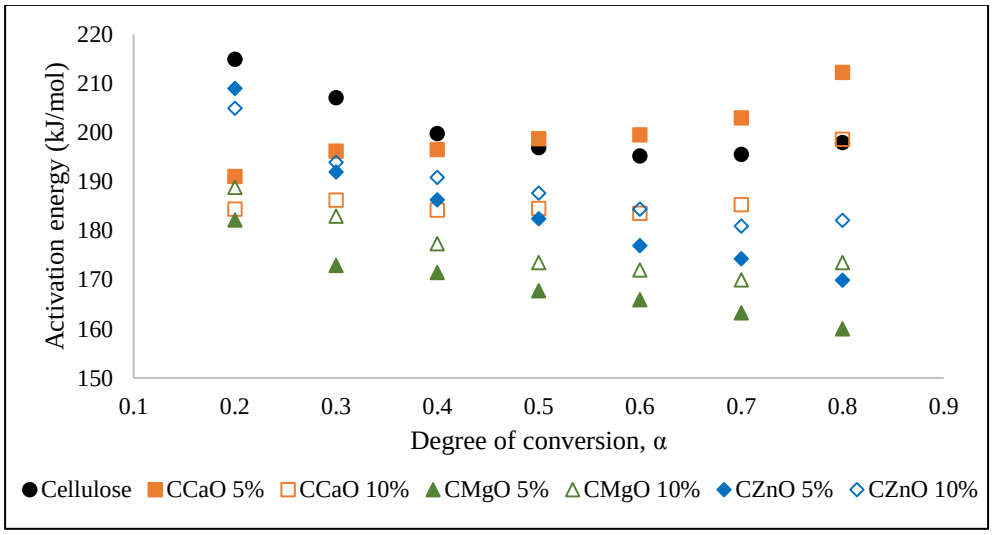

Figure 10: Activation energies of cellulose, with and without catalysts against degree of conversion using simplified DAEM

Based on Table 12, the E_{avg} obtained in the current study was 274.5 kJ/mol whereas the change in E_α with respect to α is showed in Figure 11 for EFBF. The E_α of EFBF increased gradually from conversion 0.2 to a maximum at 0.5, where the E_α was 295.04 kJ/mol and later decreased. Hence, the conversion degree of 0.2 – 0.6 and > 0.6 may be assigned to active pyrolysis and passive pyrolysis stages of the thermal decomposition of EFBF, respectively based on the weight loss rate (Nyakuma *et al.*, 2016).

Table 12: Kinetic parameters of cellulose and EFBF, with and without oxides using DAEM

Samples	Average activation energy, E (kJ/mol)	Range of frequency factor, (1/s)
Cellulose	201.0	$1.2 \times 10^{16} – 2.8 \times 10^{18}$
CCaO 5%	199.6	$1.7 \times 10^{16} – 2.2 \times 10^{17}$
CCaO 10%	190.3	$3.1 \times 10^{15} – 4.1 \times 10^{16}$
CMgO 5%	174.5	$3.1 \times 10^{13} – 3.8 \times 10^{15}$
CMgO10%	170.4	$2.1 \times 10^{13} – 1.1 \times 10^{15}$
CZnO 5%	188.4	$9.6 \times 10^{14} – 1.7 \times 10^{17}$
CZnO 10%	186.4	$2.1 \times 10^{14} – 5.7 \times 10^{17}$
EFBF	274.5	$1.9 \times 10^{20} – 6.8 \times 10^{26}$
ECaO 5%	256.6	$2.2 \times 10^{19} – 1.2 \times 10^{31}$
ECaO 10 %	263.4	$4.8 \times 10^{21} – 3.1 \times 10^{29}$
EMgO 5%	207.2	$1.4 \times 10^{12} – 2.4 \times 10^{27}$
EMgO 10%	194.8	$4.0 \times 10^{13} – 4.9 \times 10^{18}$
EZnO 5%	223.8	$5.7 \times 10^{10} – 1.6 \times 10^{26}$
EZnO 10%	206.0	$1.3 \times 10^{14} – 1.2 \times 10^{20}$

The change of E_α with regards to α altered slightly when the oxides were employed. When MgO and ZnO were added, the activation energy reached a maximum when α is 0.7 and 0.6, respectively instead of 0.5; when CaO was added, the activation energy increased from conversion 0.2 to 0.8. Since conversions above 0.6 may be regarded as the passive pyrolysis stage and is the stage where lignin, char, and heavier compounds decompose, the continuous increment in activation energies may be contributed by the formation of coke

on the oxides, as discussed in Section 4.3.1.1. Hence, higher activation energies would be required for higher conversions. Furthermore, the effects of CaO on the increment in activation energy may have been contributed by the decomposition of $Ca(OH)_2$ and $CaCO_3$ as well. The formation of the compounds has been explained in Section 4.3.1.

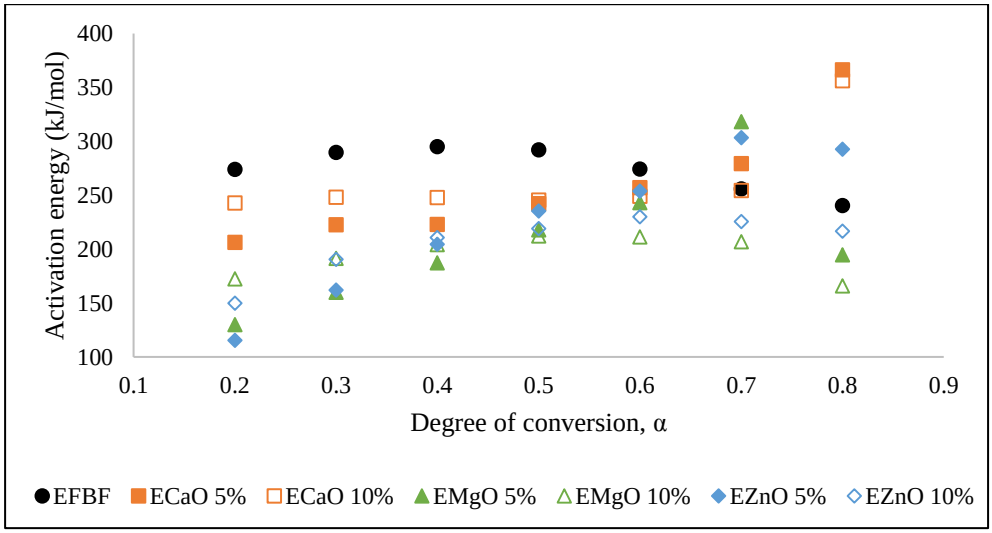

Figure 11: Activation energies of EFBF, with and without catalysts against degree of conversion using simplified DAEM

Generally, the addition of oxides lowered the average activation energy of cellulose and EFBF, indicating that the oxides posed catalytic effects on the biomasses. Nonetheless, the formation and dissociation of calcium and magnesium compounds (i.e. $Ca(OH)_2$, $CaCO_3$, and $Mg(OH)_2$) may have contributed to the decrease in activation energy as well because a lesser amount of CaO and MgO would be available for reaction with the biomass. Similarly, coke formation on the oxides may have played a role as well. Despite that, the catalytic effect posed by CaO is undeniable as both $Ca(OH)_2$ and $CaCO_3$ exert catalytic effects in the catalytic pyrolysis of wastes as well (Shah, Rasul Jan and Mabood, 2008; Claudinho and Ariza, 2017). Hence, it may be clarified that to

deduce the presence catalytic effects of CaO based solely on the decrease in activation energy may not be accurate in the current study as CaO itself reacts with moisture and CO_2. This is the same for MgO.

Further analysis on the kinetics and diffusion mechanisms during catalytic pyrolysis of cellulose and EFBF at individual stages was studied using Coats-Redfern (CR) method.

4.4.1 Kinetics and mechanisms for catalytic pyrolysis at individual stages by Coats-Redfern (CR) method

The decomposition of cellulose and EFBF were divided into stages based on DTG curve at heating rate of 20 °C/min, as presented in Section 4.3.1.1. Using CR method, the mechanisms involved in the pyrolysis of cellulose and EFBF, with and without oxides may be understood. A high correlation coefficient would indicate the kinetic model that fits the data well. The basic model functions ($f(\alpha)$) that were used in this kinetic study of solid-state reactions were presented in Table 9, which includes chemical processes or mechanisms (F series), phase boundary reactions (R series), and diffusion mechanisms (D series). The F series (F1/3, F3/4, F1, F3/2, F2, and F3) are order-based models and are the simplest models among all. For this mechanism, the reaction rate is proportional to the concentration of the reactant, raised to a particular power (Guida and Hannioui, 2016). The rate-determining step is the nucleation or chemical reaction. Phase boundary-controlled reactions (R1, R2, and R3) assume that the reaction is controlled by the movement of an interface at a constant velocity and nucleation occurs almost instantly. Then, a layer of product would cover each particle (Fink, 2013). Next, the diffusion kinetic models (D1, D2, D3, D4, D5, D6, D7, D8) are characterized by the mobility of

components in the system, usually in solid-state reactions. In these reactions, the rate of product formation decreases proportionally with the thickness of the product barrier layer (Guida and Hannioui, 2016).

The kinetic parameters obtained for cellulose and EFBF, with and without catalysts at heating rate of 20 °C/min, are presented in Table 13. Stage 1 mainly involves the dewatering of samples. While the second order chemical reaction model (F2) was in dominion for cellulose, the EFBF samples fitted well with the third order kinetic model (F3). As can be seen from the activation energies, the addition of oxides did not affect the water evaporation rate of both biomasses significantly.

Subsequently, the main devolatilization of cellulose occurs at Stage 2. At this stage, the solid-state reaction was controlled by one and a half order (F3/2) and the three-dimensional diffusion mechanism of Zhuravlev, Lasokin, Tempelman equation (D5). Here, diffusion in all three directions is important. Even though there were no changes in the kinetic models when the oxides were employed, the activation energies increased in general. This indicates that the oxides did not influence the reaction mechanisms but reduced the rate of reaction. Nevertheless, this did not affect the weight loss of cellulose at this stage (Section 4.3.1.1). An extra kinetic model showed high correlation coefficient when CaO was employed, which is the phase boundary reaction (R3). R3 is a function for a sphere reacting from the surface inward, suggesting that the presence of spherical particles may be contributed by CaO, $Ca(OH)_2$ or $CaCO_3$.

Table 13: Kinetic parameters for cellulose and EFBF, with and without oxides at heating rate of 20 °C/min using CR method

Stage	Cellulose samples	E (kJ/mol)	A (1/s)	Kinetic model	EFBF samples	E (kJ/mol)	A (1/s)	Kinetic model
1	Cellulose	98.0	6.5×10^{14}	F2	EFBF	78.7	4.8×10^{11}	F3
	CCaO 5%	99.0	9.2×10^{14}	F2	ECaO 5%	78.4	4.4×10^{11}	F3
	CCaO 10%	99.1	9.7×10^{14}	F2	ECaO 10%	81.3	1.5×10^{12}	F3
	CMgO 5%	98.2	6.2×10^{14}	F2	EMgO 5%	73.3	6.3×10^{10}	F3
	CMgO 10%	100.7	1.5×10^{15}	F2	EMgO 10%	74.7	1.1×10^{11}	F3
	CZnO 5%	100.2	1.2×10^{15}	F2	EZnO 5%	76.2	1.8×10^{11}	F3
	CZnO 10%	96.8	4.0×10^{14}	F2	EZnO 10%	80.3	9.7×10^{11}	F3
2	Cellulose	265.9	1.9×10^{22}	F3/2	EFBF	111.7	7.7×10^{09}	F2
		509.9	2.3×10^{42}	D5		182.5	1.4×10^{15}	D5
	CCaO 5%	320.9	1.1×10^{27}	F3/2	ECaO 5%	96.0	1.6×10^{08}	F1
		240.4	5.6×10^{19}	R3		85.2	4.3×10^{06}	R3
		615.5	2.6×10^{51}	D5		226.4	1.7×10^{19}	D5
	CCaO 10%	248.2	5.8×10^{27}	F3/2	ECaO 10%	95.1	1.3×10^{08}	F1
		249.1	2.9×10^{20}	R3		84.4	3.6×10^{06}	R3
		635.7	1.1×10^{53}	D5		224.3	1.1×10^{19}	D5
	CMgO 5%	294.0	4.5×10^{24}	F3/2	EMgO 5%	110.6	6.6×10^{09}	F2
		563.5	6.7×10^{46}	D5		180.3	9.8×10^{14}	D5
	CMgO 10%	318.9	5.6×10^{26}	F3/2	EMgO 10%	111.0	6.4×10^{09}	F2
		611.2	6.2×10^{50}	D5		180.7	8.8×10^{14}	D5
	CZnO 5%	273.0	7.4×10^{22}	F3/2	EZnO 5%	110.4	6.1×10^{09}	F2
		523.5	2.8×10^{43}	D5		180.3	9.2×10^{14}	D5

Table 13: Kinetic parameters for cellulose and EFBF, with and without catalysts at heating rate of 20 °C/min using CR method (continue)

	CZnO 10%	273.2	7.9×10^{22}	F3/2	EZnO 10%	110.8	6.8×10^{09}	F2
		523.8	3.1×10^{43}	D5		180.8	1.1×10^{15}	D5
3	Cellulose	122.1	1.1×10^{08}	F3	EFBF	128.2	4.9×10^{08}	F3
	CCaO 5%	185.3	1.0×10^{14}	F3	ECaO 5%	209.9	5.5×10^{15}	F3
	CCaO 10%	202.2	2.7×10^{15}	F3	ECaO 10%	227.3	1.5×10^{17}	F3
	CMgO 5%	152.2	2.8×10^{10}	F3	EMgO 5%	122.3	1.1×10^{08}	F3
	CMgO 10%	153.8	3.6×10^{10}	F3	EMgO 10%	121.0	9.7×10^{07}	F3
	CZnO 5%	156.3	5.8×10^{10}	F3	EZnO 5%	123.3	1.9×10^{08}	F3
	CZnO 10%	154.5	4.0×10^{10}	F3	EZnO 10%	116.2	5.7×10^{07}	F3
4	CCaO 5%	398.9	2.5×10^{23}	F3	ECaO 5%	237.0	6.5 x 1012	F1
						221.3	1.4 x 1011	R3
						458.3	4.9 x 1023	D3
	CCaO 10%	409.6	2.1×10^{24}	F3		253.8	6.3×10^{13}	F1
						235.5	9.3×10^{11}	R3
						486.5	2.1×10^{25}	D3

EFBF also experienced the highest weight loss at Stage 2, which may be ascribed to the devolatilization of mainly cellulose and hemicellulose. The reactions were not only controlled by second order reaction (F2) but also three-dimensional diffusion mechanism of Zhuravlev, Lasokin, Tempelman equation (D5), which is similar to that of cellulose. This further justifies the

devolatilization of cellulose at this stage. The addition of MgO and ZnO did not pose any significant effect on the kinetic model nor the activation energy of EFBF. Nonetheless, the weight loss at this stage decreased when the oxides were added (Section 4.3.1.1). As observed, the addition of oxides caused a reduction in the frequency factor (A), which, by definition signifies the probability for reaction occurrence (Valdés *et al.*, 2018). Hence, it may be hypothesized that the addition of the oxides did not affect the reaction rate of EFBF for devolatilization but rather, lowered the probability for reaction to occur. This may be possibly due to coking of the oxides, which would block the diffusion pathways of the volatiles, as observed and discussed in Section 4.3.1.1. Aside from kinetic models of F1 and D5, the addition of CaO also showed high correlation coefficient with the power law in the phase boundary reaction (R3), which is again, similar to that of cellulose. As may be interpreted from the change in activation energies shown in Table 13, CaO was able to increase the rate of nucleation for EFBF but decreased the rate for the diffusion mechanisms, due to the formation of calcium compounds (e.g. $Ca(OH)_2$ and $CaCO_3$).

EFBF exhibited higher reaction rates in dewatering of the sample and in devolatilization of the sample than in cellulose. This was reflected from the lower activation energies obtained for EFBF, indicating that the presence of metal elements in EFBF such as Mg, Ca, K, and Zn might have played a catalytic role in the thermal degradation of EFBF (Hayawin *et al.*, 2014; Mahadevan *et al.*, 2016).

Stage 3 may be attributed to the further decomposition of cellulose and additional lignin for EFBF, to form gaseous products and residual char. For all samples, the unanimous kinetic model that was most fitting is the third order

kinetic model (F3). As observed for cellulose, the activation energy increased with the addition of the MgO and ZnO. This may be because the oxides promoted the formation of coke, which was reflected by the higher residual weight obtained as presented in Section 4.3.1.1. Hence, higher activation energy would be required for the further degradation of cellulose and so, led to the decrease in the reaction rate of cellulose. On the contrary, when MgO and ZnO were added to EFBF, the activation energy decreased slightly, which explains the higher weight loss in Stage 3, as presented in Section 4.3.1.1. This suggests that MgO and ZnO are more effective in catalysing the decomposition of lignin and more complex components. Phenolic compounds are the products of lignin depolymerization and pyrolysis experiments did show that the utilization of MgO and ZnO would increase the amount of phenolic compounds in the bio-oil (Zhou *et al.*, 2013; Stefanidis *et al.*, 2016).

When CaO was added to cellulose, Stage 3 and Stage 4 may be accredited to the decomposition of $Ca(OH)_2$ and secondary reactions alongside with the decomposition of $CaCO_3$, respectively. Similarly, F3 kinetic model fits well with the data, showing that aside from secondary reactions, the decomposition rate of calcium compounds was also limited by chemical reactions.

For EFBF with CaO, while Stage 3 may be accredited to the decomposition of $Ca(OH)_2$, Stage 4 may be ascribed to the decomposition of mainly lignin together and $CaCO_3$. The degradation of $Ca(OH)_2$ obtained good linearity with the F3 kinetic model, which is the same as that of cellulose. However, for Stage 4, the solid-state reaction was controlled by first order kinetic model (F1), phase boundary reaction (R3), and Jander equation (D3). As both R3 and D3 are functions for reactions in a sphere, it is indicated that the $CaCO_3$ in the current

study are of spherical shape. Such observation was not made for cellulose probably due to the little amount of $CaCO_3$ formed as explained in Section 4.3.1.1.

4.5 Concluding remarks

In the current chapter, three oxides, namely calcium oxide (CaO), magnesium oxide (MgO), and zinc oxide (ZnO) were incorporated to investigate the influence of the oxides on the thermal behaviour and kinetic mechanisms of biomass degradation. The addition of MgO and ZnO did not affect the degradation behaviour of the biomasses. On the other hand, owing to the reaction between moisture and carbon dioxide (CO_2) adsorption ability of CaO, two major weight loss peaks were observed, which may be attributed to the decomposition of calcium hydroxide ($Ca(OH)_2$) and calcium carbonate ($CaCO_3$).

Generally, the addition of the CaO, MgO, and ZnO reduced the amount of volatile released from the biomass and the effect was more noticeable in EFBF than in cellulose. This may be attributed to the presence of other biomass components (e.g. hemicellulose and lignin) and impurities (e.g. dirt) in EFBF. Even though MgO and ZnO did not affect the reaction mechanisms and reaction rate for the devolatilization of cellulose and hemicellulose in EFBF, the weight loss at the devolatilization stage decreased. This is because the coking of the oxides may have restricted the transportation of the volatiles in EFBF and also lowered the chances of reaction to occur (based on decrement in frequency factor). Instead, both MgO and ZnO were found to be more effective in catalysing the degradation of heavier compounds such as lignin. As for CaO, the formation of the calcium compounds (e.g. $Ca(OH_2)$ and $CaCO_3$) limited the

diffusion of volatiles and hence, also caused a decrease in devolatilization of EFBF.

By definition, catalysts are agents that are able to speed up reactions without going through permanent changes itself. In the current study, CaO, MgO, and ZnO did increased the rate of reactions slightly (based on the decrease in average activation energy that is obtained from DAEM), but not significantly, and even reacted with the surrounding (e.g. moisture and CO_2). Hence, CaO, MgO, and ZnO may be considered as catalytic additives, rather than catalysts.

CHAPTER 5

5 IN-SITU CATALYTIC PYROLYSIS OF CELLULOSE AND EMPTY FRUIT BUNCH FIBRE (EFBF) WITH OXIDES: EFFECTS ON BIO-OIL PROPERTIES

5.1 Introduction

The current chapter investigates the effects of calcium oxide (CaO), magnesium oxide (MgO), and zinc oxide (ZnO), on the physical properties of bio-oil. Bio-oil was produced in a fixed bed reactor in the presence of oxides at various weight percentages (0, 5, and 10 wt.%) via catalytic intermediate pyrolysis. The bio-oil was then analysed for the chemical properties such as acidity, water content, surface structure, and major compounds. The current chapter is segregated into two sections: the first section utilized cellulose as feed, with the aim to understand the influence of oxides on bio-oil at the simplest form of lignocellulosic biomasses and to summarize possible reaction pathways based on the obtained results and literature; the latter section employed empty fruit bunch fibre (EFBF) as feed. The characterization of both feed and the oxides has been carried out in the Chapter 4, Sections 4.2 and 4.3.1, respectively.

5.2 Section 1: Effect of oxides on the properties of bio-oil from in-situ catalytic pyrolysis of cellulose

5.2.1 Textural properties of oxides

Table 14 presents the textural properties of calcium oxide (CaO), magnesium oxide (MgO), and zinc oxide (ZnO) that were used in the current study. As the current study focused on inexpensive additives, the oxides were taken for

pyrolysis without further modification other than calcination. Having a pore diameter of > 50 nm categorized the oxides as macroporous. Nevertheless, the BET surface areas of the oxides were relatively small (< 20 m^2/g).

Table 14: Textural properties of oxides

Catalysts	S_{BET} (m^2/g)	Pore diameter (nm)	Pore volume (cm^3/g)
CaO	2.25	99.73	0.10
MgO	19.84	56.15	0.27
ZnO	0.86	88.4	0.01

5.2.2 Product yield

Figure 12 illustrates the yield of products from cellulose pyrolysis, with and without the presence of different oxides. Samples labelled as "CCaO 5%" refers to cellulose sample with 5 wt.% of CaO added; "CCaO 10%" refers to that with 10 wt.% CaO added, and so on for the other samples. Without oxides, cellulose achieved a production yield of 52.3 ± 1.3 wt.%.

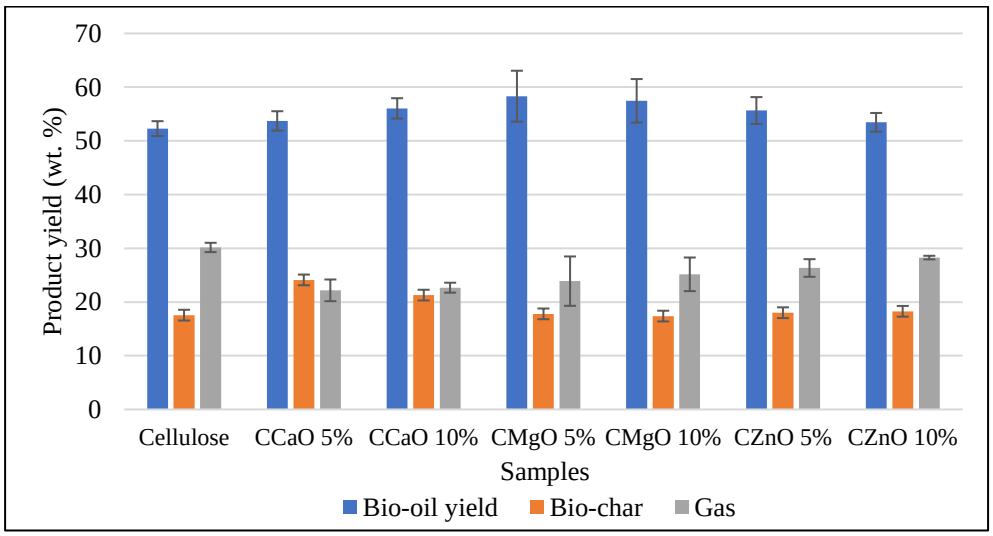

Figure 12: Product yields of cellulose pyrolysis, with and without the presence of oxides

The difference in bio-oil yields, with and without the addition of CaO, MgO, and ZnO (5 wt.% and 10 wt.%) was analysed by performing ANOVA test. From the p-values presented in Table 15, there was no adequate evidence to reject the null hypothesis regarding bio-oil yields, indicating that the increment in bio-oil yields is negligible. Therefore, the results can be interpreted as the introduction of CaO, MgO, and ZnO to the pyrolysis system would not affect the degradation of cellulose regarding bio-oil production evidently. The macroporosity of CaO, MgO, and ZnO used in current study has no significant impact on the bio-oil yield because their BET surface areas are too small and hence, may be neglected.

Table 15: p-values obtained from ANOVA analysis

Combination of data sets for comparison	p – values		
	Bio-oil yield	TAN	Water content
Cellulose, CCaO 5%, and CCaO 10%	0.0914	0.0002	0.4856
Cellulose, CMgO 5%, and CMgO 10%	0.1784	0.2253	0.0245
Cellulose, CZnO 5%, and CZnO 10%	0.3340	0.0249	0.0585

The elevation in char yield in the presence of CaO may be ascribed to the formation of calcium carbonate ($CaCO_3$) upon adsorption of carbon dioxide (CO_2), which correlates with the decrease in gas yield. CO_2 is mainly produced in the primary reaction or at early stages of cellulose pyrolysis under fast heating conditions (Li *et al.*, 2001). The decomposition of $CaCO_3$ occurs at 700 °C and so, CO_2 was not re-released in current study and the carbonate formed remained in char (Kwon *et al.*, 2018). Moreover, since the molar mass of $CaCO_3$ (100.1 g/mol) is larger than that of CaO (56.1 g/mol), the mass gain in char yield was

observed. The identification of $CaCO_3$ in the solid residual was performed and presented in Section 5.2.6.

CaO has higher CO_2 adsorption capacities as compared to MgO and thus, the decrement in gas yield was more evident when CaO was employed (Wang *et al.*, 2011). Even though MgO adsorbs CO_2 to form magnesium carbonate ($MgCO_3$), the carbonate formed decomposes at 450 °C (Bhagiyalakshmi, Lee and Jang, 2010). Most of the $MgCO_3$ was expected to have decomposed at the end of current study and therefore, did not pose an effect on the char yield. ZnO can be used for CO_2 capture but the process is favoured by low operating temperatures (varies with CO_2 pressure) (Kumar and Saxena, 2014). Consequently, the influence of ZnO on CO_2 capture in current study was negligible. Assuming that basic zinc carbonate did form from CO_2 capture reaction, the decomposition temperature was found to be low (197 – 257 °C) (Kumar and Saxena, 2014). This is the reason that ZnO did not influence the char yield in current study.

5.2.3 Acidity

Upon pyrolysis of cellulose, carboxylic acids such as acetic acid, propanoic acid, and heptanoic acids are reportedly formed (Shen and Gu, 2009; Zhao, Jiang and Chen, 2017). Based on the gas chromatography-mass spectrometry (GC-MS) results of current study that is to be discussed later in Section 5.2.7, acetic acid showed the highest weight percentage among the acids in bio-oils. Aside from organic acids, compounds such as phenolics, fatty acids and resin and hydoxy acids contribute to the acidity of the bio-oils (Oasmaa et al., 2010). The high acidity of bio-oil is corrosive to common construction materials such as

aluminium and carbon steel. The corrosion rate would even be enhanced at elevated temperatures (Czernik and Bridgwater, 2004; Lu, Li and Zhu, 2009).

The pH values and total acid number (TAN) of the bio-oils are presented in Table 16. While pH measures the concentration of hydrogen ions (H^+), TAN quantifies the amount of acidic components in the bio-oil samples. As bio-oil contains large amounts of ions and free radicals, the pH did not show much variation even though a significant difference may be observed from TAN. In Table 15, the ANOVA analysis for TAN are presented. P-values of less than or equal to 0.05 indicate that both CaO and ZnO posed great influence in reducing the acidity of the cellulose-derived bio-oils whereas that effect of MgO was negligible.

One of the reaction pathways between CaO and acids in the bio-oil is neutralization, where acids are converted to calcium carboxylate and water. Then, calcium carboxylate would decompose to ketones and $CaCO_3$ at temperature range of 400 – 500 ˚C. Current study confirmed this pathway by an increase in ketones as shown from GC-MS results in Section 5.2.7 and detailed results in Appendix 3 (Table A.25). Another reaction pathway for the removal of acids is the thermal cracking of acids to hydrocarbons and CO_2 in presence of CaO (Lu *et al.*, 2010; Wang *et al.*, 2010; Chen, Chen, *et al.*, 2017). However, current study did not notice the presence of hydrocarbons, possibly due to the lack of acid sites in CaO.

Table 16: pH, TAN, and water content of bio-oils

	pH of bio-oil	TAN of bio-oil (mg KOH/g)	Water content (wt. %)
Cellulose	2.4	42.6 ± 2.0	47.5 ± 3.8
CCaO 5%	2.5	29.7 ± 2.4	51.1 ± 3.7
CCaO 10%	2.5	28.4 ± 1.3	49.1 ± 1.4
CMgO 5%	2.4	40.7 ± 1.0	56.9 ± 3.8
CMgO 10%	2.4	38.9 ± 3.4	57.3 ± 4.0
CZnO 5%	2.3	37.0 ± 2.9	49.1 ± 4.6
CZnO 10%	2.3	34.5 ± 3.0	55.7 ± 2.9

With the utilization of MgO, carboxylic acids can be removed via ketonization, producing ketone, water, and CO_2. During decarboxylation, two molecules of pentanoic acid would form dibutyl ketone, water, and CO_2 in the presence of MgO (Khromova *et al.*, 2013). This is similar for acetic acid, where two molecules of acetic acid in the bio-oil would undergo ketonization, producing 2-propanone (acetone), water, and CO_2 (Stefanidis *et al.*, 2016). An increase in ketone compounds were noticed by adding MgO in the current study as well (Section 5.2.7 and Appendix 3 (Table A.25)). Apart from ketonization, acetic acid could also be adsorbed onto MgO and forming magnesium acetate, which would decompose to MgO, water, and CO_2 (Mekhemer *et al.*, 2005). However, an insignificant change in acidity was observed in current study even though an increase in ketone was observed, possibly caused by the secondary cracking of levoglucosan (LG), as discussed later in Section 5.2.7.

Similar to the CaO and MgO, acetic acid interacts with ZnO surface via adsorption, forming surface carboxylate species. At temperatures above 230 °C, the surface acetate would undergo dehydration and decomposes to form ketene,

acetic acid, CO_2, hydrogen (H_2), and water (Vohs and Barteau, 1988). Current study confirms this pathway by an increase in ketone/ketene (Section 5.2.7 and Appendix 3 (Table A.25)) and water content.

5.2.4 Water content

The presence of water contributes both negatively and positively to the quality of bio-oil. On the negative note, a relatively high water content decreases the heating value and encourages stratification of the bio-oil. Conversely, water would lower the viscosity of the bio-oil for good pumping and atomization during combustion, and simultaneously reduce the emission of pollutants (NO_x) (Czernik and Bridgwater, 2004). The addition of oxides to pyrolysis reactions is expected to increase the water content of the bio-oils due to neutralization and dehydration reactions posed by the oxides.

Neutralization of acids in the bio-oil in the presence of CaO, MgO, and ZnO was discussed in Section 5.2.3. On the other hand, dehydration involves the removal of oxygen from the bio-oil through the formation of water from reacting molecule, which is beneficial in enhancing the properties of bio-oil. The occurrence of dehydration reactions was justified by the increment in dehydration products such as water, furfural, furfuryl alcohol, acetic acid, and so on (Lin *et al.*, 2010; Chen, Chen, *et al.*, 2017). In current study, GC-MS analysis was used to observe the change in bio-oil compounds and is further discussed in Section 5.2.7. Based on the amounts of furan compounds and acetic acid, ZnO showed highest dehydration efficiency.

With the addition of CaO, MgO, and ZnO, the water content of the bio-oils increased in general, as observed from Table 16. In accordance to the p-values

presented in Table 15, the increment in water content of bio-oil is significant only with the employment of MgO. Magnesium ions (Mg^{2+}) has a strong hydration ability and the dehydration of the hydrated Mg^{2+} had been observed to occur even above 500 °C (Hwang *et al.*, 2015). Upon dehydration, the combination of water and Mg^{2+} breaks down and thus, contributes to the increase in the water content of bio-oil at elevated temperatures.

The neutralization reaction of acids in bio-oil with CaO was expected to cause a significant increase in water content. However, the formation of water was only significant at 600 °C (Wang *et al.*, 2010). Even though the TAN greatly decreased in the presence of CaO, the water content in bio-oil did not increase significantly as the operating temperature was around 500 °C.

While Zhou et al. (2013) carried out pyrolysis experiments with ZnO at 550 °C, Nokkosmäki et al. (2000) did that at 400 °C. The former showed a decrease in water content whereas the latter showed an increase in water content (Nokkosmäki *et al.*, 2000; Zhou *et al.*, 2013). In the current study with operating temperature of 500 °C, the water content of the bio-oil remained unchanged, suggesting that the operating temperature plays a role in affecting the water content of the bio-oil when ZnO is used.

5.2.5 Reaction pathways on carbon dioxide (CO_2) and acetic acid adsorption (neutralization)

Upon the introduction of CaO, MgO, and ZnO, the reactions involved in the adsorption of CO_2 and neutralization of carboxylic acid are shown to be complex. Based on the results and discussions presented in Sections 5.2.2, 5.2.3, and 5.2.4, the reaction pathways on CO_2 capture and neutralization of

carboxylic acids are summarized in Table 17, where acetic acid was used as the model compound. While CO_2 is captured by the oxides and forms metal carbonates, acetic acid is adsorbed onto oxides, forming surface carboxylate compounds, which would further decompose at varying temperatures (Rajadurai, 2006).

Table 17: Summary of reactions involved in CO_2 capture and neutralization of acetic acid upon employment of metal oxides

CaO	MgO	ZnO
1. CO_2 capture		
$CO_2 + CaO \rightarrow CaCO_3$	$CO_2 + MgO \rightarrow {}^{\#}MgCO_3$	$CO_2 + ZnO \rightarrow {}^{\#}ZnCO_3$
1.1 Decomposition of carbonate		
$CaCO_3 \rightarrow CO_2 + CaO$ @ 700 °C	${}^{\#}MgCO_3 \rightarrow CO_2 + MgO$ @ 450 °C	${}^{\#}ZnCO_3 \rightarrow CO_2 + ZnO$ @ 197 – 257 °C
2. Neutralization of acetic acid		
2.1 Formation of carboxylates		
$2CH_3COOH + CaO \rightarrow {}^{\#}Ca(CH_3COO)_2 + H_2O$	$2CH_3COOH + MgO \rightarrow {}^{\#}Mg(CH_3COO)_2 + H_2O$	$2CH_3COOH + ZnO \rightarrow {}^{\#}Zn(CH_3COO)_2 + H_2O$
2.2 Products from decomposition of carboxylates		
$CaCO_3 + (CH_3)_2CO$ @ 400 – 500 °C	$MgO + H_2O + CO_2$ @ 225 °C	Ketene + CH_3COOH + $CO_2 + H_2 + H_2O + Zn$ @ 230 °C
2.3 Products from ketonization of acetic acid		
-	$(CH_3)_2CO + H_2O + CO_2$	-

undetected due to decomposition temperatures of lower than operating temperature (500 °C)

5.2.6 Surface structure of bio-oil and biochar

Fourier-transform infrared spectroscopy (FTIR) is one of the powerful analytical tools to investigate the surface structure of samples. It is helpful to investigate the changes that occurs in the biomass, bio-oil, and char upon catalytic pyrolysis, by comparing the spectra of different samples in the same experimental design. Figure 13(a) presents the FTIR spectra for cellulose. Stretching bands for OH groups (3400 – 3200 cm^{-1}) and alkyl groups (2880 cm^{-1}) were observed, together with a prominent peak at 1022 cm^{-1} can be attributed to the C-O vibrations in the cellulose pyranoside units (Dorado *et al.*, 2001). Besides that, the presence of absorbance peaks at 3400 – 3200 and 1632 cm^{-1} may be accredited to the water adsorbed whereas peaks in the range of 1460 – 1298 cm^{-1} may be assigned to both alkane and alkene groups (Coates, 2006).

The FTIR spectrum of cellulose-derived bio-oil is depicted in Figure 13(b) and the disappearance of the major peak observed in cellulose at 1022 cm^{-1} suggested the cracking of the glycosidic bonds upon pyrolysis. The broad peak in the range of 3458 – 3200 cm^{-1} that can be accredited to OH stretching bonds, signifies the presence of oxygenated compounds such as alcohols and water in the bio-oil. As mentioned in Section 5.2.4, the presence of water in bio-oil may or may not be beneficial but needs to be controlled. Peaks in the ranges of 1750 – 1650 cm^{-1} and at 1640 cm^{-1} can both be assigned to the C=O stretching vibration in carbonyl groups. While the former is contributed by acids, the latter is by hydroxy unsaturated ketones and aldehydes (Lievens *et al.*, 2011). The presence of such carbonyl compounds can be reaffirmed from GC-MS results in Section 5.2.7.

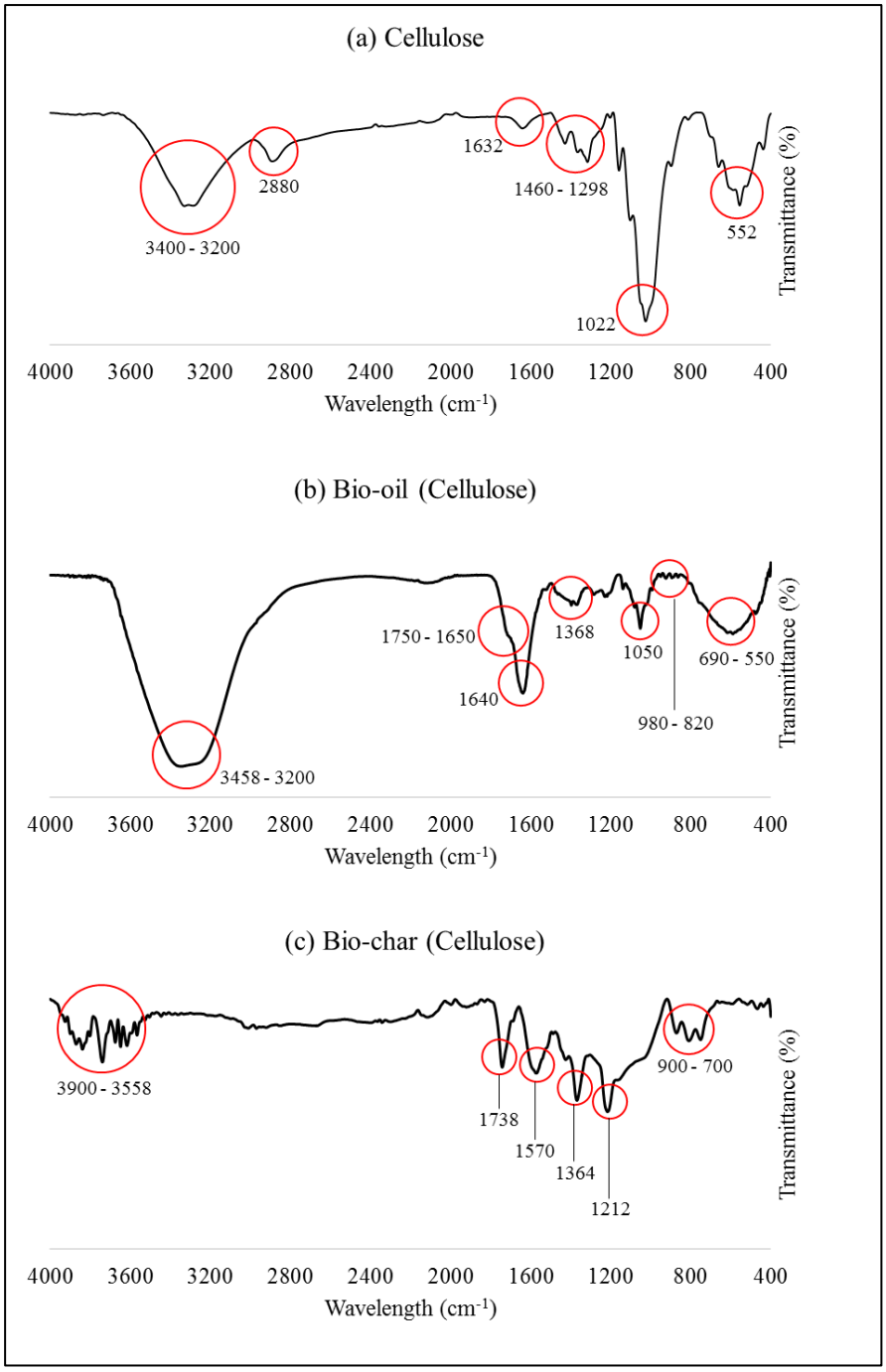

Figure 13: FTIR spectra of (a) cellulose, (b) cellulose-derived bio-oil, and (c) biochar

Apart from that, absorbance peak at 1368 cm^{-1} may be ascribed to alkyl groups (Rutkowski and Kubacki, 2006). Several peaks were observed at 1050 and 980 – 820 cm^{-1}, revealing the presence of alcohols and aromatics in the bio-oil. Among these ranges of peaks, the C-O stretch that is attributed to primary

alcohol at 1050 cm^{-1} is the most prominent one. However, only 1,2-cyclohexadiol, a secondary alcohol, was detected from GC-MS.

Upon pyrolysis at a temperature of 500 ± 20 °C, the biochar presented in Figure 14(c) showed obvious signs of dehydration. One of the signs is the reduction in intensity of the broad peak at 3900 – 3558 cm^{-1}. Besides that, the presence of carbonyl structures (C=O) at 1738 cm^{-1}, and C=C structures at 1570 cm^{-1} confirms the dehydration of hydroxyl (OH) groups in cellulose as well (Long *et al.*, 2017). Alcohols, phenols, and aromatic compounds were also found in the char as shown in peaks 1364, 1212 and 900 – 700 cm^{-1}, respectively.

The presence of CaO, MgO, and ZnO did not pose significant changes to the FTIR spectra of cellulose bio-oil, apart from the slight intensification of the peak at 1050 cm^{-1} by MgO and ZnO. This indicates that both MgO and ZnO encouraged the formation of primary alcohol in the bio-oil. FTIR analysis may be interpreted as the addition of CaO, MgO and ZnO did not significantly affect the chemical bonds in cellulose-derived bio-oil. The FTIR spectra are presented in Appendix 4 (Figure A.28)).

Figure 14 compares the FTIR spectra of the remaining solids with that of cellulose biochar. Residual solids from catalytic pyrolysis showed weaker peaks, especially C=O carbonyl (1738 cm^{-1}) together with C-O alcohol (1212 cm^{-1}). There is an obvious difference in the FTIR spectra for the residual with CaO. Three peaks including the intense one at 1404 cm^{-1}, narrow one at 874 cm^{-1}, and that at 714 cm^{-1} are known to be the fundamental modes of $CaCO_3$, contributed by carbonate ions (CO_3^{2-}) in the sample (Coates, 2006). The formation of $CaCO_3$ is discussed previously in Sections 5.2.2 and 5.2.3. Since addition of 5

wt.% oxides have similar spectra on solid residual to those with 10 wt.%, the former is presented in Appendix 4 (Figure A.29).

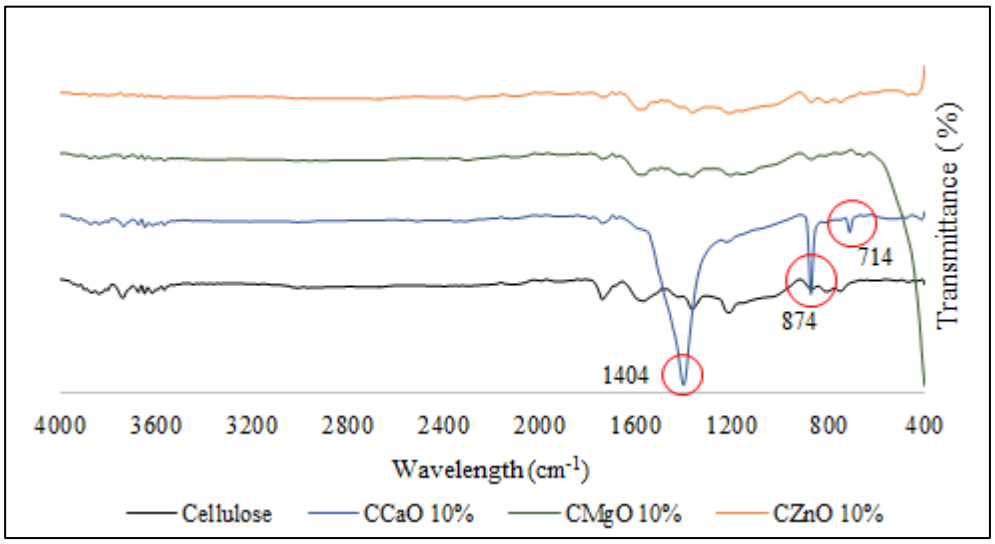

Figure 14: FTIR spectra of cellulose solid residual, with and without the presence of 10 wt.% oxides

5.2.7 Major compounds in bio-oil

The main products that are quantified in current study are levoglucosan (LG), acetic acid, furans (e.g. furfural and 5-hydroxymethylfurfural) where the results obtained are presented in Table 18 and the detailed detected compounds are presented in Appendix 3 (Table A.25). The chemical pathways that relate the main products mentioned have been compiled and presented in Figure 15.

LG and isomers were dominant products in the bio-oil. LG from cellulose pyrolysis was formed from the cleavage of 1,4-glycosidic linkage in the cellulose polymer, followed by intramolecular rearrangement of the monomer units. Similarly, 3,4-anhydro-d-galactosan and 2,3-anhydro-d-mannosan (isomers of LG) were initiated from the free hydroxyl radicals, followed by chemical structure rearrangement (Li *et al.*, 2001). These saccharides were

targeted compounds in various studies due to their attractive application as a renewable non-petroleum feedstock for the chemical and pharmaceutical industry (Dobele *et al.*, 2005; Lu *et al.*, 2014). In the presence of oxides, the amount of these products increased consequentially, with the weight percentages increasing from 8.1 wt. % to a maximum of 15.1 wt. % when ZnO was used. This indicates that the employed oxides induced the cracking of the cellulose, where both MgO and ZnO were more effective in doing so than CaO.

Table 18: Main products from pyrolysis of cellulose, with and without the presence of oxides

Quantified compounds (wt.%)							
Compounds	Cellulose	CCaO 5%	CCaO 10%	CMgO 5%	CMgO 10%	CZnO 5%	CZnO 10%
Levoglucosan and isomers	8.1 ± 0.3	11.7 ± 0.3	10.0 ± 0.4	15.0 ± 0.2	13.7 ± 1.1	14.6 ± 0.9	15.1 ± 2.6
Acetic acid	1.3 ± 0.2	1.0 ± 0.1	0.9 ± 0.1	0.9 ± 0.2	0.9 ± 0.2	1.0 ± 0.1	1.0 ± 0.2
Furan	1.3 ± 0.6	2.3 ± 1.1	2.0 ± 1.5	2.2 ± 1.6	2.2 ± 1.6	2.2 ± 2.2	2.3 ± 2.2
Total area of compounds (area %)							
Anhydrosugars	14.36	30.79	29.39	38.02	35.91	36.38	36.39
Furan	14.36	18.7	20.36	20.23	18.95	20.89	21.36
Ketones	2.68	4.74	4.85	4.27	4.08	4.07	3.86
Esters	0.39	0.28	0.30	0.15	0.22	0	0
Alcohols	0.36	0.91	0.46	0.88	0.96	0.52	0.95
Methoxys alkanes/alkenes	0.50	1.69	1.98	1.44	1.08	1.93	1.74

Upon the addition of the oxides, the amount of acetic acid decreased slightly but not as significant as reflected from the results of TAN analysis (Section

5.2.3). Acetic acid can be produced from LG either by direct pyrolysis or char-catalysed decomposition (Hosoya, Kawamoto and Saka, 2007; Ronsse *et al.*, 2012). As mentioned in Section 5.2.5, acetic acid is also a product from the dehydration reactions. The decrease in TAN may have been contributed by the decrement of other carboxylic acids such as formic acid and benzoic acid (Czernik and Bridgwater, 2004).

Furan compounds are thermally stable oxygenates that are either formed from the secondary cracking of LG and its isomers or from the opening and reforming of the pyranoid ring in cellulose (Liao, Wang and Ma, 2004). Among furan compounds, á-methoxy-(S)-2-furanethanol, which is formed from the breaking and recombining of C=O linkages in furfural and 2-furancarboxyaldehyde showed the highest peak area (%). For all three of the oxides, the furan selectivity was increased, especially when ZnO was utilized.

Carbonyl compounds that were detected from GC-MS analysis include 1-hydroxy-2-butanone, 1, 2-cyclopentanedione, 2, 3-pentanedione, and 3-methyl-2-cyclopenten-1-one, which can be specifically classified as ketones. According to GC-MS results as presented in Table 18, the area % of carbonyl compounds increased with the addition of the oxides in the current study. Such observation can be associated with the deacidification properties of the catalysts, as discussed in Section 5.2.3 previously. Relative increase in all carbonyl compounds without compromising the bio-oil yield showed the potential of these oxides in capturing carbon from gas to liquid and in improving the pH of bio-oil.

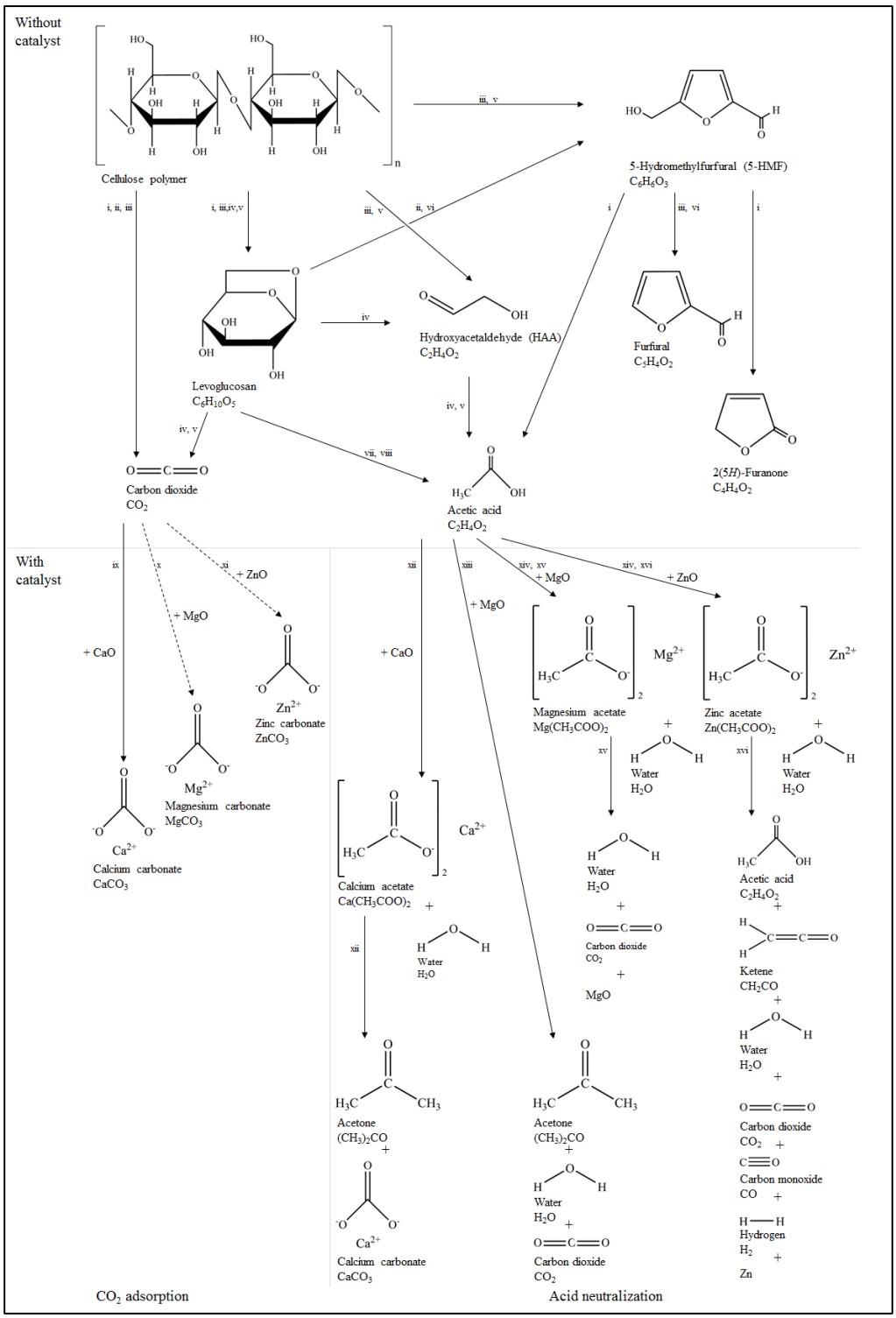

Figure 15: Pathways related to main products from pyrolysis of cellulose at 500 °C, with and without the presence of CaO, MgO, and ZnO; i: (Wang *et al.*, 2012); ii: (Shafizadeh and Yuan-Zong, 1975); iii: (Luo *et al.*, 2004); iv: (Piskorz, Radlein and Scott, 1986); v: (Shen and Gu, 2009); vi: (Shafizadeh and Y.Z., 1966); vii: (Hosoya, Kawamoto and Saka, 2007); vii: (Ronsse *et al.*, 2012); ix: (Wang *et al.*, 2011); x: (Bhagiyalakshmi, Lee and Jang, 2010); xi: (Kumar and Saxena, 2014); xii: (Chen, Chen, *et al.*, 2017); xiii: (Stefanidis *et al.*, 2016); xiv: (Rajadurai, 2006); xv: (Mekhemer *et al.*, 2005); xvi: (Vohs and Barteau, 1988)

5.2.8 Comparison of results with literature

The results obtained from current study were compared to literature, presented in Section 2.3.3.2. Most studies that utilized CaO, MgO, and ZnO for pyrolysis of lignocellulosic biomass focused on the physical properties of the bio-oil (e.g. yield, water content, and acidity) whereas pyrolysis of cellulose would focus on targeted compounds (e.g. LG and furan compounds). Besides, several studies were carried out at micro-scale, which may produce varying results upon scale-up.

Mohammed IY (2016) reported a strong interaction between cellulose and hemicellulose during pyrolysis, which would inhibit the production of LG (Yakub Mohammed, 2016). Such observation may be deduced from the current study as well, where the production of LG increased in cellulose with the oxides but decreased in EFBF. Based on Table 4 and Table 5, several contradicting results between those of biomass and of cellulose were observed as well, such as 1) yield of LG upon the utilization of CaO; 2) changes in bio-oil yield, LG, and furan compounds when MgO was added, and 3) changes in yield, water content, acidity of the bio-oil, and also LG production when ZnO employed.

5.3 Section 2: Effect of oxides on the properties of bio-oil from in-situ catalytic pyrolysis of palm empty fruit bunch fibre (EFBF)

5.3.1 Product yield

The product yields that were derived from EFBF, with and without the presence of oxides are presented in Table 19. Samples labelled as "ECaO 5%" refers to EFBF sample with 5 wt.% of CaO added; "ECaO 10%" refers to that with 10 wt.% CaO added, and so on for the other samples. The bio-oil yield obtained

from the intermediate pyrolysis of EFBF is within the range of literature, as discussed in Section 2.3. Based on the p-values obtained from ANOVA analysis as presented in Table 20, there was no adequate evidence to indicate a significant change in the bio-oil, suggesting that the addition of CaO, MgO and ZnO would not affect bio-oil yield substantially.

Table 19: Product yield from EFBF pyrolysis, with and without the presence of oxides

Samples	Bio-oil yield (wt. %)	Char yield (wt. %)	Gas yield (wt. %)*
EFBF	42.3 ± 1.5	27.2 ± 0.2	30.5 ± 1.4
ECaO 5%	39.9 ± 0.6	29.4 ± 0.7	30.7 ± 1.1
ECaO 10%	40.4 ± 0.4	30.7 ± 0.7	28.9 ± 1.1
EMgO 5%	39.3 ± 1.5	29.0 ± 0.4	31.6 ± 1.1
EMgO 10%	42.3 ± 1.8	25.7 ± 0.4	32.0 ± 1.5
EZnO 5%	44.7 ± 1.6	27.0 ± 1.5	28.2 ± 0.8
EZnO 10%	42.2 ± 0.7	26.8 ± 0.8	31.0 ± 0.4

*from difference

Upon catalytic pyrolysis, the char yields increased when CaO and MgO were utilized but remained unaffected by the employment of ZnO. For CaO, comparable results were obtained in the catalytic pyrolysis of cellulose (Section 5.2.2). As mentioned, CaO has CO_2 capture property which would form $CaCO_3$ as a product. The identification of $CaCO_3$ in the solid residual was performed in Section 5.3.4

As for the addition of MgO, the increase in char yield may be attributed to coke deposition yields, as concluded from Chapter 4 and from literature (Pütün, 2010; Stefanidis *et al.*, 2011). Coke depositions are formed from secondary reactions

or from the contaminants in the feed, which would cause the deactivation of catalysts (Bartholomew, 2001).

As observed from Table 19, the employment of the oxides did not affect the gas yields from EFBF evidently.

Table 20: p-values obtained from ANOVA analysis

Combination of data sets for comparison	p-values		
	Bio-oil yield	TAN	Water content
EFBF, CaO 5%, CaO 10%, CaO 20%	0.7414	0.0002	0.0340
EFBF, MgO 5%, and MgO 10%	0.0978	0.0036	0.0345
EFBF, ZnO 5%, and ZnO 10%	0.0924	0.3970	0.0054

5.3.2 Acidity

The pH and TAN of the bio-oils together with the ANOVA analysis p-value for TAN are presented in Table 21 and Table 20, respectively. P-values proved that the addition of CaO and MgO affect the acidity of bio-oils significantly. Among the three oxides, CaO was clearly found to be the best one for deacidification of the bio-oil and has been concluded in other studies and was discussed in Section 5.3.4.

As can be seen in Table 20, p-values that are less than or equal to 0.05 for TAN showed that besides CaO, MgO also posed great contribution in reducing the acidity of the EFBF-derived bio-oils. The change presented by the presence of ZnO was negligible. Nonetheless, based on previous studies that utilized ZnO in the catalytic pyrolysis of biomass, the results varied. Further studies were carried out to investigate the change in quantity of acidic compounds present in the bio-oils and the results are presented in Section 5.3.5.

Table 21: pH, TAN, and water content of bio-oils

Samples	pH of bio-oil	TAN of bio-oil (mg KOH/g)	Water content (wt. %)
EFBF	3.5	64.6 ± 3.9	45.0 ± 0.2
ECaO 5%	3.9	38.0 ± 2.6	47.5 ± 0.8
ECaO 10%	3.9	32.9 ± 2.2	56.6 ± 4.1
EMgO 5%	3.5	59.3 ± 1.0	55.7 ± 3.6
EMgO 10%	3.5	53.4 ± 0.2	54.6 ± 2.0
EZnO 5%	3.5	58.8 ± 4.1	53.9 ± 1.6
EZnO 10%	3.5	58.1 ± 2.8	62.4 ± 2.6

5.3.3 Water content

Generally, the total water content of bio-oil increased, as oxides tend to promote dehydration reaction of oxygenated species during pyrolysis. The water content in each bio-oil is given in Table 21 and with reference to the p-values presented in Table 20, all three oxides showed significant increase in the bio-oil water content.

In addition to dehydration reactions, the great decrease in TAN and significant increase in water content reflects the superior deacidification property of CaO, presented in Section 5.3.2. This may also interpreted as CaO has the potential of fixing oxygen-rich active groups in the bio-oil into the solid phase (Lin *et al.*, 2010).

As discussed in Section 5.2, the strong hydration ability and the dehydration of the hydrated Mg^{2+} contributes to the increase in the water content of bio-oil at elevated temperatures, like 500 ± 20 °C in current study.

The employment of ZnO showed substantial increase in the water content of bio-oil, which could be accredited to the active role of ZnO in dehydration of anhydrosugar, producing furan compounds, acetic acid, and water (Branca, Di Blasi and Galgano, 2010; Fanchiang and Lin, 2012). This explanation is to be justified in Section 5.3.5.

5.3.4 Surface structure of EFBF-derived bio-oil and biochar

As the FTIR spectra of EFBF-derived bio-oil and biochar with the addition of both 5 and 10 wt.% are similar, only those of the latter are presented in Figure 16 whereas the former is presented in Appendix 5 (Figure A.30 and Figure A.31).

The presence of a broad band in the range of 3400 – 3200 cm^{-1} can be accredited to stretching vibrations of O-H bonds in oxygenated compounds such as phenols, alcohols, and water in the bio-oil (Hassan, Steele and Ingram, 2009). Besides, C-H stretching vibrations at peaks 2924 and 2854 cm^{-1} together with C-H deformation vibrations at peaks 1458 and 1366 cm^{-1} signify the presence of methylene and methyl groups of alkanes in the bio-oil, respectively (Coates, 2006). On the other hand, presence of carbonyl groups in ketones and, aldehydes, carboxylic acids contribute to the C=O stretching vibrations at 1700 cm^{-1} whereas the presence of alkenes and aromatics contribute to C=C stretching vibrations at 1600 and 1506 cm^{-1} (Coates, 2006; Lievens *et al.*, 2011). The several peaks between 1225 and 950 cm^{-1} can be ascribed to the bending of aromatic C-H groups (Coates, 2006). Aside from that, monocyclic, polycyclic, and substituted aromatic groups can also be found in the bio-oil as shown by the transmittance peaks in the range of 900 – 700 cm^{-1} (Das, Sreelatha and Ganesh, 2004).

The introduction of CaO and MgO seem to pose several notable effects on the surface structure of the bio-oil but ZnO did not. Upon the addition of CaO and MgO, the peaks at 2924, 1700, and 1212 cm^{-1} are less intense comparatively. The weakening of the peaks shows that the addition of CaO and MgO reduced alkanes, carbonyl groups (e.g. carboxylic acids), and aromatics in the bio-oil.

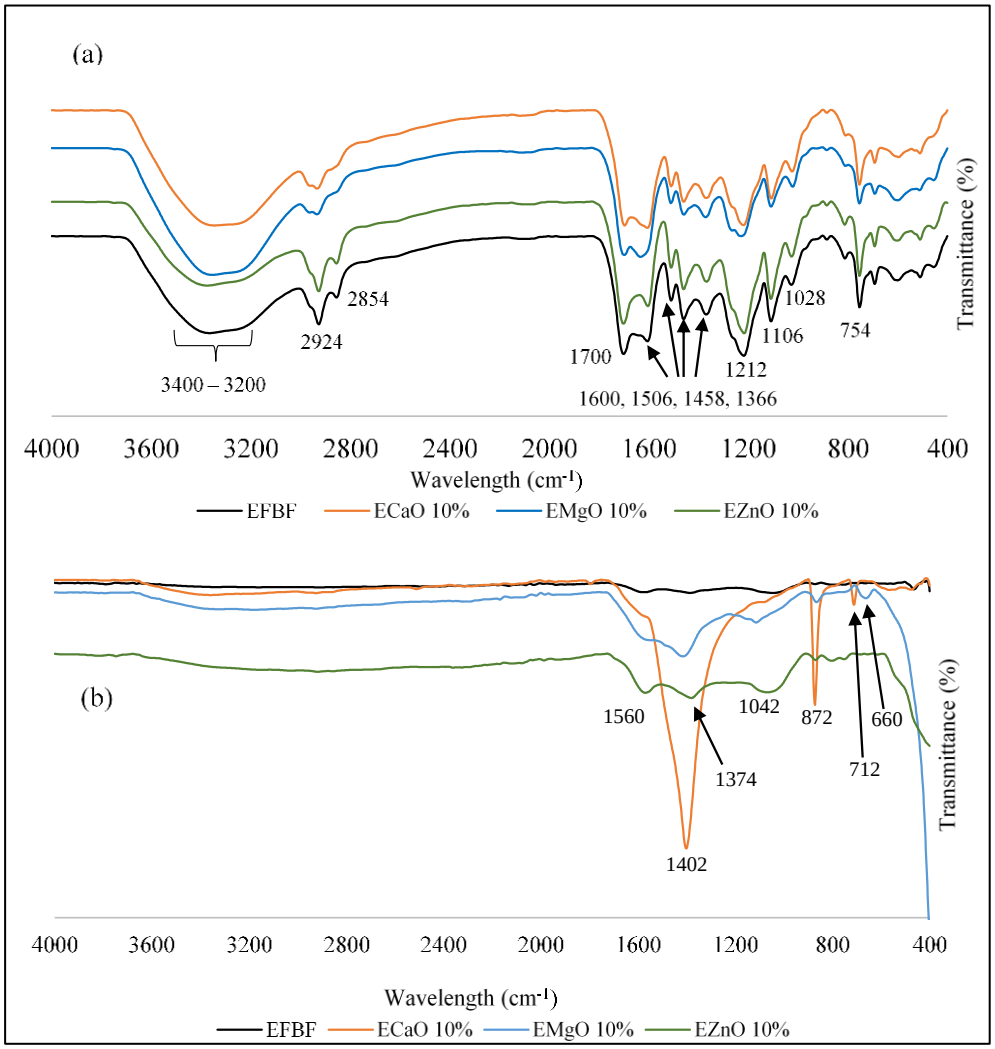

Figure 16: (a) FTIR spectra of EFBF-derived bio-oil; (b) FTIR spectra of biochar

As for biochar spectra as shown in Figure 16(b), the appearance of both peaks at 1560 and 1374 cm^{-1} can be attributed to carboxylate functional group, which reflects the presence of carboxylic acid salt (Coates, 2006). Carboxylic acid salt is the salt formed when a carboxylic acid reacts with a base, which in this study

is the oxides. The presence of the salt shows that CaO, MgO, and ZnO reacted with the acids in pyrolysis vapour prior to condensation. This in turn lowered the acidity of bio-oils, as discussed in Section 5.3.2. While the peak at 1042 cm^{-1} shows the presence of C-O in carbonyl group, that at 660 cm^{-1} shows the presence of O-H group out-of-plane bending in alcohols (Coates, 2006).

There is an obvious difference in the FTIR spectra for the remaining solids with CaO. The intense peak at 1402 cm^{-1} together with the narrow peak at 872 cm^{-1} are contributed by the carbonate ions (CO_3^{2-}) in the sample (Coates, 2006). These two peaks including the one at 712 cm^{-1} are also known to be the fundamental modes of $CaCO_3$. The presence of these peaks revealed that during the catalytic pyrolysis of EFBF with CaO, the oxide reacted with the components in the bio-oil. Similar results were obtained when cellulose was used as feed (Section 5.2.5), and concluded that as the CaO neutralizes the acids in the bio-oil, calcium carboxylate and water were formed. Then, at the temperature range of 400 – 500 °C, calcium carboxylate would decompose to form ketones and $CaCO_3$ (Wang *et al.*, 2010). The sharp drop observed for remaining solids with MgO below wavelength 600 cm^{-1} might be contributed by the scattering of infrared light. This may occur if the sample has a rough surface or contains inorganic compounds. To further characterize the solids, theoretical light scattering models such as T-matrix simulations may be further applied (Meland *et al.*, 2010).

5.3.5 Gas chromatography-mass spectrometry (GC-MS) results

The compounds that were detected via GC-MS are presented in Appendix 6 (Table A.26). Here, four of the main compounds that are typically present in

bio-oils namely acetic acid, anhydrosugar, furan compounds, and phenolic compounds are presented in Table 22.

Table 22: Quantification of main products in bio-oil in wt.%

Samples	Acetic acid (wt.%)	Anhydrosugar (wt.%)	Furan (wt.%)	Phenol (wt.%)
EFBF	1.95	0.22	0.38	1.54
ECaO 5%	1.53	0.07	0.39	1.17
ECaO 10%	0.90	0.10	0.38	0.64
EMgO 5%	2.32	0.06	0.49	1.11
EMgO 10%	2.08	0.04	0.46	0.85
EZnO 5%	2.29	0.07	0.41	1.20
EZnO 10%	2.23	0.10	0.52	1.20

5.3.5.1 Acetic acid

Acetic acid is one of the main carboxylic acids present in bio-oils, which is mainly produced from the deacetylation of hemicellulose, and a small fraction from the cracking of cellulose-derived products (Shen and Gu, 2009). With the addition of oxides, two molecules of carboxylic acids would be adsorbed by the oxides, which then produce a heavy ketone, together with CO_2 and water.

As shown in Section 5.3.2, CaO was the best oxide for the deacidification of EFBF-derived bio-oil. This can be justified from the decrement in the weight percentage of acetic acid, as presented in Table 22.

Unexpectedly, the employment of MgO and ZnO did not show reduction in the weight percentages of acetic acid as TAN revealed (Section 5.3.2), and even

slightly increased. One of the explanations is that the decrease in TAN was not contributed only by a reduction in acetic acid but also the lessening of other acids such as hexadecenoic and dodecanoic acid, as reflected from the decrease in area % of the acids, presented in Appendix 6 (Table A.26). Besides that, based on product distribution, MgO exhibited stronger effect on the secondary cracking of the bio-oil, which might have led to an increment in light compounds, such as acetic acid. Acetic acid is also a product from dehydration reactions of LG. Adam et al. reported that pore enlargement and incorporation of transition metals (e.g. Al) on such catalysts may reduce the yield of acetic acid (Adam *et al.*, 2005).

5.3.5.2 Anhydrosugars

Levoglucosan (LG) is the main anhydrosugar that is produced from the depolymerization of cellulose in lignocellulosic biomass. Table 22 reveals that with the addition of the oxides (CaO, MgO, and ZnO), the weight percentage of LG decreased substantially. As inferred from the discussion presented by Lin et al. (2010) in a comprehensive manner, a decrease in LG content is able to reflect the decrease in the oxygen content of the bio-oil (Lin *et al.*, 2010). Besides that, it was mentioned in Section 5.3.3 that LG may play an active role in dehydration of the bio-oil, producing furan compounds, acetic acid, and water. Hence, based on the observations made in the terms of increase in water content and acetic acid, together with the reduction in LG, it may be deduced that CaO, MgO, and ZnO have potential in the deoxygenation of bio-oil via dehydration.

5.3.5.3 Furfural

Furan compounds are thermally stable oxygenates that are formed from depolymerization of cellulose, hemicellulose, and from the dehydration of anhydrosugars (Liao, Wang and Ma, 2004). They are considered a bridge between renewable energy and petrochemicals, owing to them being widely used in the production of medicines, resins, fuel additives, and so on. As presented in Section 5.3.5.2, all three oxides were expected to increase the production of furan compounds. In the current study, furfural showed the highest peak among the furan compounds and except for CaO, the amount of furan compounds did increase upon the utilization of both MgO and ZnO. With the employment of 10 wt.% of ZnO, the weight percentage of furan compounds increased from 0.38 to 0.52 wt.%.

5.3.5.4 Phenol

Phenolic compounds are mainly derived from the lignin component in the biomass and contributes greatly to the high molecular weight and viscosity of bio-oils. Hence, the cracking of phenols into lighter ones is advantageous in enhancing the bio-oil quality (Lu *et al.*, 2010). Chemical compounds heavier than vanillin were classified as heavy phenols (Samolada, Papafotica and Vasalos, 2000).

Overall, the employment of CaO, MgO, and ZnO decreased the weight percentages of phenolic compounds in the bio-oil. This may be accredited to the decarbonylation property of the oxides, where oxygen is removed from the bio-oil in the form of carbon monoxide (CO), which would in turn decrease the amount of phenolic compounds (Franklin *et al.*, 1981; Chen, Chen, *et al.*, 2017).

The results from Table 22 reflects that CaO was the best oxide for deoxygenation of the bio-oil via decarbonylation.

5.3.6 Thermal stability

The selection of a suitable oxide for the study on thermal stability of the bio-oil was done based on its ability to reduce the acidity and the amount of oxygenated compounds in the bio-oil, without compromising extensively with the bio-oil yield. Upon comparing the effects of the three oxides, CaO showed better deacidification and deoxygenation abilities overall. Upon aging at both 16 h and 24 h, gum formation was observed on the walls of the sample bottles. As the gum formed was too sticky and viscous, the analysis conducted for thermal stability were done separately for the liquid and solid parts. The liquid portion of the samples were subjected to viscosity, TAN, water content, and FTIR analyses, whereas the solid fractions were studied using FTIR.

5.3.6.1 Stability analyses

Under storage conditions at an ambient of 20 °C, diesel fuel may be expected to stay in a useable condition for 12 months and 6 – 12 months at an ambient temperature higher than 30 °C. Upon aging, diesel would react with oxygen in the air to form fine sediment and gum forms. Such phenomenon is undesirable as fuel filters would be blocked, leading to the engine stopping. At the end of the aging test for diesel (ASTM D2274), having less than 20 mg/L of sediment and gum in the diesel is considered acceptable (Beyond Petroleum, 2005).

In the current study, upon aging, phase separation occurred in the bio-oil, where highly viscous and sticky gum was formed on the walls of the sample bottles and were considered as solids in this study. The formation of gum may be

explained by the polymerization of the bio-oil, studied thoroughly by Fratini et al. (2006). To summarize, lignin oligomers that was formed during pyrolysis would polymerize in the course of storage, and the heaviest lignin-rich fraction would separate out as viscous sludge (Fratini *et al.*, 2006). Upon aging EFBF bio-oil for 16 h and 24 h, the amount of solids in the raw bio-oil increased significantly, as presented in Table 23. Besides that, the change of solid content present in both raw and upgraded bio-oils is considered insignificant. This result indicates that the EFBF-derived bio-oil is unsuitable for long term storage and CaO-upgraded bio-oil did not improve the stability of the bio-oil in terms of polymerization.

Table 23: Solid content of aged bio-oil samples

	Solid content of raw bio-oil (g)	Solid content of aged bio-oil on walls of sample bottles (g)	
	t = 0	t = 16 h	t = 24 h
EFBF	0.01	0.10	0.07
ECaO 10%	0.01	0.09	0.11
ECaO 20%	0.01	0.10	0.09

Figure 17 shows the change in viscosity, TAN, and water content of the liquid sections of both raw and upgraded bio-oil with regards to time. In the current study, the viscosity of the bio-oil unexpectedly decreased upon aging, contradicting with previous studies (Abdullah, Sulaiman and Gerhauser, 2011; Meng *et al.*, 2015; Rajamohan and Kasimani, 2018). However, if the viscous portion of the aged bio-oil was taken into consideration, a different trend may be observed. As can be seen from Figure 17(a), with the increase in the weight percentages of CaO, the change in viscosity of the bio-oil was smaller. This indicates that the addition of CaO for pyrolysis reactions has the potential for

the stabilization of bio-oils to a certain extent. Nevertheless, the utilization of the catalyst should not over-compromise other properties of the bio-oil such as water content and TAN.

The decrease in viscosity of the aged bio-oils might also be affected by the increase in water content over aging time. The increment in water content is contributed by various aging reactions such as esterification (alcohols with organic acids) and acetalization (aldehydes and alcohols) (Diebold, 2000). Alongside this, though the test conditions that was applied in current study is equivalent to storing the bio-oil at ambient temperature for 1 year, this is true for bio-oils with water content of approximately 25 wt.% (Oasmaa and Peacocke, 2010). Therefore, with the application of the thermal stability test on bio-oils with high water content as such in the current study, aging effects on the viscosity of bio-oils may be dissimilar from other studies.

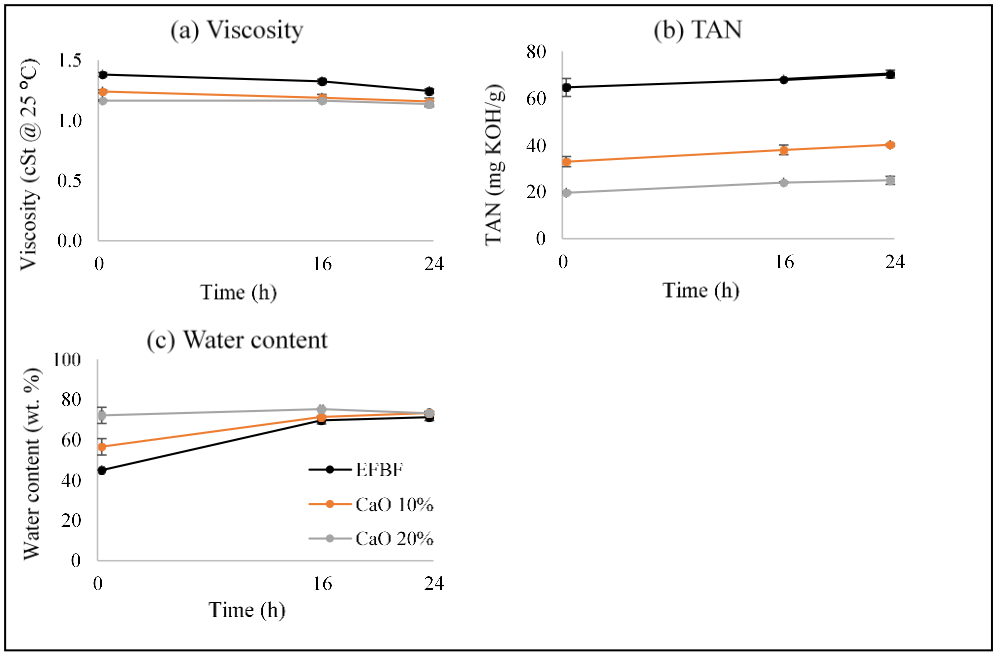

Figure 17: Change in (a) viscosity, (b) TAN, and (c) water content of 24 h aged bio-oils (liquid fraction) over time

For TAN, a slight increase was observed for all the bio-oil samples in relation to time, which may be caused by air oxidation of alcohols and aldehydes to carboxylic acids (Diebold, 2000). The current study showed that the highest increment in TAN was 7.2 wt.%, exhibited by CaO 10% bio-oil upon being aged for 24 h.

5.3.6.2 Surface structure of aged bio-oil (liquid and solid fractions)

The FTIR spectra of aged bio-oil (16 h and 24 h) for both liquid and solid fractions are presented in Appendix 7 (liquid: Figure A.32 and Figure A.33; solid: Figure A.34 and Figure A.35), where aged samples of both 16 h and 24 h exhibited similar spectra. Compared to the bio-oil before aging, in the liquid fraction, peaks that relate the deformation vibration of C-H bonds (2924, 2854, 1458, and 1366 cm^{-1}) to the presence of alkanes in the bio-oil disappeared. Bending of aromatic C-H groups that were indicated from peaks between 1225 and 950 cm^{-1} faded as well. The vanishing of the peaks reveals the breakage of C-H bonds during aging. On the other hand, a peak at 1634 cm^{-1} in the liquid fraction of aged bio-oil appeared, which can be accredited to alkenyl C=C stretch. However, Meng et al. (2015) attributed the increase in C=C bond to newly formed bio-oil compounds that have non-aromatic double bonds (e.g. furfural or olefins) that are produced from the dehydration reactions of sugar, instead of aromatic hydrocarbon. This is because aromatic hydrocarbons are expected to be stable upon aging. (Meng *et al.*, 2015).

On the other hand, in comparison with the FTIR spectra of raw bio-oil presented in Section 5.2.6, the FTIR spectra of the solid fraction is closely similar. The observations are all similar for bio-oil samples, produced with and without the presence of CaO.

5.4 Concluding remarks

The catalytic effects of the calcium oxide (CaO), magnesium oxide (MgO), and zinc oxide (ZnO) on the enhancement of bio-oil from cellulose and empty fruit bunch fibre (EFBF) were evident for intermediate pyrolysis, in terms of reducing the amounts of acids and oxygenated compounds to form compounds such as furan compounds. Comparatively, among the three oxides, CaO exhibited the best performance in terms of reducing the acidity for the bio-oils whereas MgO and ZnO were good in deoxygenation of the bio-oils via dehydration. One of the favourable notes is that the bio-oil yields were not affected by the oxides upon upgrading.

Section 1 of the chapter compiled the reaction pathways involved in bio-oil upgrading when the oxides were used. Upon comparing the results of current study with literature, though the reaction pathways are agreeable, the effects of the oxides on the physical properties of the bio-oils varied. This may be attributed to the difference in feed, operating conditions, scale of experiment, amount of oxides used, and type of reactors. Hence, the study may be used as a reference to get an overview of the reactions involved but may not exactly reflect the absolute effects of the oxides on bio-oil properties.

Upon selecting CaO as the oxide with the best performance, Section 2 of the chapter further investigated the effects of the CaO on EFBF bio-oil aging. The addition of CaO for pyrolysis reactions showed potential in stabilizing the EFBF-derived bio-oil in terms of viscosity without influencing the surface structure of the bio-oil but not the polymerization of bio-oil. Nevertheless, the utilization of the oxide should not over-compromise other properties of the bio-oil such as the water content and acidity.

CHAPTER 6

6 CONCLUSIONS AND FUTURE WORK

6.1 Introduction

The aim of the current project was to investigate the effects of oxides, namely calcium oxide (CaO), magnesium oxide (MgO), and zinc oxide (ZnO) on the upgrading of bio-oil, which was derived from palm empty fruit bunch fibre (EFBF) via catalytic intermediate pyrolysis. Cellulose was utilized as feed to study the effects of the oxides on lignocellulosic biomass at the simplest form. The project started with evaluating the effects of oxides on the kinetics and mechanisms involved, and then to examining the influences on the physical properties of bio-oil. The current chapter presents the key findings for the project and recommendations for future work.

6.2 Conclusions

The key findings for chapters 4 and 5 are as follows:

- The addition of MgO and ZnO did not affect the degradation behaviour of both cellulose and EFBF. Nevertheless, because CaO is prone to adsorb moisture and carbon dioxide (CO_2), an additional weight loss stage was observed for both studies. As EFBF consists of other components such as hemicellulose and lignin, the effects of the oxides on devolatilization of EFBF is more significant than in cellulose. Even though the oxides did not affect the activation energy and mechanism of EFBF devolatilization, the amount of volatiles released reduced due to the restriction posed by the oxides, because of coking (MgO and ZnO)

and formation of other compounds (e.g. calcium hydroxide and calcium carbonate, formed from CaO). For pyrolysis samples, the amount of volatiles released reduced by 36.2 %, 14.3 %, and 11.5 %, when 10 wt.% of CaO, MgO, and ZnO were introduced, respectively. Despite hinting the existence of catalytic effects exerted by the oxides, the alteration of the oxides at the end of the experiment categorizes CaO, MgO, and ZnO as catalytic additives, rather than catalysts. (Chapter 4)

- CaO, MgO, and ZnO were able to enhance the bio-oil quality via deacidification and deoxygenation (e.g. dehydration, decarbonylation, and decarboxylation) reactions without affecting the bio-oil yields of EFBF (42.3 wt.%), which is a favourable finding. While the utilization of cellulose as feed may act as a guide to understand the effects of CaO, MgO, and ZnO on the physical properties of bio-oil, the effects may not be absolute for all biomasses. CaO-upgraded bio-oil showed improvement in stability in terms of viscosity but not in polymerization of the bio-oil, as compared to those of raw EFBF-derived bio-oil. (Chapter 5)

The key findings obtained in the current project showed that CaO, MgO, and ZnO are promising oxides for enhancing the quality of EFBF-derived bio-oil with the role as catalytic additives. Each of the oxides is superior in varying properties of the bio-oil during catalytic pyrolysis (e.g. increment in furan compounds). Hence, based on the targeted compounds and properties of the bio-oil, the selection of oxides may vary.

To date, a number of industrial scale demonstration of pyrolysis technologies are available. Nevertheless, one of the challenges faced is the high cost in bio-

oil upgrading processes and low bio-oil yield. Based on the conclusions drawn from this work, CaO, MgO, and ZnO have the potential to improve the bio-oil quality in the upstream processing and so, would make downstream bio-oil upgrading more sustainable. In addition, these oxides are relatively cheap and may be obtained from natural resources. Hence, for industrial applications, the utilization of theses oxides as catalytic additives is favourable due to the low cost and abundance. Moreover, since CaO is basic oxide, it can be used as catalysts for esterification. Therefore, some studies were conducted in order to evaluate CaO as a catalyst for esterification.

6.2.1 Preliminary study for future work (Esterification of empty fruit bunch fibre (EFBF)-derived bio-oil with calcium oxide (CaO) and methanol (MeOH))

The utilization of calcium oxide (CaO) for biofuel production via processes such as catalytic pyrolysis and transesterification showed great potential and studies have been flourishing. Nevertheless, the investigation of CaO as catalyst for esterification of bio-oil has not been carried out. Ideally, the intrinsic carboxylic acids in the bio-oil would be converted to esters. The current section presents the experiment carried out to investigate the prospective of CaO in the esterification of empty fruit bunch fibre (EFBF)-derived bio-oil with methanol (MeOH).

6.2.1.1 Variation of methanol (MeOH) volume

Initially, esterification experiments were carried out with 1.5 wt.% of CaO (with respect to raw bio-oil) while volume ratio of methanol (MeOH)/bio-oil was varied from 0 to 1. As observed from Table 24, even when no MeOH was added,

acid conversion of approximately 27 % was achieved. This may be attributed to the neutralization effect posed by the CaO catalyst. Upon the addition of MeOH, the acid conversion increased to approximately 30 % at MeOH/bio-oil volume ratio of 0.5 and remained the same at higher ratios.

Table 24: Acid conversion (%) at varying volume ratios of MeOH/bio-oil with 1.5 wt.% of CaO at reaction temperature of 50 °C for 5 h

Volume ratio of MeOH/bio-oil	Acid conversion (%)
0	27.7 ± 0.7
0.25	29.3 ± 1.7
0.50	30.2 ± 2.6
0.75	30.2 ± 0.4
1	30.3 ± 0.8

When the alcohol is in excess, higher reactions rates and higher equilibrium conversions are bound to occur as the reaction would be driven towards completion (Yaakob and Bhatia, 2004; Ding, Xia and Lu, 2012). In the current study, the maximum conversion was achieved at MeOH/bio-oil volume ratio of 0.5 when 1.5 wt.% of CaO (with respect to raw bio-oil) was employed.

6.2.1.2 Variation of CaO catalyst added

At constant MeOH/bio-oil volume ratio of 0.5, the amount of CaO (wt.% of raw bio-oil) added to the reaction was manipulated. Based on the observation from Figure 18, acid conversion increased with the amount of CaO to approximately 100 % when 5 wt.% of CaO (with respect to raw bio-oil) was added to the reaction. According to Wang et al. (2010), the esterification degree of intrinsic acids in bio-oil is reflected by the change in total acid number (TAN) (Wang,

Chang and Fan, 2010). Nevertheless, as CaO is basic and an efficient deacidification catalyst, a challenge lies in differentiating whether the decrease in bio-oil acidity is contributed by esterification or neutralization reaction. Hence, further analyses were carried out and presented in Section 6.2.1.5 to identify the major contributor.

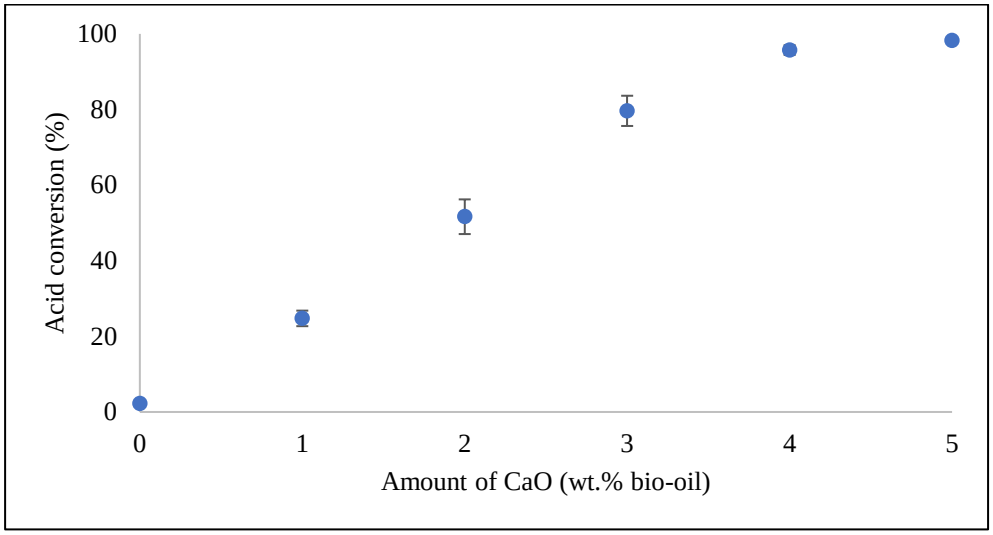

Figure 18: Conversion of intrinsic acids in bio-oil over varying amounts of CaO with MeOH/bio-oil volume ratio of 0.5 at reaction temperature of 50 °C for 5 h

Esterification (Eqn. 9) involves the reaction of carboxylic acids with MeOH in the presence of a catalyst to esters. On the other hand, neutralization (Eqn. 10) occurs upon the reaction of the acids with CaO to form their respective salts and water (Wang *et al.*, 2010). As acetic acid (CH_3COOH) is one of the common carboxylic acids in bio-oils, acetic acid is taken as the model acid and the reaction equations are presented as follows:

Esterification

$$CH_3COOH + CH_3OH \leftrightarrow CH_3COOCH_3 + H_2O \quad (9)$$

Neutralization

$$2\ CH_3COOH + CaO \rightarrow Ca(CH_3COO)_2 + H_2O \quad (10)$$

6.2.1.3 Water content

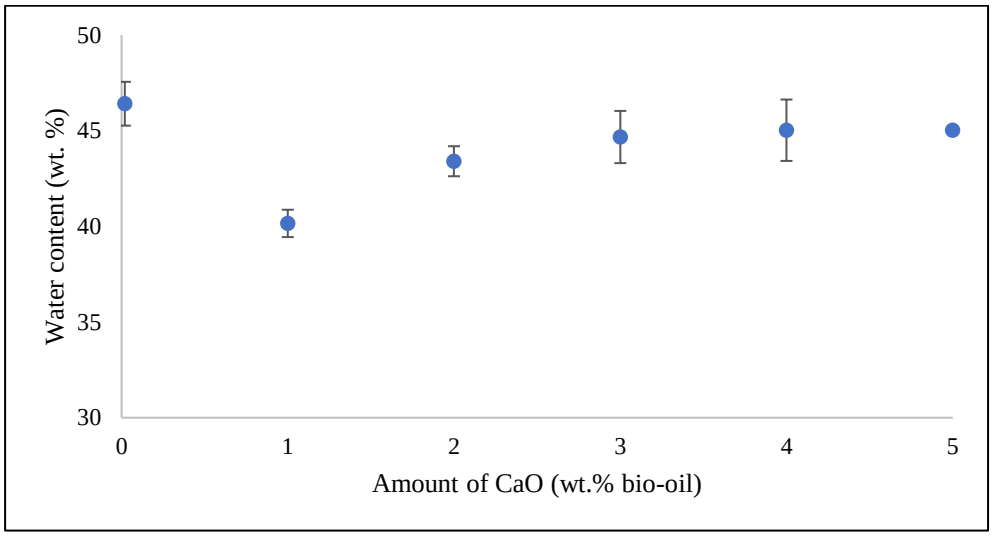

Figure 19: Water content of mixture after reaction over varying amounts of CaO

As mentioned in the previous Section 6.2.1.2, two of the reactions that may occur upon the addition of CaO are neutralization and esterification. A common side product obtained from the reactions is water.

The presence of water is disadvantageous as it would participate in the hydrolysis of esters (reverse reaction) back to starting materials, which in turn reduces acid conversion efficiency (Sundqvist, Oasmaa and Koskinen, 2015). The optimum water content in bio-oil for positive effects in terms of speeding up the reaction and increasing the purity of methyl ester via transesterification is 3 wt.% (Prasertsit, Phoosakul and Sukmanee, 2014). As observed from Figure 19, the addition of CaO reduced the amount of water in the bio-oil mixture, which may be attributed to the reaction of CaO with water to form calcium hydroxide ($(CaOH)_2$). Then, the water content of the mixture increased with the increase in CaO added, indicating the occurrence of neutralization and esterification reactions.

6.2.1.4 Solid content

Upon centrifuge, the insignificant amount of solids left on the centrifuge tube led to the deduction that CaO was unrecyclable in the current study. Nevertheless, the little amount of solids that were left on the centrifuge tube of 0.5M5C sample was retrieved and subjected to analysis, presented in Section 6.2.1.6.

The solid content of the mixtures after reaction was determined and compared to theoretical values. As observed from the results presented in Figure 20, the solid contents of the mixtures increased non-linearly with the amount of CaO added and are lower than the theoretical values. These indicate that a fraction of CaO did dissolve in MeOH.

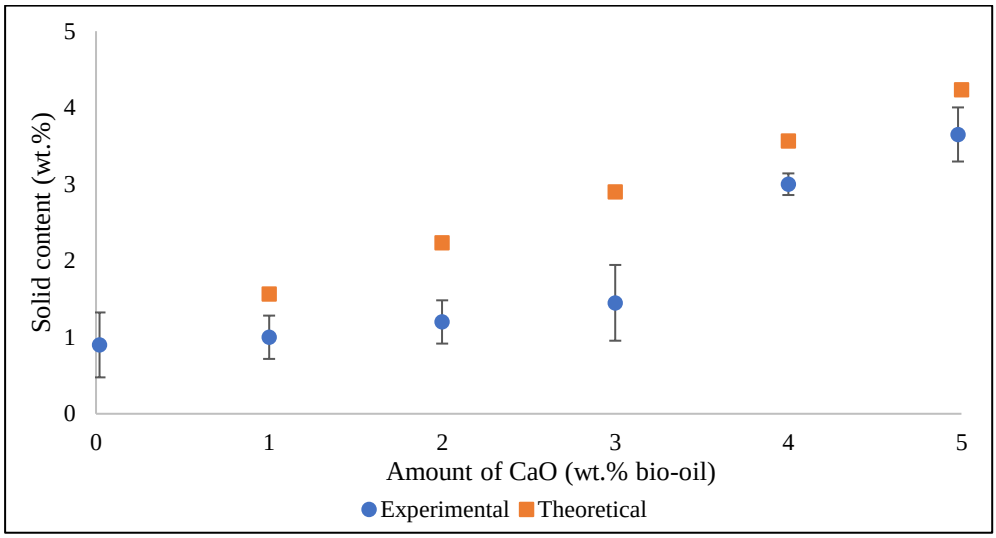

Figure 20: Solid content of mixture after reaction over varying amounts of CaO

Similar observation was made in transesterification reactions, where Urasaki et al. (2012) attributed the observation to the dissolution of CaO in MeOH. In addition, Yan et al. (2007) observed that CaO existed as suspensoid in the reaction mixture due to its poor mechanical strength (Yan *et al.*, 2007; Urasaki *et al.*, 2012). The unavailability to separate CaO from the bio-oil mixture after

reaction poses negative effects such as equipment blockage. To ease the removal of CaO, supporting of CaO onto carriers may be beneficial.

6.2.1.5 Methyl acetate and acetic acid in bio-oil

Identification of acetic acid and methyl acetate in the bio-oils were carried out using gas chromatography-flame ionization detector (GC-FID) and were quantified using external standard method. The results are presented in Figure 21.

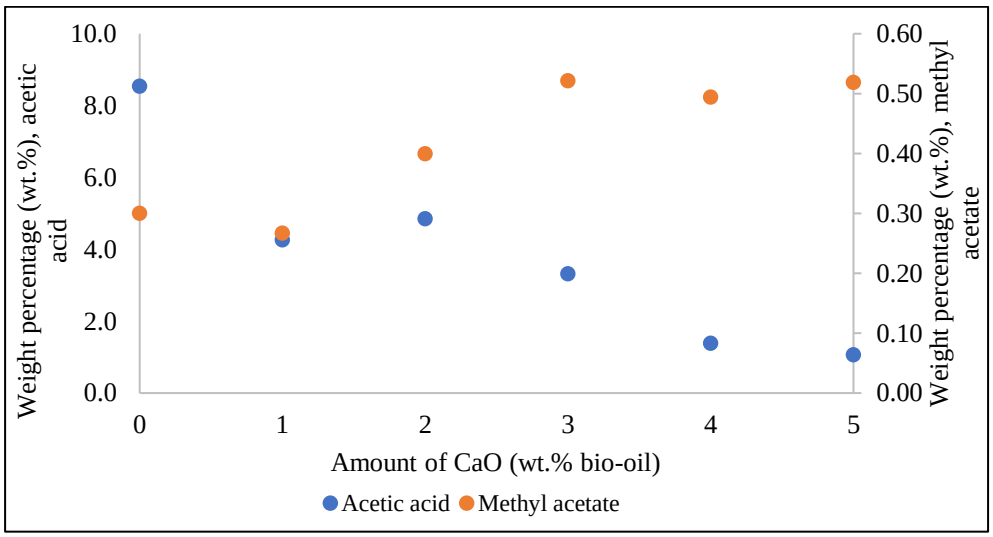

Figure 21: Weight percentages (wt.%) of acetic acid and methyl acetate in bio-oil mixture with varying amounts of CaO

As can be observed, with the increase in CaO, weight percentage of acetic acid decreased whereas that of methyl acetate increased. This indicates the occurrence of esterification reactions in the bio-oil mixture. Upon the addition of 5 wt.% CaO, methyl acetate in bio-oil increased by 72.9 wt.% as compared to that without CaO addition.

Knowing from Eq. (9) that one mole of acetic acid would produce one mole of methyl acetate upon esterification, the change in moles for acetic acid and

methyl acetate were both calculated. By comparing the mole percentages of the compounds with and without the presence of 5 wt.% CaO, acetic acid decreased by 87.5 mol %. Nevertheless, of the acetic acid converted, only 15.8 mol % may be attributed to the formation of methyl acetate. Therefore, it may be inferred that the neutralization reaction of acetic acid was more dominant than the esterification reaction of acetic acid to methyl acetate.

6.2.1.6 Surface properties of mixture and solids

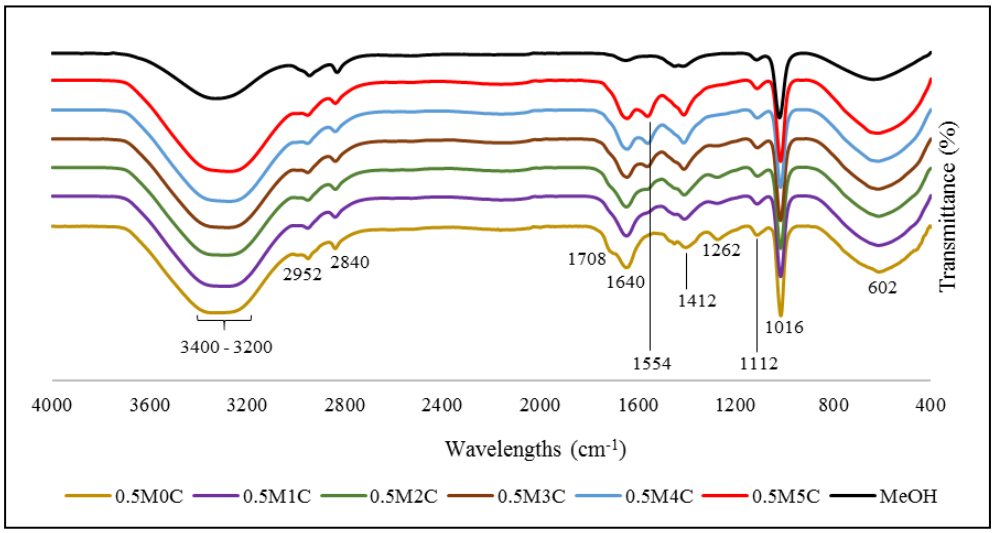

Figure 22: FTIR spectra of bio-oil mixtures with various amounts of CaO and constant MeOH/bio-oil volume ratio of 0.5

The FTIR spectra of the bio-oil mixtures after reaction are presented in Figure 22, together with that of MeOH to exclude the influence of MeOH in the bio-oil mixtures. The broad band observed in the range of 3400 – 3200 cm^{-1} and may be ascribed to stretching vibrations of O-H bonds in oxygenated compounds (e.g phenols, alcohols, and water) in the bio-oil (Hassan, Steele and Ingram, 2009). Next, appearance of both peaks at 2952 and 2840 cm^{-1} reveals the presence of methyl C-H stretch, which in the current study, may be deduced to be contributed by MeOH (Coates, 2006). Following that, the peak at 1708

cm^{-1} may be accredited to C=O stretching vibration in carboxylic acids (Lievens *et al.*, 2011). The peak at 1640 cm^{-1} may be assigned to C-C bonds, contributed by alkenes or by unsaturated carboxylic acids (Rutkowski and Kubacki, 2006). Subsequently, the presence of both peaks at 1554 and 1412 cm^{-1} may be ascribed to carboxylic acid salt (carboxylate) (Coates, 2006). The peak at 1262 cm^{-1} may be contributed by C-O vibrations from alcohol and phenol (Elleuch, Halouani and Li, 2016). While both peaks at 1112 and 1016 cm^{-1} have been fingerprinted as C-O stretch in MeOH, the peak at 602 cm^{-1} may be ascribed to O-H out-of-plane bend of alcohol (Coates, 2006; Coldea *et al.*, 2013).

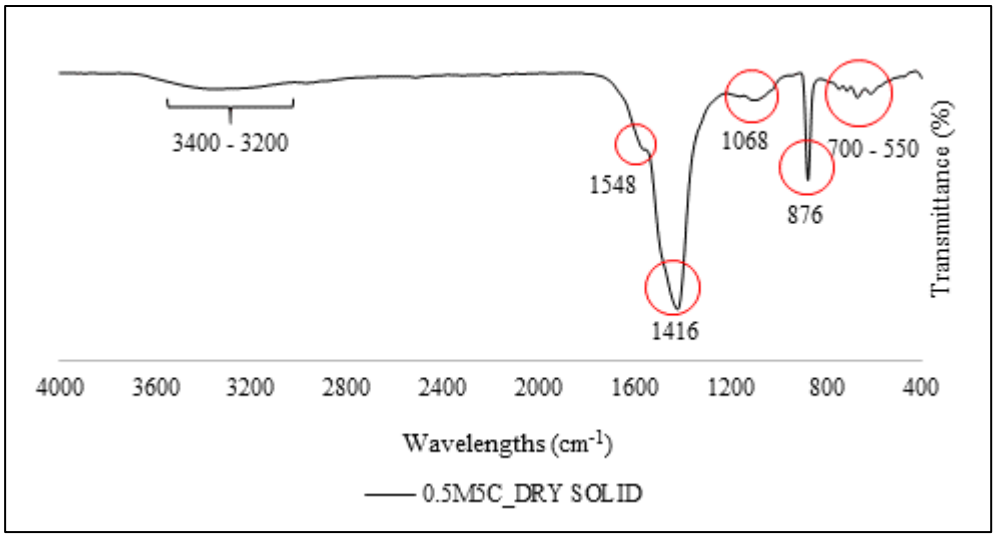

Figure 23: FTIR of solids retrieved from bio-oil mixture with 5 wt.% CaO and MeOH/bio-oil volume ratio of 0.5

With the increase in CaO amount added to the bio-oil mixture, the peak regarding carboxylic acids (1708 cm^{-1}) disappears whereas both peaks contributed by carboxylates (1554 and 1412 cm^{-1}) increase in intensity. Such observation reveals the neutralization reaction of CaO with the intrinsic carboxylic acids in bio-oil such as acetic acid to form their respective

carboxylates (e.g. calcium acetate). The FTIR spectra did not show strong indication of esters in the bio-oil mixtures.

Solid that were retrieved from 0.5M5C samples after centrifuge were washed with ethanol and dried in the oven at 70 ˚C. The FTIR spectrum of the dried solid is presented in Figure 23. The appearance of both peaks at 1548 and 1416 cm^{-1} may be ascribed to the presence of carboxylate, a product from the neutralization of intrinsic carboxylic acids in the bio-oil sample by CaO. Similarly, the pair of peaks at 1416 and 876 cm^{-1} may be attributed to carbonate ion (CO_3^{2-}), probably from calcium carbonate ($CaCO_3$) (Coates, 2006). CaO captures CO_2 even at ambient temperature to form $CaCO_3$, which would only decompose at 700 °C. Here, CaO might have captured CO_2 from air to form $CaCO_3$ and since the experiments in the current study were carried out at 50 °C, the $CaCO_3$ remained as solids in the bio-oil mixture even after the experiments (Kwon *et al.*, 2018). As for the weak peaks at 3400 – 3200, 1068, and 700 – 550 cm^{-1}, they may be accredited to O-H stretch, C-O stretch, and O-H out-of-plane bend in alcohol, respectively (Coates, 2006). Upon washing and drying, all alcohols are expected to have evaporated from the solids. Nevertheless, calcium carboxylates (e.g calcium acetate) in the bio-oil mixture might have reacted with ethanol during washing and precipitate to form a gel. Hence, a fraction of alcohol residue was left in the dried solids.

6.2.1.7 Concluding remarks

The potential of calcium oxide (CaO) in esterification of bio-oil from fast pyrolysis of palm empty fruit bunch fibre (EFBF) with methanol (MeOH) was investigated. The esterification degree of the bio-oil was initially based on the change in the total acid number (TAN) of the bio-oil. When 5 wt.% of CaO

(with respect to bio-oil) was added, the conversion of acids was almost complete. Nevertheless, since CaO is a basic oxide and would neutralize the acids in the bio-oil, a challenge laid in determining the dominant reaction that reduced the amount of acid in the bio-oil. Upon quantifying the weight percentages of both methyl acetate and acetic acid in the bio-oil and calculating their change in mole weight percentages, it was deduced that the neutralization reaction of acetic acid in the bio-oil is more superior to the esterification reaction.

6.3 Future work

The current project was able to provide an insight on the positive effects of CaO, MgO, and ZnO in the catalytic upgrading of bio-oil via catalytic intermediate pyrolysis. While the prospective of these oxides in biofuel upgrading were observed, limitations were recognized. One of the limits is the quenching of vapours in the pyrolysis system, where a fraction of vapours escaped from the condensers. Besides that, the current study did not investigate the scalability and economics of the process, which may incur more challenges. Even though the current study was able to provide significant insights on utilizing oxides for catalytic intermediate pyrolysis, further investigation on the applicability of the upgraded bio-oil in current available technologies or engines is required.

The properties of the upgraded bio-oil may be further enhanced to develop a more ideal system for biofuel production. Further improvements and future works are recommended based on the current work to provide a more comprehensive understanding and evaluation on the subject.

- In the preliminary study for the future work (Section 6.2.1), where EFBF-derived bio-oil was subjected to esterification reaction in the

presence of CaO and methanol, it was observed that neutralization reaction was more dominant than esterification reaction. Hence, further study on the effects of CaO on the other major compounds in the bio-oil (e.g. levoglucosan, furan compounds, and phenolic compounds) may be carried out to explore the potential of CaO in improving the bio-oil quality under esterification conditions. In addition, esterification studies with MgO and ZnO may be explored.

- Upon the catalytic pyrolysis of EFBF with CaO, MgO, and ZnO, the amount of levoglucosan (LG) in the bio-oil decreased significantly as compared to raw bio-oil. Since LG was identified as one of the compounds that is responsible for the immiscibility of bio-oil with diesel, the emulsification of the upgraded bio-oil with diesel may be further explored.
- As received from palm oil mills, palm wastes such as EFBF have considerably high-water contents (approximately 67 wt.%), the pre-drying of EFBF requires high energy cost. Since hydrothermal liquefaction of biomass does not require pre-drying of the biomass for biofuel production, catalytic hydrothermal liquefaction of EFBF with the oxides (CaO, MgO, and ZnO) might be worth studying.

REFERENCES

Abdullah, N. and Gerhauser, H. (2008) ‘ Bio-oil derived from empty fruit bunches’, *Fuel*. Elsevier, 87(12), pp. 2606–2613. doi: 10.1016/j.fuel.2008.02.011.

Abdullah, N. and Sulaim, F. (2013) ‘ The Oil Palm Wastes in Malaysia’, in *Biomass Now - Sustainable Growth and Use*. doi: 10.5772/55302.

Abdullah, N., Sulaiman, F. and Gerhauser, H. (2011) ‘ Characterisation of oil palm empty fruit bunches for fuel application’, *Journal of Physical Science*, 22(1), pp. 1–24.

Abnisa, F. *et al.* (2013) ‘ Characterization of Bio-oil and Bio-char from Pyrolysis of Palm Oil Wastes’, *Bioenergy Research*, 6(2), pp. 830–840. doi: 10.1007/s12155-013-9313-8.

Abnisa, F., Mohd, W. and Daud, A. W. (2014) ‘ A review on co-pyrolysis of biomass: An optional technique to obtain a high-grade pyrolysis oil’, *Energy Conversion and Management*, 87, pp. 71–85. doi: 10.1016/j.enconman.2014.07.007.

Abu Bakar, M. S. and Titiloye, J. O. (2013) ‘ Catalytic pyrolysis of rice husk for bio-oil production’, in *Journal of Analytical and Applied Pyrolysis*. Elsevier, pp. 362–368. doi: 10.1016/j.jaap.2012.09.005.

Adam, J. *et al.* (2005) ‘ Pyrolysis of biomass in the presence of Al-MCM-41 type catalysts’, *Fuel*, 84(12–13), pp. 1494–1502. doi: 10.1016/j.fuel.2005.02.006.

Adhikari, S., Thangalazhy-Gopakumar, S. and Taylor, S. (2012) ‘ Integrated Forest Biorefineries: Gasification and Pyrolysis for Fuel and Power Production’, in *Integrated Forest Biorefineries: Challenges and Opportunities*. The Royal Society of Chemistry, pp. 211–255. doi: 10.1039/9781849735063-00211.

Ahmad, R., Rohim, R. and Ibrahim, N. (2014) ‘ Effect of Pyrolysis Parameter and Catalyst on Oil Production from Empty Fruit Bunch’, pp. 10–11. Available at: https://www.researchgate.net/publication/277916868.

Ahmed, Y. A. (2013) ‘ Standard Test Method for Ash from Petroleum Products’, *ASTM International*, pp. 8–11. doi: 10.1520/D0482-13.In.

Aho, A. *et al.* (2008) ‘ Catalytic pyrolysis of woody biomass in a fluidized bed reactor: Influence of the zeolite structure’, *Fuel*. Elsevier, 87(12), pp. 2493–2501. doi: 10.1016/J.FUEL.2008.02.015.

Akhtar, J. and Saidina Amin, N. (2012) ‘ A review on operating parameters for optimum liquid oil yield in biomass pyrolysis’, *Renewable and Sustainable Energy Reviews*, pp. 5101–5109. doi: 10.1016/j.rser.2012.05.033.

Alshehri, S. . *et al.* (2000) ‘ Kinetics of the thermal decomposition of γ-irradiated cobaltous acetate’, *Thermochimica Acta*, 363(1), pp. 61–70. doi: 10.1016/S0040-6031(00)00602-X.

Anja, O. (2013) ‘ Development of Stability Test for Fast Pyrolysis Bio-oils’, (May), pp. 1–11. Available at: http://www.pyne.co.uk/Resources/user/Development of Stability Test for Fast Pyrolysis Bio_v6.pdf.

Aphane, M. E. (2009) ‘ The Hydration of Magnesium Oxide With Different Reactivities by Water and Magnesium Acetate’, *Thesis*, (March). Available at: http://uir.unisa.ac.za/handle/10500/2326.

Asadieraghi, M. and Wan Daud, W. M. A. (2015) ‘ In-situ catalytic upgrading of biomass pyrolysis vapor: Using a cascade system of various catalysts in a multi-zone fixed bed reactor’, *Energy Conversion and Management*, 101, pp. 151–163. doi: 10.1016/j.enconman.2015.05.008.

Auta, M., Ern, L. M. and Hameed, B. H. (2014) ‘ Fixed-bed catalytic and non-catalytic empty fruit bunch biomass pyrolysis’, *Journal of Analytical and Applied Pyrolysis*, 107(Supplement C), pp. 67–72. doi: 10.1016/j.jaap.2014.02.004.

Bajpai, P. (2016) ‘ Structure of Lignocellulosic Biomass’, in, pp. 7–12. doi: 10.1007/978-981-10-0687-6_2.

Balasundram, V. *et al.* (2018) ‘ Thermogravimetric catalytic pyrolysis and kinetic studies of coconut copra and rice husk for possible maximum production of pyrolysis oil’, *Journal of Cleaner Production*, 167, pp. 218–228. doi: 10.1016/j.jclepro.2017.08.173.

Baldwin, R. M. and Feik, C. J. (2013) ‘ Bio-oil stabilization and upgrading by hot gas filtration’, *Energy and Fuels*, 27(6), pp. 3224–3238. doi: 10.1021/ef400177t.

Barrios, A. M. *et al.* (2018) ‘ Hydrodeoxygenation of phenol over niobia supported Pd catalyst’, *Catalysis Today*. Elsevier, 302, pp. 115–124. doi: 10.1016/j.cattod.2017.03.034.

Bartholomew, C. H. (2001) ‘ Mechanisms of catalyst deactivation’, *Applied Catalysis A: General*, 212(1–2), pp. 17–60. doi: 10.1016/S0926-860X(00)00843-7.

BE-Sustainable (2012) *Malaysia’ s biomass potential*. Available at: http://www.besustainablemagazine.com/cms2/malaysias-biomass-potential/.

Bensidhom, G. *et al.* (2018) ‘ Pyrolysis of Date palm waste in a fixed-bed reactor: Characterization of pyrolytic products’, *Bioresource Technology*, 247, pp. 363–369. doi: 10.1016/j.biortech.2017.09.066.

Beyond Petroleum (2005) ‘ Long Term Storage of Diesel’, pp. 1–3. Available at: http://www.bp.com/content/dam/bp-country/en_au/media/fuel-news/long-term-storage-diesel.pdf.

Bhagiyalakshmi, M., Lee, J. Y. and Jang, H. T. (2010) ‘ Synthesis of mesoporous magnesium oxide: Its application to CO2 chemisorption’, *International Journal of Greenhouse Gas Control*, 4(1), pp. 51–56. doi: 10.1016/j.ijggc.2009.08.001.

Branca, C., Di Blasi, C. and Galgano, A. (2010) ‘ Pyrolysis of corncobs catalyzed by zinc chloride for furfural production’, *Industrial and Engineering Chemistry Research*, 49(20), pp. 9743–9752. doi: 10.1021/ie101067v.

Bu, Q. *et al.* (2016) ‘ A thermal behavior and kinetics study of the catalytic pyrolysis of lignin’, *RSC Adv.* Royal Society of Chemistry, 6(103), pp. 100700–100707. doi: 10.1039/C6RA22967K.

Bui, V. N. *et al.* (2011) ‘ Hydrodeoxygenation of guaiacol with CoMo

catalysts. Part I: Promoting effect of cobalt on HDO selectivity and activity', *Applied Catalysis B: Environmental*. Elsevier, 101(3–4), pp. 239–245. doi: 10.1016/J.APCATB.2010.10.025.

Cheah, W. Y. *et al.* (2018) ' Microalgae cultivation in palm oil mill effluent (POME) for lipid production and pollutants removal', *Energy Conversion and Management*, 174, pp. 430–438. doi: 10.1016/j.enconman.2018.08.057.

Chen, D., Li, M. and Zhu, X. (2012) ' TG-DSC method applied to drying characteristics and heat requirement of cotton stalk during drying', *Heat and Mass Transfer/Waerme- und Stoffuebertragung*, 48(12), pp. 2087–2094. doi: 10.1007/s00231-012-1050-6.

Chen, T. *et al.* (2011) ' Effect of hot vapor filtration on the characterization of bio-oil from rice husks with fast pyrolysis in a fluidized-bed reactor', *Bioresource Technology*, 102(10), pp. 6178–6185. doi: 10.1016/j.biortech.2011.02.023.

Chen, X., Yang, H., *et al.* (2017) ' Catalytic fast pyrolysis of biomass to produce furfural using heterogeneous catalysts', *Journal of Analytical and Applied Pyrolysis*. Elsevier, 127, pp. 292–298. doi: 10.1016/j.jaap.2017.07.022.

Chen, X., Chen, Y., *et al.* (2017) ' Fast pyrolysis of cotton stalk biomass using calcium oxide', *Bioresource Technology*, 233, pp. 15–20. doi: 10.1016/j.biortech.2017.02.070.

Cheng, S., Li, A. and Yoshikawa, K. (2015) ' High Quality Oil Recovery from Oil Sludge Employing a Pyrolysis Process with Oil Sludge Ash

Catalyst', *International Journal of Waste Resources*. OMICS International, 05(02). doi: 10.4172/2252-5211.1000176.

Chiaramonti, D. *et al.* (2003) ' Development of emulsions from biomass pyrolysis liquid and diesel and their use in engines - Part 1: Emulsion production', *Biomass and Bioenergy*, 25(1), pp. 85–99. doi: 10.1016/S0961-9534(02)00183-6.

Chong, C. *et al.* (2015) ' The use of energy in Malaysia: Tracing energy flows from primary source to end use', *Energies*, 8(4), pp. 2828–2866. doi: 10.3390/en8042828.

Chow, L. W. *et al.* (2018) ' Sludge as a Relinquishing Catalyst in Co-Pyrolysis with Palm Empty Fruit Bunch Fiber', *Journal of Analytical and Applied Pyrolysis*. doi: 10.1016/j.jaap.2018.03.015.

Claudinho, J. E. M. and Ariza, O. J. C. (2017) ' A study on thermo - Catalytic degradation of PET (polyethylene terephthalate) waste for fuel production and chemical products', *Chemical Engineering Transactions*, 57, pp. 259–264. doi: 10.3303/CET1757044.

Coates, J. (2006) ' Interpretation of Infrared Spectra, A Practical Approach', in *Encyclopedia of Analytical Chemistry*. John Wiley & Sons, Ltd. doi: 10.1002/9780470027318.a5606.

Coats, A. W. and Redfern, J. P. (1964) ' Kinetic Parameters from Thermogravimetric Data', *Nature*, 201(4914), pp. 68–69. doi: 10.1038/201068a0.

Coldea, T. E. *et al.* (2013) ' Rapid quantitative analysis of ethanol and

prediction of methanol content in traditional fruit brandies from romania, using FTIR spectroscopy and chemometrics', *Notulae Botanicae Horti Agrobotanici Cluj-Napoca*, 41(1), pp. 143–149.

Collard, F.-X. and Blin, J. (2014) ' A review on pyrolysis of biomass constituents: Mechanisms and composition of the products obtained from the conversion of cellulose, hemicelluloses and lignin', *Renewable and Sustainable Energy Reviews*, 38, pp. 594–608. doi: 10.1016/j.rser.2014.06.013.

Cooley, S. and Antal, M. J. (1988) ' Kinetics of cellulose pyrolysis in the presence of nitric oxide', *Journal of Analytical and Applied Pyrolysis*, 14(2–3), pp. 149–161. doi: 10.1016/0165-2370(88)85005-8.

Cortés, A. M. and Bridgwater, A. V. (2015) ' Kinetic study of the pyrolysis of miscanthus and its acid hydrolysis residue by thermogravimetric analysis', *Fuel Processing Technology*, 138, pp. 184–193. doi: 10.1016/j.fuproc.2015.05.013.

Criado, J. M., Sánchez-Jiménez, P. E. and Pérez-Maqueda, L. A. (2008) ' Critical study of the isoconversional methods of kinetic analysis', *Journal of Thermal Analysis and Calorimetry*. Springer Netherlands, 92(1), pp. 199–203. doi: 10.1007/s10973-007-8763-7.

Czernik, S. and Bridgwater, A. V (2004) ' Overview of applications of biomass fast pyrolysis oil', *Energy and Fuels*, 18(2), pp. 590–598. doi: 10.1021/ef034067u.

Das, P., Sreelatha, T. and Ganesh, A. (2004) ' Bio oil from pyrolysis of

cashew nut shell-characterisation and related properties', *Biomass and Bioenergy*, 27(3), pp. 265–275. doi: 10.1016/j.biombioe.2003.12.001.

Derman, E. *et al.* (2018) ' Oil palm empty fruit bunches as a promising feedstock for bioethanol production in Malaysia', *Renewable Energy*, 129, pp. 285–298. doi: 10.1016/j.renene.2018.06.003.

Diebold, J. (2000) ' A review of the chemical and physical mechanisms of the storage stability of fast pyrolysis bio-oils', (January 2000), pp. 1–59. doi: 10.2172/753818.

Diebold, J. P. and Czernik, S. (1997) ' Additives to lower and stabilize the viscosity of pyrolysis oils during storage', *Energy and Fuels*. American Chemical Society, 11(5), pp. 1081–1091. doi: 10.1021/ef9700339.

Ding, J., Xia, Z. and Lu, J. (2012) ' Esterification and deacidification of a waste cooking oil (TAN 68.81 mg KOH/g) for biodiesel production', *Energies*, 5(8), pp. 2683–2691. doi: 10.3390/en5082683.

Dit, M. (2007) ' Palm Kernel Shell (PKS) is more than Biomass for Alternative Fuel after 2005', *Proceedings of Chemistry and Technology Conference*, pp. 275–287. doi: 10.1016/S0399-077X(05)81545-8.

Dobele, G. *et al.* (2005) ' Application of catalysts for obtaining 1,6-anhydrosaccharides from cellulose and wood by fast pyrolysis', in *Journal of Analytical and Applied Pyrolysis*, pp. 401–405. doi: 10.1016/j.jaap.2004.11.031.

Dorado, J. *et al.* (2001) ' Infrared spectroscopy analysis of hemp (Cannabis sativa) after selective delignification by Bjerkandera sp. at different nitrogen

levels’, *Enzyme and Microbial Technology*, 28(6), pp. 550–559. doi: 10.1016/S0141-0229(00)00363-X.

Du, Y. *et al.* (2014) ‘ Thermal behavior and kinetics of bio-ferment residue/coal blends during co-pyrolysis’, *Energy Conversion and Management*, 88, pp. 459–463. doi: 10.1016/j.enconman.2014.08.068.

El-Sayed, S. A. and Khairy, M. (2015) ‘ Effect of heating rate on the chemical kinetics of different biomass pyrolysis materials’, *Biofuels*, 6(3–4), pp. 157–170. doi: 10.1080/17597269.2015.1065590.

Elleuch, A., Halouani, K. and Li, Y. (2016) ‘ Direct Utilization of Pyrolysis Bio-Oil in a Solid Oxide Fuel Cell’, in *Refrigeration Energy and Environment, Hammamet,At: Hammamet, Tunisia*.

Fanchiang, W. L. and Lin, Y. C. (2012) ‘ Catalytic fast pyrolysis of furfural over H-ZSM-5 and Zn/H-ZSM-5 catalysts’, *Applied Catalysis A: General*, 419–420, pp. 102–110. doi: 10.1016/j.apcata.2012.01.017.

Faridah, M. M. *et al.* (2018) ‘ Recent advances in the preparation of oil palm waste-based adsorbents for removal of environmental pollutants - a review’, *Malaysian Journal of Analytical Sciences*, 22(2), pp. 175–184. doi: 10.17576/mjas-2018-2202-02.

Fei, J. *et al.* (2012) ‘ Synergistic effects on co-pyrolysis of lignite and high-sulfur swelling coal’, *Journal of Analytical and Applied Pyrolysis*, 95, pp. 61–67. doi: 10.1016/j.jaap.2012.01.006.

Fermoso, J. *et al.* (2017) ‘ Bio-oil production by lignocellulose fast-pyrolysis: Isolating and comparing the effects of indigenous versus external catalysts’,

Fuel Processing Technology. Elsevier, 167, pp. 563–574. doi: 10.1016/J.FUPROC.2017.08.009.

Fink, D. (2013) *Transport processes in ion-irradiated polymers*.

Franklin, H. D. *et al.* (1981) ‘ Effects of Calcium Minerals on the Rapid Pyrolysis of a Bituminous Coal’, *Industrial and Engineering Chemistry Process Design and Development*, 20(4), pp. 670–674. doi: 10.1021/i200015a016.

Fratini, E. *et al.* (2006) ‘ SANS analysis of the microstructural evolution during the aging of pyrolysis oils from biomass’, *Langmuir*, 22(1), pp. 306–312. doi: 10.1021/la051990a.

Fu, P. *et al.* (2011) ‘ Effect of temperature on gas composition and char structural features of pyrolyzed agricultural residues’, *Bioresource Technology*, 102(17), pp. 8211–8219. doi: 10.1016/j.biortech.2011.05.083.

Ghetti, P., Ricca, L. and Angelini, L. (1996) ‘ Thermal analysis of biomass and corresponding pyrolysis products’, *Fuel*. Elsevier, 75(5), pp. 565–573. doi: 10.1016/0016-2361(95)00296-0.

Gil, M. V. *et al.* (2010) ‘ Thermal behaviour and kinetics of coal/biomass blends during co-combustion’, *Bioresource Technology*, 101(14), pp. 5601–5608. doi: 10.1016/j.biortech.2010.02.008.

Griffin, M. B. *et al.* (2016) ‘ Role of the Support and Reaction Conditions on the Vapor-Phase Deoxygenation of m-Cresol over Pt/C and Pt/TiO2Catalysts’, *ACS Catalysis*, 6(4), pp. 2715–2727. doi: 10.1021/acscatal.5b02868.

Grønli, M. G., Várhegyi, G. and Di Blasi, C. (2002) ‘ Thermogravimetric analysis and devolatilization kinetics of wood’, *Industrial and Engineering Chemistry Research*, 41(17), pp. 4201–4208. doi: 10.1021/ie0201157.

Guda, V. K. and Toghiani, H. (2017) ‘ Catalytic pyrolysis of pinewood using metal oxide catalysts in an integrated reactor system’, *Biofuels*, 8(5), pp. 527–536. doi: 10.1080/17597269.2016.1231960.

Guida, M. Y. and Hannioui, A. (2016) ‘ Evaluation of Reliability of Coats-Redfern and Criado Methods for Kinetics Analysis of Olive Mill Solid Waste and Olive Mill Wastewater’, *International Journal of Scientific & Engineering Research*, 7(11), pp. 193–203.

Guo, J. and Lua, A. C. (2000) ‘ Kinetic study on pyrolysis of extracted oil palm fiber: Isothermal and non-isothermal conditions’, *Journal of Thermal Analysis and Calorimetry*, 59, pp. 763–774. doi: 10.1023/A:1010149619877.

Guo, Z., Wang, S. and Wang, X. (2014) ‘ Stability mechanism investigation of emulsion fuels from biomass pyrolysis oil and diesel’, *Energy*, 66, pp. 250–255. doi: 10.1016/j.energy.2014.01.010.

Gutierrez, A. *et al.* (2009) ‘ Hydrodeoxygenation of guaiacol on noble metal catalysts’, *Catalysis Today*. Elsevier, 147(3–4), pp. 239–246. doi: 10.1016/j.cattod.2008.10.037.

Gutiérrez, A. (2013) *Noble Metal Catalysts in the Production of Biofuels*. Available at: http://urn.fi/URN:ISBN:978-952-60-5323-3.

Harmsen, P. and Huijgen, W. (2010) ‘ Literature Review of Physical and Chemical Pretreatment Processes for Lignocellulosic Biomass’, (September),

pp. 1–49.

Haryati, Z. *et al.* (2018) ‘ Pilot scale biochar production from palm kernel shell (PKS) in a fixed bed allothermal reactor’, *Journal of Oil Palm Research*, 30(3), pp. 485–494. doi: 10.21894/jopr.2018.0043.

Hassan, E. B. M., Steele, P. H. and Ingram, L. (2009) ‘ Characterization of fast pyrolysis bio-oils produced from pretreated pine wood’, in *Applied Biochemistry and Biotechnology*, pp. 182–192. doi: 10.1007/s12010-008-8445-3.

Hayawin, Z. N. *et al.* (2014) ‘ The growth and reproduction of Eisenia fetida and Eudrilus eugeniae in mixtures of empty fruit bunch and palm oil mill effluent’, *Compost Science and Utilization*, 22(1), pp. 40–46. doi: 10.1080/1065657X.2014.882247.

Hernando, H. *et al.* (2017) ‘ Biomass catalytic fast pyrolysis over hierarchical ZSM-5 and Beta zeolites modified with Mg and Zn oxides’, *Biomass Conversion and Biorefinery*. Springer Berlin Heidelberg, 7(3), pp. 289–304. doi: 10.1007/s13399-017-0266-6.

Hornung, A. (2013) ‘ Intermediate pyrolysis of biomass’, *Biomass Combustion Science, Technology and Engineering*, pp. 172–186. doi: 10.1533/9780857097439.2.172.

Hosoya, T., Kawamoto, H. and Saka, S. (2007) ‘ Cellulose-hemicellulose and cellulose-lignin interactions in wood pyrolysis at gasification temperature’, *Journal of Analytical and Applied Pyrolysis*. Elsevier, 80(1), pp. 118–125. doi: 10.1016/j.jaap.2007.01.006.

Hwang, H. *et al.* (2015) ‘ Catalytic effects of magnesium on the characteristics of fast pyrolysis products - Bio-oil, bio-char, and non-condensed pyrolytic gas fractions’, *Journal of Analytical and Applied Pyrolysis*. Elsevier, 113, pp. 27–34. doi: 10.1016/j.jaap.2014.09.028.

Iliopoulou, E. F. *et al.* (2012) ‘ Catalytic upgrading of biomass pyrolysis vapors using transition metal-modified ZSM-5 zeolite’, *Applied Catalysis B: Environmental*, 127, pp. 281–290. doi: 10.1016/j.apcatb.2012.08.030.

Index Mundi (2019) *Malaysia Palm Oil Production by Year*. Available at: https://www.indexmundi.com/agriculture/?commodity=palm-oil.

Jiang, J., Liu, Z. and Liu, Q. (2017) ‘ Synergetic Catalysis of Calcium Oxide and Iron in Hydrogasification of Char’, *Energy & Fuels*, 31(1), pp. 198–204. doi: 10.1021/acs.energyfuels.6b02026.

Johannes, I., Tiikma, L. and Luik, H. (2013) ‘ Synergy in co-pyrolysis of oil shale and pine sawdust in autoclaves’, *Journal of Analytical and Applied Pyrolysis*, 104, pp. 341–352. doi: 10.1016/j.jaap.2013.06.015.

Jukić, A. (2013) ‘ Petroleum Refining and Petrochemical Processes Crude oil : main properties Ante Jukić’. Available at: https://www.fkit.unizg.hr/_download/repository/PRPP_2013_Crude_oil_composition.pdf.

Khor, K. H. *et al.* (2009) ‘ Characterization of Bio-Oil : A By-Product from Slow Pyrolysis of Oil Palm Empty Fruit Bunches School of Physics , School of Mechanical Engineering , Engineering Campus’, *American Journal of Applied Sciences*, 6(9), pp. 1647–1652. doi: 10.3844/ajassp.2009.1647.1652.

Khromova, S. A. *et al.* (2013) ‘ Magnesium-containing catalysts for the decarboxylation of bio-oil’, *Catalysis in Industry*, 5(3), pp. 260–268. doi: 10.1134/S2070050413030069.

Kilzer, F. J. and Broido, A. (1965) ‘ Speculations on the Nature of Cellulose Pyrolysis’, *Pyrodynamics*, 2, pp. 151–163. doi: 10.1143/JPSJ.20.457.

Krerkkaiwan, S. *et al.* (2013) ‘ Synergetic effect during co-pyrolysis/gasification of biomass and sub-bituminous coal’, *Fuel Processing Technology*, 115, pp. 11–18. doi: 10.1016/j.fuproc.2013.03.044.

Kumar, S. and Saxena, S. K. (2014) ‘ A comparative study of CO2 sorption properties for different oxides’, *Materials for Renewable and Sustainable Energy*, 3(3), p. 30. doi: 10.1007/s40243-014-0030-9.

Kwon, E. E. *et al.* (2018) ‘ Effects of calcium carbonate on pyrolysis of sewage sludge’, *Energy*, 153, pp. 726–731. doi: 10.1016/j.energy.2018.04.100.

Lau, H. S. *et al.* (2018) ‘ Torrefaction of oil palm fronds for co-firing in coal power plants’, *Energy Procedia*, 144, pp. 75–81. doi: 10.1016/j.egypro.2018.06.010.

Lee, H. *et al.* (2016) ‘ Environment-Friendly Heterogeneous Alkaline-Based Mixed Metal Oxide Catalysts for Biodiesel Production’, *Energies*. Multidisciplinary Digital Publishing Institute, 9(8), p. 611. doi: 10.3390/en9080611.

Lee, X. J. *et al.* (2017) ‘ Biochar potential evaluation of palm oil wastes through slow pyrolysis: Thermochemical characterization and pyrolytic

kinetic studies', *Bioresource Technology*. Elsevier, 236, pp. 155–163. doi: 10.1016/j.biortech.2017.03.105.

Li, S. *et al.* (2001) ' Real-time evolved gas analysis by FTIR method: An experimental study of cellulose pyrolysis', *Fuel*. Elsevier, 80(12), pp. 1809–1817. doi: 10.1016/S0016-2361(01)00064-3.

Liao, Y. fen, Wang, S. rong and Ma, X. qian (2004) ' Study of reaction mechanisms in cellulose pyrolysis', *ACS Division of Fuel Chemistry, Preprints*, 49(1), pp. 407–411.

Lievens, C. *et al.* (2011) ' An FT-IR spectroscopic study of carbonyl functionalities in bio-oils', *Fuel*, 90(11), pp. 3417–3423. doi: 10.1016/j.fuel.2011.06.001.

Lin, Y. *et al.* (2010) ' Deoxygenation of bio-oil during pyrolysis of biomass in the presence of CaO in a fluidized-bed reactor', *Energy and Fuels*, 24(10), pp. 5686–5695. doi: 10.1021/ef1009605.

Lin, Z. *et al.* (2018) ' Cobalt-modified molybdenum carbide as a selective catalyst for hydrodeoxygenation of furfural', *Applied Catalysis B: Environmental*, 233, pp. 160–166. doi: 10.1016/j.apcatb.2018.03.113.

Liu, C. *et al.* (2014) ' Catalytic fast pyrolysis of lignocellulosic biomass', *Chem. Soc. Rev.* The Royal Society of Chemistry, 43(22), pp. 7594–7623. doi: 10.1039/C3CS60414D.

Liu, J. *et al.* (2009) ' Pyrolysis treatment of oil sludge and model-free kinetics analysis', *Journal of Hazardous Materials*, 161(2), pp. 1208–1215. doi: 10.1016/j.jhazmat.2008.04.072.

Liu, N. A. *et al.* (2002) ‘ Kinetic modeling of thermal decomposition of natural cellulosic materials in air atmosphere’, *Journal of Analytical and Applied Pyrolysis*, 63(2), pp. 303–325. doi: 10.1016/S0165-2370(01)00161-9.

Long, Y. *et al.* (2017) ‘ Acid-catalysed cellulose pyrolysis at low temperatures’, *Fuel*. Elsevier Ltd, 193, pp. 460–466. doi: 10.1016/j.fuel.2016.12.067.

López-Fonseca, R. *et al.* (2007) ‘ A kinetic study of the combustion of porous synthetic soot’, *Chemical Engineering Journal*, 129(1), pp. 41–49. doi: 10.1016/j.cej.2006.10.029.

Lu, M. *et al.* (2017) ‘ Catalytic Hydrodeoxygenation of Guaiacol over Palladium Catalyst on Different Titania Supports’, *Energy and Fuels*, 31(10), pp. 10858–10865. doi: 10.1021/acs.energyfuels.7b01498.

Lu, Q. *et al.* (2010) ‘ Catalytic upgrading of biomass fast pyrolysis vapors with nano metal oxides: An analytical Py-GC/MS study’, *Energies*, 3(11), pp. 1805–1820. doi: 10.3390/en3111805.

Lu, Q. *et al.* (2014) ‘ Catalytic fast pyrolysis of cellulose and biomass to produce levoglucosenone using magnetic SO4 2-/TiO2-Fe3O4’, *Bioresource Technology*, 171, pp. 10–15. doi: 10.1016/j.biortech.2014.08.075.

Lu, Q. *et al.* (2018) ‘ Catalytic fast pyrolysis of biomass with noble metal-like catalysts to produce high-grade bio-oil: Analytical Py-GC/MS study’, *Catalysis Today*. Elsevier, 302, pp. 169–179. doi: 10.1016/j.cattod.2017.08.029.

Lu, Q., Li, W. Z. and Zhu, X. F. (2009) ‘ Overview of fuel properties of

biomass fast pyrolysis oils', *Energy Conversion and Management*. Pergamon, 50(5), pp. 1376–1383. doi: 10.1016/j.enconman.2009.01.001.

Luo *et al.* (2004) ' Mechanism Study of Cellulose Rapid Pyrolysis', *Industrial & Engineering Chemistry Research*, 43(18), pp. 5605–5610. doi: 10.1021/ie030774z.

Ma, B. and Agblevor, F. A. (2014) ' Polarity-based separation and chemical characterization of fast pyrolysis bio-oil from poultry litter', *Biomass and Bioenergy*, 64, pp. 337–347. doi: 10.1016/j.biombioe.2014.03.003.

Ma, Z. *et al.* (2014) ' Selective deoxygenation of lignin during catalytic fast pyrolysis', *Catalysis Science & Technology*. The Royal Society of Chemistry, 4(3), p. 766. doi: 10.1039/c3cy00704a.

Ma, Z., Troussard, E. and van Bokhoven, J. A. (2012) ' Controlling the selectivity to chemicals from lignin via catalytic fast pyrolysis', *Applied Catalysis A: General*, pp. 130–136. doi: 10.1016/j.apcata.2012.02.027.

Mahadevan, R. *et al.* (2016) ' Effect of Alkali and Alkaline Earth Metals on in-Situ Catalytic Fast Pyrolysis of Lignocellulosic Biomass: A Microreactor Study', *Energy and Fuels*, 30(4), pp. 3045–3056. doi: 10.1021/acs.energyfuels.5b02984.

Mahfouz, R. M. *et al.* (2012) ' Kinetic studies of isothermal decomposition of unirradiated and γ-irradiated gallium acetylacetonate: new route for synthesis of gallium oxide nanoparticles', *Progress in Reaction Kinetics and Mechanism*, 37(3), pp. 249–262. doi: 10.3184/146867812X13377012276288.

Majhi, A., Sharma, Y. K. and Naik, D. V. (2012) ' Blending optimization of

Hempel distilled bio-oil with commercial diesel', *Fuel*, 96, pp. 264–269. doi: 10.1016/j.fuel.2012.01.039.

Malaysian Palm Oil Board (2018) *Monthly FFB yield*. Available at: http://www.palmoilworld.org/about_mpob.

Martin, J. A. and Boateng, A. A. (2014) ' Combustion performance of pyrolysis oil/ethanol blends in a residential-scale oil-fired boiler', *Fuel*, 133, pp. 34–44. doi: 10.1016/j.fuel.2014.05.005.

Martin, J. A., Mullen, C. A. and Boateng, A. A. (2014) ' Maximizing the Stability of Pyrolysis Oil/Diesel Fuel Emulsions', *Energy & Fuels*, 28(9), pp. 5918–5929. doi: 10.1021/ef5015583.

Mekhemer, G. A. H. *et al.* (2005) ' Ketonization of acetic acid vapour over polycrystalline magnesia: In situ Fourier transform infrared spectroscopy and kinetic studies', *Journal of Catalysis*, 230(1), pp. 109–122. doi: 10.1016/j.jcat.2004.09.030.

Meland, B. *et al.* (2010) ' Correlated IR spectroscopy and visible light scattering measurements of mineral dust aerosol', *Journal of Geophysical Research Atmospheres*, 115(20). doi: 10.1029/2010JD014389.

Meng, J. *et al.* (2015) ' Thermal and Storage Stability of Bio-Oil from Pyrolysis of Torrefied Wood', *Energy and Fuels*, 29(8), pp. 5117–5126. doi: 10.1021/acs.energyfuels.5b00929.

Miura, K. and Maki, T. (1998) ' A simple method for estimating f(E) and k0(E) in the Distrubuited Activation Energy Model', *Energy & Fuels*, 0(11), pp. 864–869.

Mohamed, A. R., Hamzah, Z. and Daud, M. Z. M. (2014) ‘ Optimization of the pyrolysis process of empty fruit bunch (EFB) in a fixed-bed reactor through a central composite design (CCD)’, in *AIP Conference Proceedings*, pp. 1172–1177. doi: 10.1063/1.4887756.

Mohammed, I. Y. *et al.* (2016) ‘ Catalytic intermediate pyrolysis of Napier grass in a fixed bed reactor with ZSM-5, HZSM-5 and zinc-exchanged zeolite-a as the catalyst’, *Energies*, 9(4). doi: 10.3390/en9040246.

Mohammed, M. A. A. *et al.* (2012) ‘ Gasification of oil palm empty fruit bunches: A characterization and kinetic study’, *Bioresource Technology*. Elsevier, 110, pp. 628–636. doi: 10.1016/j.biortech.2012.01.056.

Mortensen, P. M. *et al.* (2013) ‘ Screening of catalysts for hydrodeoxygenation of phenol as a model compound for bio-oil’, *ACS Catalysis*, 3(8), pp. 1774–1785. doi: 10.1021/cs400266e.

Mu, L. *et al.* (2016) ‘ Evaluation of co-pyrolysis petrochemical wastewater sludge with lignite in a thermogravimetric analyzer and a packed-bed reactor: Pyrolysis characteristics, kinetics, and products analysis’, *Bioresource Technology*. Elsevier Ltd, 221, pp. 147–156. doi: 10.1016/j.biortech.2016.09.011.

Nam, S.-B. *et al.* (2016) ‘ Catalytic application of metallic iron from the dyeing sludge ash for benzene steam reforming reaction in tar emitted from biomass gasification’, *Korean J. Chem. Eng*, 33(2), pp. 465–472. doi: 10.1007/s11814-015-0159-y.

Nan, W. *et al.* (2014) ‘ Catalytic upgrading of switchgrass-derived pyrolysis

oil using supported ruthenium and rhodium catalysts', in *Energy and Fuels*, pp. 4588–4595. doi: 10.1021/ef500826k.

Ninduangdee, P. and Kuprianov, V. I. (2015) ' Combustion of an oil palm residue with elevated potassium content in a fluidized-bed combustor using alternative bed materials for preventing bed agglomeration', *Bioresource Technology*, 182, pp. 272–281. doi: 10.1016/j.biortech.2015.01.128.

Nokkosmäki, M. . *et al.* (1998) ' A novel test method for catalysts in the treatment of biomass pyrolysis oil', *Catalysis Today*, 45(1), pp. 405–409. doi: 10.1016/S0920-5861(98)00276-4.

Nokkosmäki, M. I. *et al.* (2000) ' Catalytic conversion of biomass pyrolysis vapours with zinc oxide', *Journal of Analytical and Applied Pyrolysis*, 55(1), pp. 119–131. doi: 10.1016/S0165-2370(99)00071-6.

Nyakuma, B. B. *et al.* (2016) ' Thermogravimetric and kinetic analyses of oil palm empty fruit bunch (OPEFB) Pellets using the distributed activation energy model', *Journal of Physical Science*, 27(3), pp. 67–83. doi: 10.21315/jps2016.27.3.5.

Oasmaa, A., Elliott, D. C. and Korhonen, J. (2010) ' Acidity of biomass fast pyrolysis bio-oils', *Energy and Fuels*, 24(12), pp. 6548–6554. doi: 10.1021/ef100935r.

Oasmaa, A. and Peacocke, C. (2010) ' Properties and fuel use of biomass-derived fast pyrolysis liquids. A guide', *Vtt Publications*, 731, p. 79 p. + app. 46 p.

Ogunsina *et al.* (2014) ' Pyrolytic conversion of spent palm fruit bunches into

bio-fuels’, *JOMAR*, 8(2), pp. 50–60. Available at: http://eprints.covenantuniversity.edu.ng/5382/1/New Article with RMRDC.pdf.

Paenpong, C., Inthidech, S. and Pattiya, A. (2013) ‘ Effect of filter media size, mass flow rate and filtration stage number in a moving-bed granular filter on the yield and properties of bio-oil from fast pyrolysis of biomass’, *Bioresource Technology*, 139, pp. 34–42. doi: 10.1016/j.biortech.2013.03.200.

Park, L. K. E. *et al.* (2016) ‘ Separation of Switchgrass Bio-Oil by Water/Organic Solvent Addition and pH Adjustment’, *Energy and Fuels*, 30(3), pp. 2164–2173. doi: 10.1021/acs.energyfuels.5b02537.

Park, Y. K. *et al.* (2015) ‘ Catalytic fast pyrolysis of waste pepper stems over HZSM-5’, *Renewable Energy*, 79(1), pp. 20–27. doi: 10.1016/j.renene.2014.10.005.

Parker, W. (1968) ‘ Kinetics of the formation of strontium zirconate’, *Masters Theses*. Available at: http://scholarsmine.mst.edu/masters_theses.

Patwardhan, P. R. *et al.* (2010) ‘ Influence of inorganic salts on the primary pyrolysis products of cellulose’, *Bioresource Technology*, 101(12), pp. 4646–4655. doi: 10.1016/j.biortech.2010.01.112.

Pérez-Maqueda, L. A. and Criado, J. M. (2000) ‘ The Accuracy of Senum and Yang’s Approximations to the Arrhenius Integral’, *Journal of Thermal Analysis and Calorimetry*, 60, pp. 909–915.

Pérez, J. *et al.* (2002) ‘ Biodegradation and biological treatments of cellulose, hemicellulose and lignin: an overview’, *International Microbiology*, 5(2), pp.

53–63. doi: 10.1007/s10123-002-0062-3.

Piskorz, J., Radlein, D. and Scott, D. S. (1986) ‘ On the mechanism of the rapid pyrolysis of cellulose’, *Journal of Analytical and Applied Pyrolysis*. Elsevier, 9(2), pp. 121–137. doi: 10.1016/0165-2370(86)85003-3.

Prasertsit, K., Phoosakul, P. and Sukmanee, S. (2014) ‘ Use of calcium oxide in palm oil methyl ester production’, *Songklanakarin J. Sci. Technol*, 36(2), pp. 195–200. doi: 10.1016/j.cej.2010.03.050.

Pütün, E. (2010) ‘ Catalytic pyrolysis of biomass: Effects of pyrolysis temperature, sweeping gas flow rate and MgO catalyst’, *Energy*, 35(7), pp. 2761–2766. doi: 10.1016/j.energy.2010.02.024.

Quan, C. *et al.* (2014) ‘ Co-pyrolysis of biomass and coal blend by TG and in a free fall reactor’, *Journal of Thermal Analysis and Calorimetry*. Springer Netherlands, 117(2), pp. 817–823. doi: 10.1007/s10973-014-3774-7.

Rajadurai, S. (2006) ‘ Pathways for Carboxylic Acid Decomposition on Transition Metal Oxides’, *Catalysis Reviews*, 36(3), pp. 385–403. doi: 10.1080/01614949408009466.

Rajamohan, S. and Kasimani, R. (2018) ‘ Studies on the effects of storage stability of bio-oil obtained from pyrolysis of Calophyllum inophyllum deoiled seed cake on the performance and emission characteristics of a direct-injection diesel engine’, *Environmental Science and Pollution Research*, 25(18), pp. 17749–17767. doi: 10.1007/s11356-018-1986-2.

Rantuch, P. and Balog, K. (2014) ‘ Thermogravimetric analysis of cellulose insulation and determination of activation energy of its thermo-oxidation using

non-isothermal, model-free methods’, *Polymers for Advanced Technologies*, 25(10), pp. 1169–1174. doi: 10.1002/pat.3373.

Reeb, C. W., Hays, T. and Venditti, R. A. (2014) ‘ Supply Chain Analysis, Delivered Cost, and Life Cycle Assessment of Oil Palm Empty Fruit Bunch Biomass for Green Chemical Production in Malaysia’, *BioResources*, 9(3), pp. 5385–5416. Available at: https://ojs.cnr.ncsu.edu/index.php/BioRes/article/view/BioRes_09_3_5385_Reeb_Supply_Chain_Analysis_Delivered_Cost.

Refaat, A. A. (2011) ‘ Biodiesel production using solid metal oxide catalysts’, *Int. J. Environ. Sci. Tech*, 8(1), pp. 203–221. Available at: http://www.bioline.org.br/pdf?st11020.

Ronsse, F. *et al.* (2012) ‘ Secondary reactions of levoglucosan and char in the fast pyrolysis of cellulose’, *Environmental Progress and Sustainable Energy*. John Wiley & Sons, Inc., 31(2), pp. 256–260. doi: 10.1002/ep.11633.

Routray, K., Barnett, K. J. and Huber, G. W. (2017) ‘ Hydrodeoxygenation of Pyrolysis Oils’, *Energy Technology*, 5(1), pp. 80–93. doi: 10.1002/ente.201600084.

Ruddy, D. A. *et al.* (2014) ‘ Recent advances in heterogeneous catalysts for bio-oil upgrading via “ ex situ catalytic fast pyrolysis”: catalyst development through the study of model compounds’, *Green Chemistry*, 16(2), pp. 454–490. doi: 10.1039/c3gc41354c.

Rutkowski, P. and Kubacki, A. (2006) ‘ Influence of polystyrene addition to cellulose on chemical structure and properties of bio-oil obtained during

pyrolysis’, *Energy Conversion and Management*. Pergamon, 47(6), pp. 716–731. doi: 10.1016/j.enconman.2005.05.017.

Salman, B., Nomanbhay, S. and Salema, A. A. (2019) ‘ Microwave-synthesised hydrothermal co-pyrolysis of oil palm empty fruit bunch with plastic wastes from Nigeria’, *Biofuels*, pp. 1–17. doi: 10.1080/17597269.2019.1626000.

Salman, Z. (2015) *Biomass Wastes from Palm Oil Mills*. Available at: http://www.bioenergyconsult.com/palm-biomass/.

Samolada, M. C., Papafotica, A. and Vasalos, I. A. (2000) ‘ Catalyst Evaluation for Catalytic Biomass Pyrolysis’, *Energy and Fuels*, 14(6), pp. 1161–1167. doi: 10.1021/ef000026b.

Samolada, M. C. and Zabaniotou, A. A. (2014) ‘ Comparative assessment of municipal sewage sludge incineration , gasification and pyrolysis for a sustainable sludge-to-energy management in Greece’, *Waste Management*. Elsevier Ltd, 34(2), pp. 411–420. doi: 10.1016/j.wasman.2013.11.003.

Sembiring, K. C., Rinaldi, N. and Simanungkalit, S. P. (2015) ‘ Bio-oil from Fast Pyrolysis of Empty Fruit Bunch at Various Temperature’, *Energy Procedia*, 65, pp. 162–169. Available at: https://www.sciencedirect.com/science/article/pii/S1876610215000533.

Shafizadeh, F. and Y.Z., L. (1966) ‘ Thermal Degradation of 1,6-Anhydro-p-D-glucopyranose’, *Journal of Organic Chemistry*, 1964(12), pp. 2139–2143. doi: 10.1002/star.19630150503.

Shafizadeh, F. and Yuan-Zong, L. (1975) ‘ Thermal degradation of 3-deoxy-

D-erythro-hexosulose’, *Carbohydrate Research*, 40(2), pp. 263–274. doi: 10.1016/S0008-6215(00)82608-7.

Shah, J., Rasul Jan, M. and Mabood, F. (2008) ‘Catalytic pyrolysis of waste tyre rubber into hydrocarbons via base catalysts’, *Iranian Journal of Chemistry and Chemical Engineering*, 27(2), pp. 103–109.

Shao, J. and Agblevor, F. (2015) ‘New Rapid Method for the Determination of Total Acid Number (Tan) of Bio-Oils’, *American Journal of Biomass and Bioenergy*, 4(1), pp. 1–9. doi: 10.7726/ajbb.2015.1001.

Shen, D. K. and Gu, S. (2009) ‘The mechanism for thermal decomposition of cellulose and its main products’, *Bioresource Technology*, 100(24), pp. 6496–6504. doi: 10.1016/j.biortech.2009.06.095.

Shimada, N., Kawamoto, H. and Saka, S. (2008) ‘Different action of alkali/alkaline earth metal chlorides on cellulose pyrolysis’, *Journal of Analytical and Applied Pyrolysis*. Elsevier, 81(1), pp. 80–87. doi: 10.1016/j.jaap.2007.09.005.

Shuit, S. H. *et al.* (2009) ‘Oil palm biomass as a sustainable energy source: A Malaysian case study’, *Energy*. Elsevier Ltd, 34(9), pp. 1225–1235. doi: 10.1016/j.energy.2009.05.008.

de Souza, P. M. *et al.* (2017) ‘Hydrodeoxygenation of Phenol over Pd Catalysts. Effect of Support on Reaction Mechanism and Catalyst Deactivation’, *ACS Catalysis*, 7(3), pp. 2058–2073. doi: 10.1021/acscatal.6b02022.

Speight, J. G. (2014) *Crude Oil Assay Database. Knovel. Online version*.

Available at: https://app.knovel.com/web/toc.v/cid:kpCOAD0005/viewerType:toc/root_slug:crude-oil-assay-database/url_slug:table-1-crude-oil-assay.

Stefanidis, S. D. *et al.* (2011) ‘ In-situ upgrading of biomass pyrolysis vapors: Catalyst screening on a fixed bed reactor’, *Bioresource Technology*. Elsevier, 102(17), pp. 8261–8267. doi: 10.1016/j.biortech.2011.06.032.

Stefanidis, S. D. *et al.* (2016) ‘ Natural magnesium oxide (MgO) catalysts: A cost-effective sustainable alternative to acid zeolites for the in situ upgrading of biomass fast pyrolysis oil’, *Applied Catalysis B: Environmental*, 196, pp. 155–173. doi: 10.1016/j.apcatb.2016.05.031.

Strezov, V. *et al.* (2015) ‘ Lignocellulosic biomass pyrolysis : A review of product properties and effects of pyrolysis parameters and effects of pyrolysis parameters’, *Renewable and Sustainable Energy Reviews*, 57(January 2016), pp. 1126–1140. doi: 10.1016/j.rser.2015.12.185.

Sudiyani, Y. *et al.* (2013) ‘ Utilization of biomass waste empty fruit bunch fiber of palm oil for bioethanol production using pilot - Scale unit’, *Energy Procedia*. Elsevier B.V., 32, pp. 31–38. doi: 10.1016/j.egypro.2013.05.005.

Sukiran, M. A. *et al.* (2009) ‘ Optimization of Pyrolysis of Oil Palm Empty Fruit Bunches’, *American Journal of Applied Sciences*, 21(6), pp. 653–658. doi: 10.3844/ajas.2009.869.875.

Sukiran, M. A., Chin, C. M. and Bakar, N. K. A. (2009) ‘ Bio-oils from pyrolysis of oil palm empty fruit bunches’, *American Journal of Applied Sciences*, 6(5), pp. 869–875. Available at:

http://eprints.um.edu.my/6238/1/1.pdf.

Sun, L. *et al.* (2016) ‘ Comparision of catalytic fast pyrolysis of biomass to aromatic hydrocarbons over ZSM-5 and Fe/ZSM-5 catalysts’, *Journal of Analytical and Applied Pyrolysis*. Elsevier, 121, pp. 342–346. doi: 10.1016/j.jaap.2016.08.015.

Sundqvist, T., Oasmaa, A. and Koskinen, A. (2015) ‘ Upgrading fast pyrolysis bio-oil quality by esterification and azeotropic water removal’, *Energy and Fuels*, 29(4), pp. 2527–2534. doi: 10.1021/acs.energyfuels.5b00238.

Suruhanjaya Tenaga (Energy Commission) (2018) *2017 Malaysia Energy Statistics Handbook*. Available at: http://www.statcan.gc.ca/pub/57-601-x/57-601-x2012001-eng.pdf%5Cnpapers2://publication/uuid/792EFC7D-A6CF-40B5-A139-8FA59714AA41.

Thangalazhy-Gopakumar, S. *et al.* (2015) ‘ Utilization of palm oil sludge through pyrolysis for bio-oil and bio-char production’, *Bioresource Technology*. Elsevier Ltd, 178, pp. 65–69. doi: 10.1016/j.biortech.2014.09.068.

U.S. Energy Information Agency (2017) *US Energy Information Administration, International Energy Outlook 2017 Overview, International Energy Outlook*. doi: EIA-0484(2013).

Urasaki, K. K. *et al.* (2012) ‘ Effect of the kinds of alcohols on the structure and stability of calcium oxide catalyst in triolein transesterification reaction’, *Applied Catalysis A: General*, 411–412, pp. 44–50. doi:

10.1016/j.apcata.2011.10.019.

Valdés, C. F. *et al.* (2018) ‘ Effects of pyrolysis atmosphere on the porous structure and reactivity of chars from middle and high rank coals’, *Ingenieria e Investigacion*, 38(1), pp. 31–45. doi: 10.15446/ing.investig.v38n1.64516.

Varhegyi, G. *et al.* (1989) ‘ Kinetics of the thermal decomposition of cellulose, hemicellulose, and sugarcane bagasse’, *Energy & Fuels*. American Chemical Society, 3(3), pp. 329–335. doi: 10.1021/ef00015a012.

Várhegyi, G. *et al.* (1997) ‘ Kinetic modeling of biomass pyrolysis’, *Journal of Analytical and Applied Pyrolysis*, 42(1), pp. 73–87. doi: 10.1016/S0165-2370(96)00971-0.

Viswanadham, N. *et al.* (2010) ‘ A comparative study of the esterification activity of nanosized H-ZSM-5 with commercial H-ZSM-5 and H-beta zeolite’, *Petroleum Science and Technology*, 28(3), pp. 219–224. doi: 10.1080/10916460903438867.

Vlaev, L. *et al.* (2008) ‘ A comparative study of non-isothermal kinetics of decomposition of calcium oxalate monohydrate’, *Journal of Analytical and Applied Pyrolysis*, 81(2), pp. 253–262. doi: 10.1016/j.jaap.2007.12.003.

Vohs, J. M. and Barteau, M. A. (1988) ‘ Reaction pathways and intermediates in the decomposition of acetic and propionic acids on the polar surfaces of zinc oxide’, *Surface Science*, 201(3), pp. 481–502. doi: 10.1016/0039-6028(88)90499-2.

Vyazovkin, S. (2001) ‘ Modification of the integral isoconversional method to account for variation in the activation energy’, *Journal of Computational*

Chemistry. John Wiley & Sons, Inc., 22(2), pp. 178–183. doi: 10.1002/1096-987X(20010130)22:2<178::AID-JCC5>3.0.CO;2-#.

Wachs, I. E. (2005) ‘ Recent conceptual advances in the catalysis science of mixed metal oxide catalytic materials’, in *Catalysis Today*, pp. 79–94. doi: 10.1016/j.cattod.2004.12.019.

Wang, D. *et al.* (2010) ‘ Comparison of catalytic pyrolysis of biomass with MCM-41 and CaO catalysts by using TGA-FTIR analysis’, *Journal of Analytical and Applied Pyrolysis*. Elsevier B.V., 89(2), pp. 171–177. doi: 10.1016/j.jaap.2010.07.008.

Wang, J. J., Chang, J. and Fan, J. (2010) ‘ Upgrading of bio-oil by catalytic esterification and determination of acid number for evaluating esterification degree’, *Energy and Fuels*, 24(5), pp. 3251–3255. doi: 10.1021/ef1000634.

Wang, S. *et al.* (2007) ‘ Mechanism study on cellulose pyrolysis using thermogravimetric analysis coupled with infrared spectroscopy’, *Frontiers of Energy and Power Engineering in China*, 1(4), pp. 413–419. doi: 10.1007/s11708-007-0060-8.

Wang, S. *et al.* (2011) ‘ Recent advances in capture of carbon dioxide using alkali-metal-based oxides’, *Energy and Environmental Science*, 4(10), pp. 3805–3819. doi: 10.1039/c1ee01116b.

Wang, S. *et al.* (2012) ‘ Mechanism research on cellulose pyrolysis by Py-GC/MS and subsequent density functional theory studies’, *Bioresource Technology*, 104, pp. 722–728. doi: 10.1016/j.biortech.2011.10.078.

Wei, Y. *et al.* (2014) ‘ Liquid-liquid extraction of biomass pyrolysis bio-

oil’, *Energy and Fuels*, 28(2), pp. 1207–1212. doi: 10.1021/ef402490s.

White, J. E., Catallo, W. J. and Legendre, B. L. (2011) ‘ Biomass pyrolysis kinetics: A comparative critical review with relevant agricultural residue case studies’, *Journal of Analytical and Applied Pyrolysis*, 91(1), pp. 1–33. doi: 10.1016/j.jaap.2011.01.004.

Wu, J. C. (2015) *Oil palm offers cheap biofuels and bioplastics, A*STAR Research*. doi: 10.1002/bab.1188.

Xie, H. *et al.* (2013) ‘ Pyrolysis characteristics and kinetics of lignin derived from three agricultural wastes’, *Journal of Renewable and Sustainable Energy*, 5(6), p. 063119. doi: 10.1063/1.4841215.

Yaakob, A. Q. and Bhatia, S. (2004) ‘ Esterification of Palmitic Acid with Methanol in the Presence of Macroporous Ion Exchange Resin as Catalyst’, *IIUM Engineering Journal*, 5(2). doi: 10.31436/iiumej.v5i2.380.

Yahya, M. *et al.* (2015) ‘ Chemical Conversion of Palm-based Lignocellulosic Biomass to Nano-Cellulose: Review’, *Polymer Research Journal*, 9(4), pp. 1–22. Available at: https://umexpert.um.edu.my/file/publication/00005895_124309.pdf.

Yakub, M. I. *et al.* (2015) ‘ Pyrolysis of Oil Palm Residues in a Fixed Bed Tubular Reactor’, *Journal of Power and Energy Engineering*, 3(April), pp. 185–193. doi: 10.4236/jpee.2015.34026.

Yakub Mohammed, I. (2016) ‘ Pyrolysis of Napier Grass To Bio-Oil and Catalytic Upgrading To High Grade Bio-Fuel’.

Yan, S. *et al.* (2007) ‘ Solid base catalysts for transesterification of oil with methanol to produce biodiesel’, *Huagong Xuebao/Journal of Chemical Industry and Engineering (China)*, 58(10), pp. 2506–2512.

Yang, H. *et al.* (2007) ‘ Characteristics of hemicellulose, cellulose and lignin pyrolysis’, *Fuel*, 86(12–13), pp. 1781–1788. doi: 10.1016/j.fuel.2006.12.013.

Yang, H. *et al.* (2014) ‘ Overview of upgrading of pyrolysis oil of biomass’, *Energy Procedia*, 61, pp. 1306–1309. doi: 10.1016/j.egypro.2014.11.1087.

Yoo, H. M. *et al.* (2014) ‘ The fast pyrolysis characteristics of palm empty fruit bunch: The yield and homogeneity of biocrudeoil affected by ash’, in *Environmental Progress and Sustainable Energy*, pp. 706–710. doi: 10.1002/ep.11931.

Yorulmaz, S. Y. and Atimtay, A. T. (2009) ‘ Investigation of combustion kinetics of treated and untreated waste wood samples with thermogravimetric analysis’, *Fuel Processing Technology*, 90(7), pp. 939–946. doi: 10.1016/j.fuproc.2009.02.010.

Yusoff, S. (2006) ‘ Renewable energy from palm oil - Innovation on effective utilization of waste’, *Journal of Cleaner Production*, 14(1), pp. 87–93. doi: 10.1016/j.jclepro.2004.07.005.

Zabeti, M. *et al.* (2012) ‘ In situ catalytic pyrolysis of lignocellulose using alkali-modified amorphous silica alumina’, *Bioresource Technology*. Elsevier, 118, pp. 374–381. doi: 10.1016/j.biortech.2012.05.034.

Zanuttini, M. S. *et al.* (2013) ‘ Deoxygenation of m-cresol on Pt/γ-Al2O3 catalysts’, in *Catalysis Today*. Elsevier, pp. 9–17. doi:

10.1016/j.cattod.2013.04.011.

Zhang, H. *et al.* (2009) ‘ Comparison of non-catalytic and catalytic fast pyrolysis of corncob in a fluidized bed reactor’, *Bioresource Technology*. Elsevier, 100(3), pp. 1428–1434. doi: 10.1016/J.BIORTECH.2008.08.031.

Zhang, Q., Wang, T. and Wu, C. (2007) ‘ Upgrading bio-oil by catalytic esterification’, *ISES Solar World Congress 2007, ISES 2007*, 4, pp. 1–6. doi: 10.1186/1744-9081-4-16.

Zhao, C., Jiang, E. and Chen, A. (2017) ‘ Volatile production from pyrolysis of cellulose, hemicellulose and lignin’, *Journal of the Energy Institute*. Elsevier, 90(6), pp. 902–913. doi: 10.1016/J.JOEI.2016.08.004.

Zhou, L. *et al.* (2013) ‘ Catalytic pyrolysis of rice husk by mixing with zinc oxide: Characterization of bio-oil and its rheological behavior’, *Fuel Processing Technology*, 106, pp. 385–391. doi: 10.1016/j.fuproc.2012.09.003.

Zhu, X. *et al.* (2015) ‘ Co-pyrolysis behaviors and kinetics of sewage sludge and pine sawdust blends under non-isothermal conditions’, *Journal of Thermal Analysis and Calorimetry*. Springer Netherlands, 119(3), pp. 2269–2279. doi: 10.1007/s10973-014-4321-2.

Zullaikah, S. *et al.* (2018) ‘ Effect of blending ratio to the liquid product on co-pyrolysis of low rank coal and oil palm empty fruit bunch’, *MATEC Web of Conferences*, 156, p. 03023. doi: 10.1051/matecconf/201815603023.

APPENDICES

Appendix 1: TGA curves of cellulose and EFBF, with and without oxides

(a) CCaO 5%

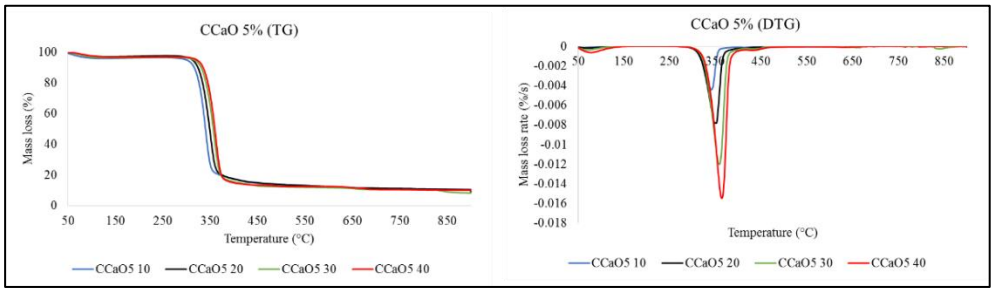

(b) CCaO 10%

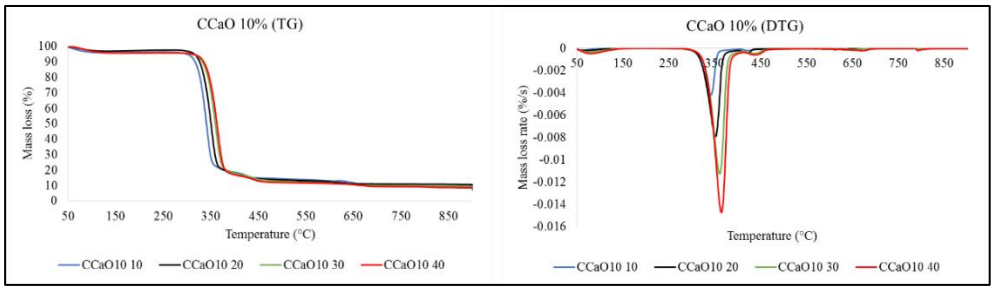

(c) CMgO 5%

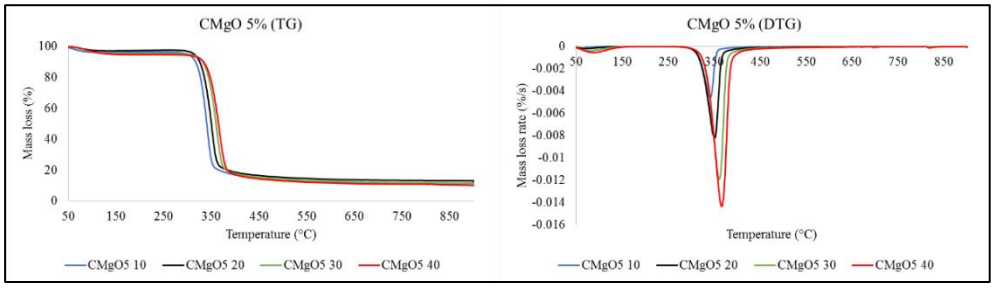

(d) CMgO 10%

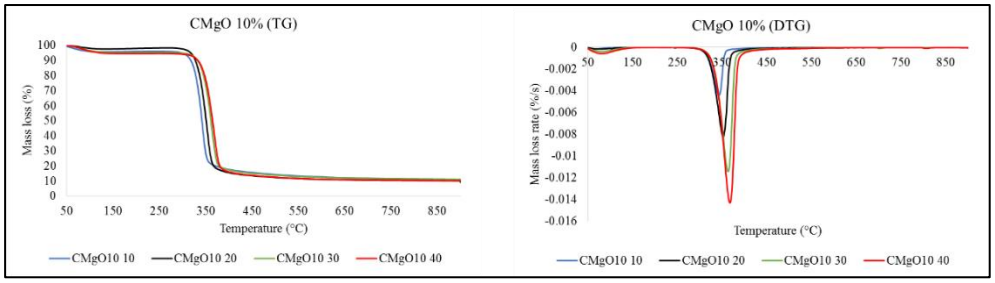

(e) CZnO 5%

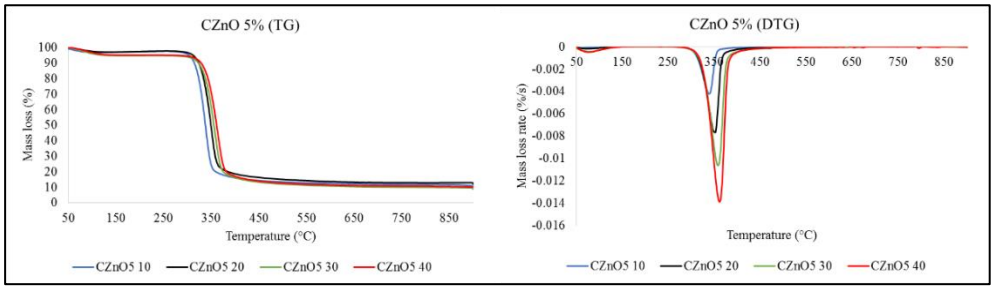

(f) CZnO 10%

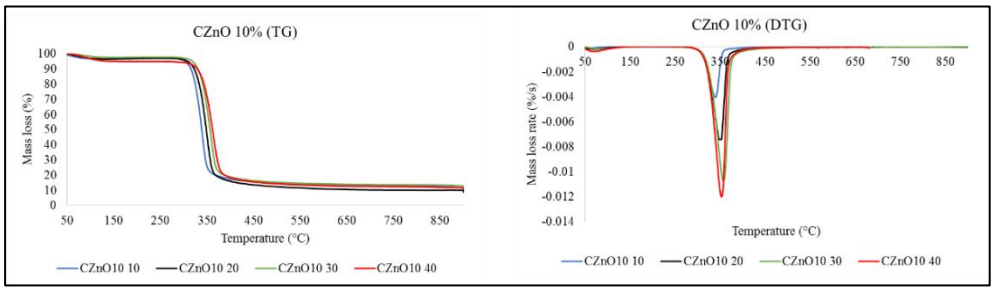

Figure A.24: TG and DTG curves of cellulose with oxides at various heating rates (10, 20, 30, and 40 ˚C/min): (a) 5 wt.% CaO; (b) 10 wt.% CaO; (c) 5 wt.% MgO; (d) 10 wt.% MgO; (e) 5 wt.% ZnO; (f) 10 wt.% ZnO

(g) ECaO 5%

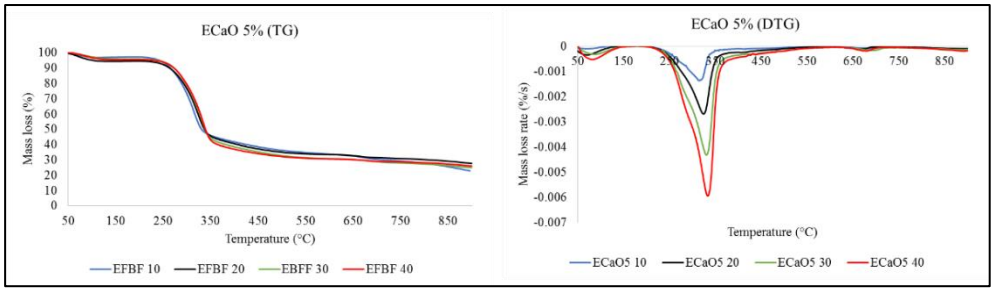

(h) ECaO 10%

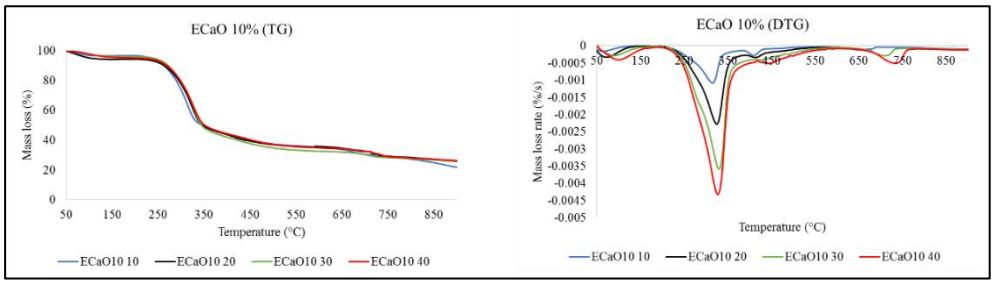

(i) EMgO 5%

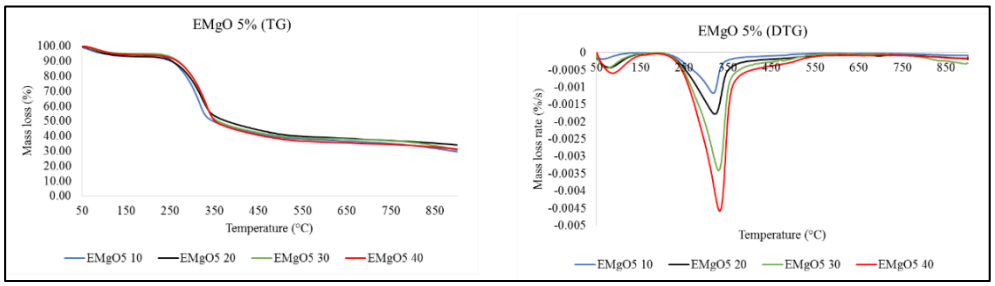

(l) EMgO 10%

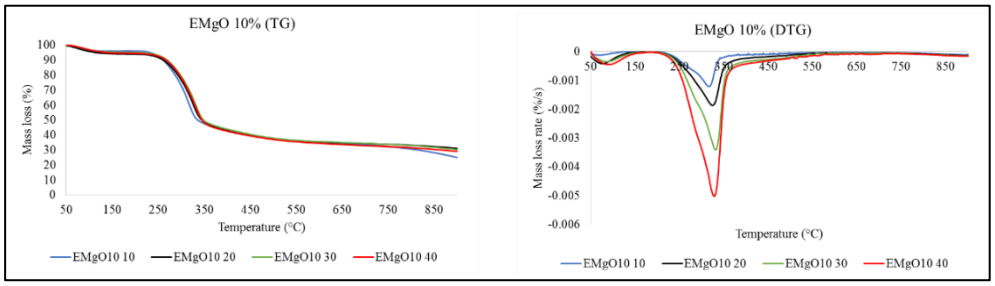

(m) EZnO 5%

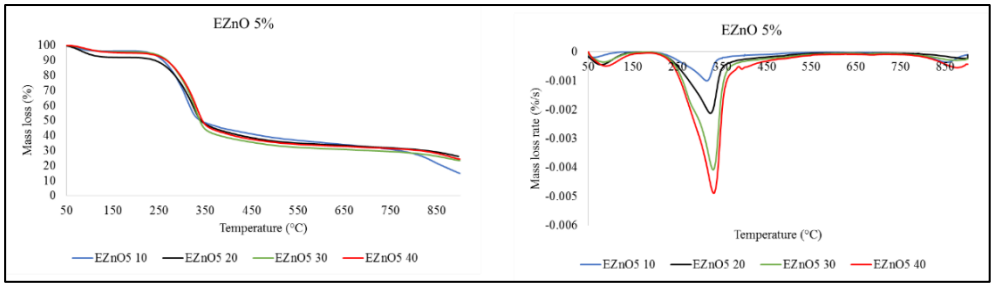

(n) EZnO 10%

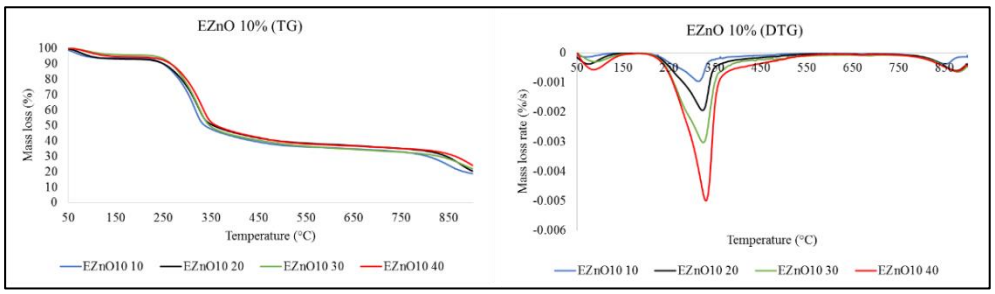

Figure A.25: TG and DTG curves of EFBF with oxides at various heating rates (10, 20, 30, and 40 ˚C/min): (g) 5 wt.% CaO; (h) 10 wt.% CaO; (i) 5 wt.% MgO; (l) 10 wt.% MgO; (m) 5 wt.% ZnO; (n) 10 wt.% ZnO

Appendix 2: ln $(\frac{\beta}{T^2})$ against $\frac{1000}{T}$ graphs to determined activation energies and frequency factors via simplified distributed activation energy model (DAEM)

(a) Cellulose

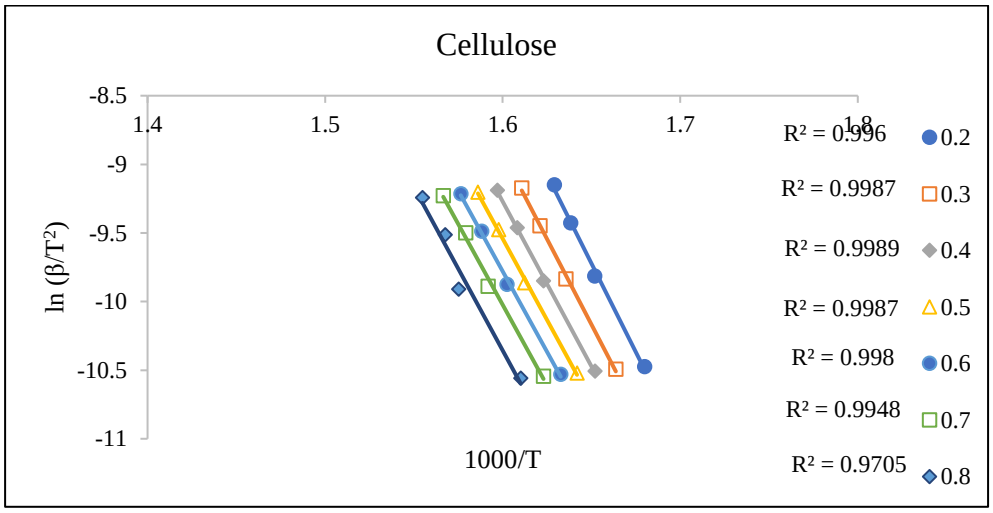

(b) CCaO 5% and 10%

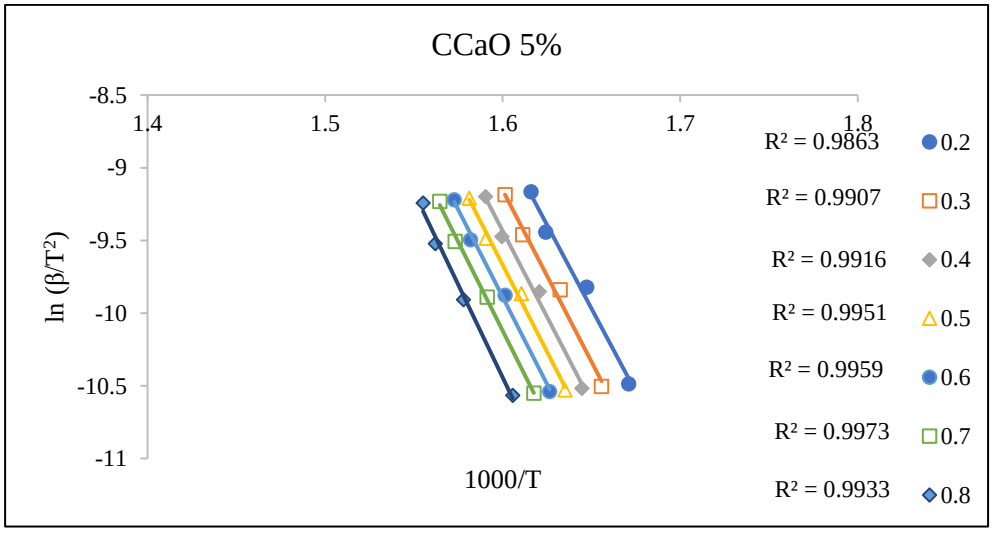

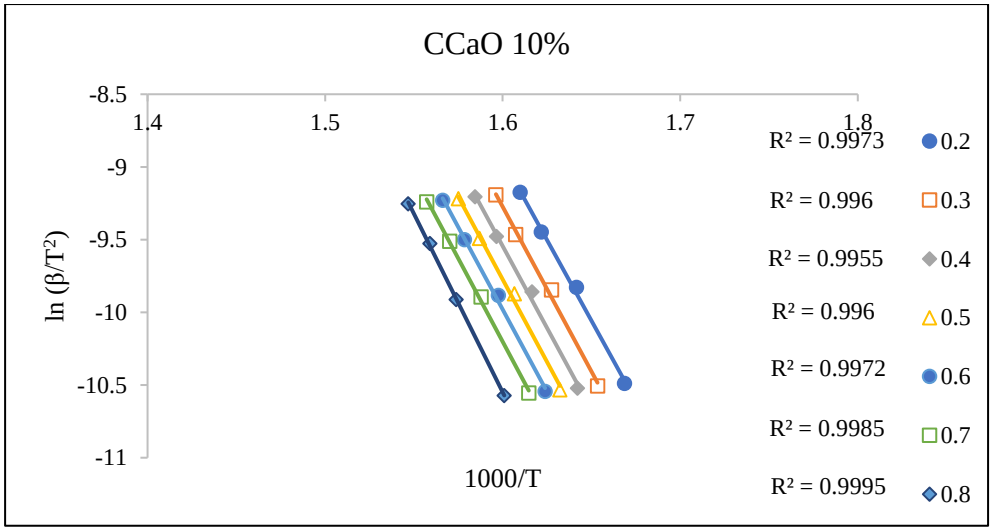

(c) CMgO 5% and 10%

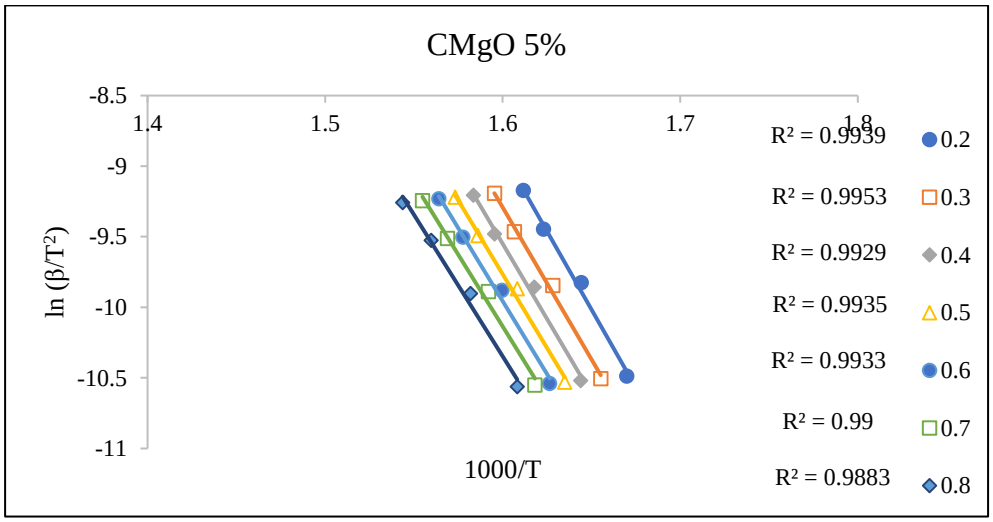

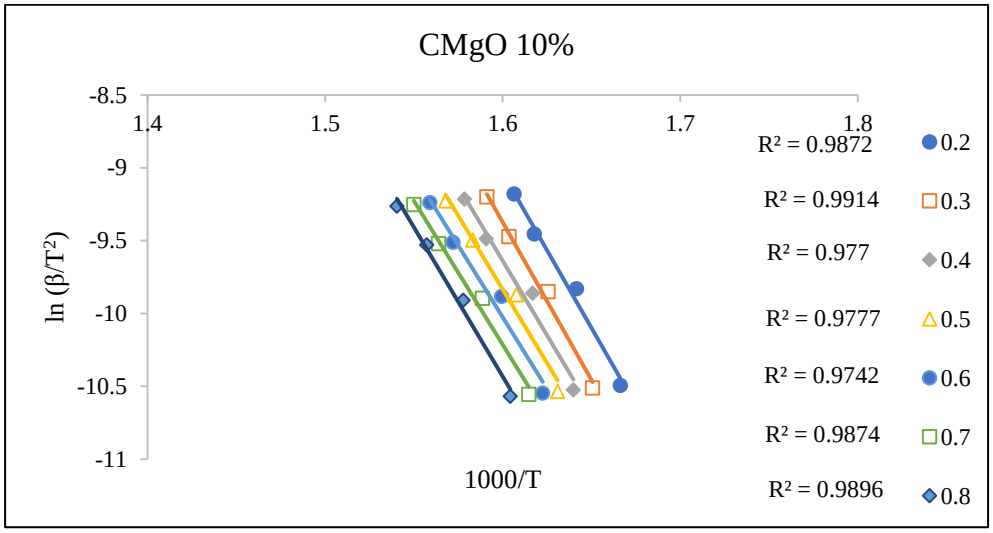

(d) CZnO 5% and CZnO 10%

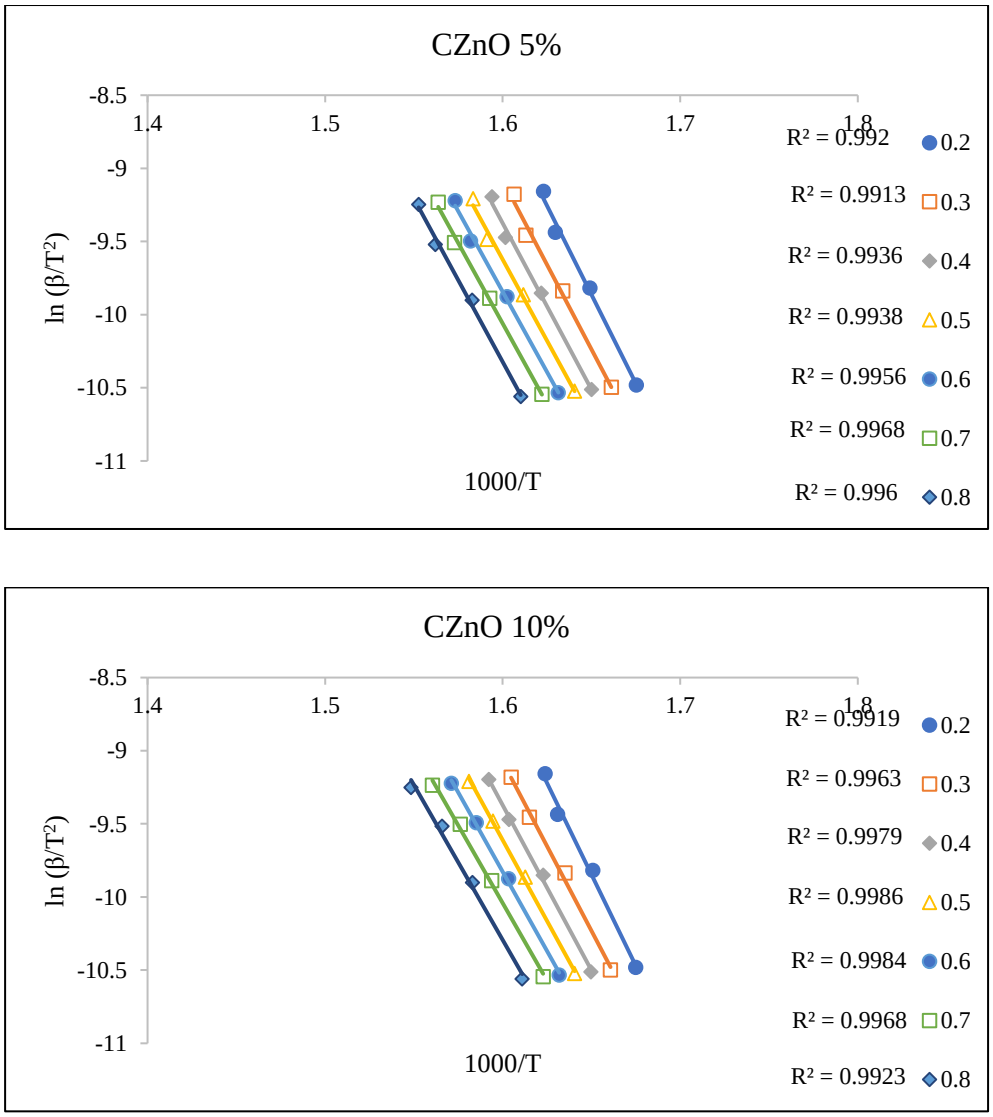

Figure A.26: ln (β/T2) versus 1000/T at conversion degrees of 0.2 – 0.8 for: (a) cellulose; (b) with 5 and 10 wt.% of CaO; (c) with 5 and 10 wt.% of MgO; (d) with 5 and 10 wt.% of ZnO

(e) EFBF

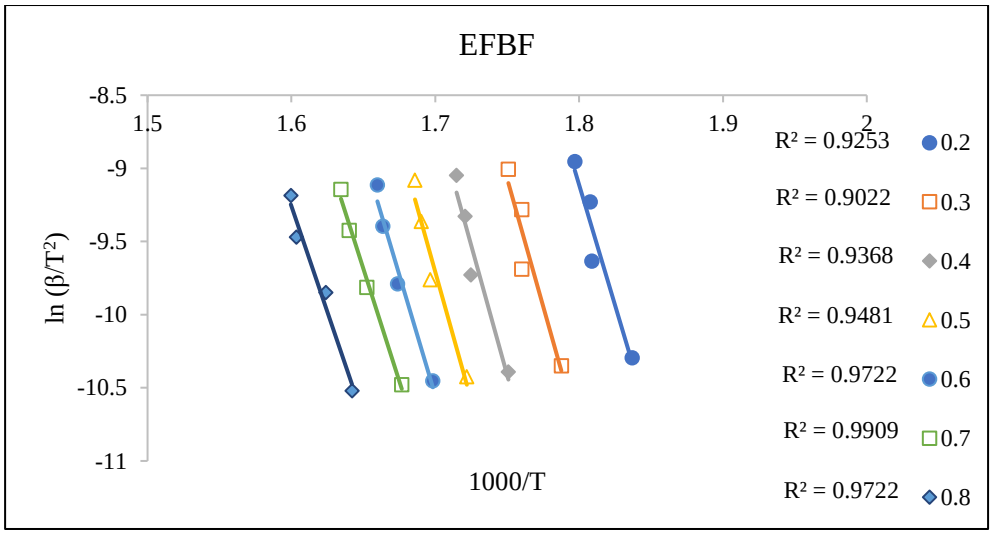

(f) ECaO 5% and 10%

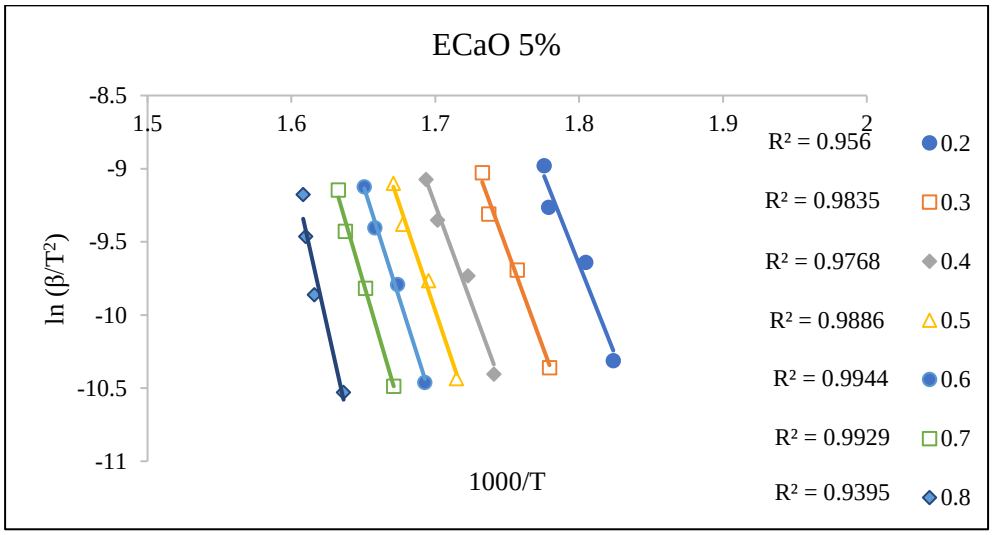

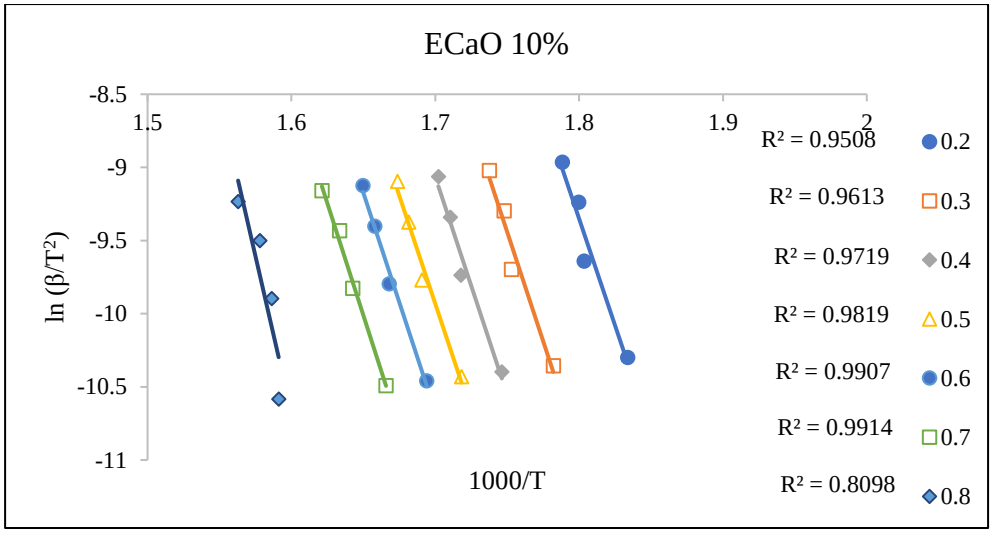

(g) EMgO 5% and 10%

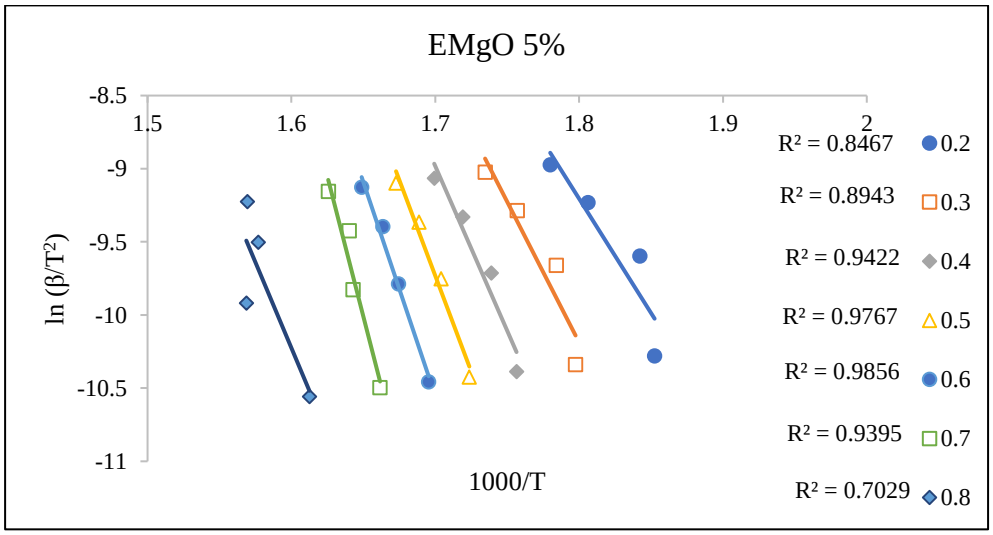

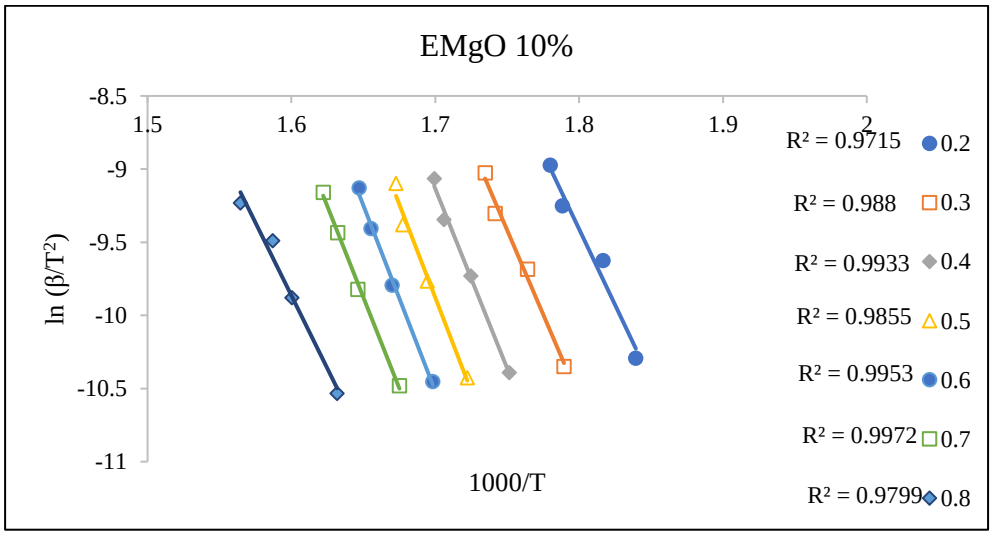

(h) EZnO 5% and 10%

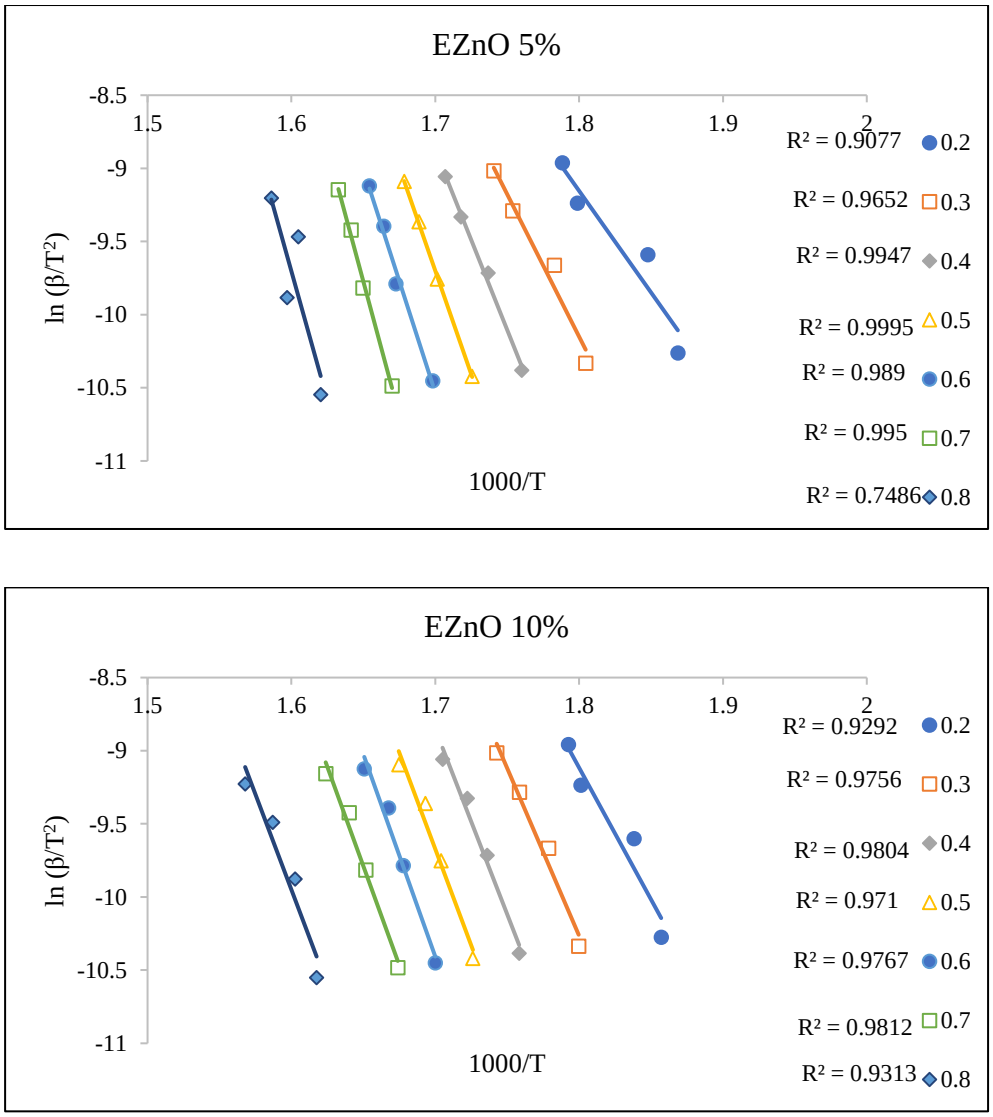

Figure A.27: ln (β/T^2) versus 1000/T at conversion degrees of 0.2 – 0.8 for: (e) EFBF; (f) with 5 and 10 wt.% of CaO; (g) with 5 and 10 wt.% of MgO; (h) with 5 and 10 wt.% of ZnO

Appendix 3: Detailed results from gas chromatography mass spectrometry (GC-MS) for catalytic intermediate pyrolysis of cellulose

Table A.25: Main products from catalytic intermediate pyrolysis of cellulose as obtained from GC-MS chromatogram as area%

No.	RT (min)	Compounds	Formula	Cellulose	CaO 5%	CaO 10%	MgO 5%	MgO 10%	ZnO 5%	ZnO 10%
Anhydrosugars										
1	11.55	Levoglucosenone	$C_6H_6O_3$	0.65	1.10	0.74	0.78	0.21	0.49	0.42
2	12.50	1,4:3,6-Dianhydro-à-d-glucopyranose	$C_6H_8O_4$	1.58	3.55	2.47	2.92	2.79	2.28	2.42
3	13.00	3,4-Anhydro-d-galactosan	$C_6H_8O_3$	-	-	0.27	0.17	-	-	-
4	13.07	2,3-Anhydro-d-mannosan	$C_6H_8O_4$	0.14	0.35	0.43	0.21	-	0.23	0.17
5	15.22	à-D-Glucopyranose, 4-O-á-D-galactopyranosyl-	$C_{12}H_{22}O_{11}$	-	0.29	-	0.30	0.25	0.22	0.24

Table A.25: Main products from catalytic intermediate pyrolysis of cellulose as obtained from GC-MS chromatogram as area% (continue)

6	17.297	1,6-Anhydro-á-d-talopyranose	$C_6H_{12}O_6$	0.33	0.80	0.68	0.96	0.89	-	-
7	18.08	D-Allose	$C_6H_{12}O_6$	11.02	23.24	23.42	30.47	29.66	31.08	31.07
8	19.69	1,6-Anhydro-à-d-galactofuranose	$C_6H_{10}O_5$	0.64	1.46	1.38	2.21	2.11	2.08	2.07
Furans										
9	6.15	Furfural (FF)	$C_5H_4O_2$	2.19	3.48	3.71	2.43	4.27	1.89	1.82
10	7.07	2,4-Dimethylfuran	C_6H_8O	0.38	0.83	0.91	0.61	0.65	0.54	0.50
11	7.32	2-Furanethanol, á-methoxy-(S)-	$C_6H_8O_2$	9.43	11.15	12.25	13.58	10.89	14.98	15.55
12	8.41	2-Furancarboxaldehyde, 5-methyl-	$C_6H_6O_2$	0.65	0.89	0.90	0.76	0.73	0.75	0.73

Table A.25: Main products from catalytic intermediate pyrolysis of cellulose as obtained from GC-MS chromatogram as area% (continue)

13	9.07	2(5H)-Furanone	$C_4H_4O_2$	0.27	0.34	-	0.31	-	0.37	0.34
24	10.22	2,5-Dimethyl-4-hydroxy-3(2H)-furanone	$C_6H_8O_3$	-	0.29	0.35	0.35	0.39	0.27	0.30
15	11.17	4-Methyl-5H-furan-2-one	$C_5H_6O_2$	0.18	0.30	0.29	0.25	0.19	0.33	0.24
16	13.75	5-(Hydroxymethyl)-2-(dimethoxymethyl)furan	$C_8H_{12}O_4$	0.17	-	0.32	0.35	0.42	0.55	0.71
17	14.10	5-Hydroxymethylfurfural (HMF)	$C_6H_6O_3$	1.09	1.42	1.63	1.59	1.41	1.21	1.17
Carbonyl compounds										
18	3.60	Cyclobutene, 2-propenylidene-	C_7H_8	0.26	-	0.21	0.19	0.18	0.26	0.25
19	5.12	1-Hydroxy-2-butanone	$C_4H_8O_2$	-	0.44	-	0.29	0.30	0.32	0.29

Table A.25: Main products from catalytic intermediate pyrolysis of cellulose as obtained from GC-MS chromatogram as area% (continue)

20	7.98	1,2-Cyclopentanedione	$C_5H_6O_2$	1.10	1.86	2.15	1.72	1.64	1.84	1.67
21	8.51	2,3-Pentanedione	$C_5H_8O_2$	0.27	0.53	0.68	0.45	0.54	0.42	0.37
22	8.55	2-Butanone, 1-(acetyloxy)-	$C_6H_{10}O_3$	0.20	0.56	0.45	0.33	0.34	0.28	0.27
23	8.64	2-Cyclopenten-1-one, 3-methyl-	C_6H_8O2	0.16	0.29	0.38	0.21	0.25	0.21	0.19
24	10.64	Furyl hydroxymethyl ketone	$C_6H_6O_3$	0.22	0.24	0.20	0.28	0.24	0.28	0.27
25	10.89	2,2-Dimethyl-3-heptanone	$C_9H_{18}O$	0.27	0.52	0.54	0.46	0.40	-	-
26	11.84	4H-Pyran-4-one, 3,5-dihydroxy-2-methyl-	$C_6H_6O_4$	0.20	0.30	0.24	0.34	0.19	0.46	0.55

Table A.25: Main products from catalytic intermediate pyrolysis of cellulose as obtained from GC-MS chromatogram as area% (continue)

Ester										
27	6.07	Pentanoic acid, 5-methoxy-, methyl ester	$C_7H_{14}O_3$	-	0.24	0.28	0.15	0.22	-	-
28	9.40	Cyclopropanecarboxylic acid, 2-methoxy-, methyl ester	$C_7H_{12}O_3$	0.19	0.28	0.30	-	-	-	-
29	11.21	Propanoic acid, ethyl ester	$C_5H_{10}O_2$	0.20	-	-	-	-	-	-
Alcohol										
30	14.55	1,2-Cyclohexanediol	$C_6H_{12}O_2$	0.36	0.91	0.46	0.88	0.96	0.52	0.95

Table A.25: Main products from catalytic intermediate pyrolysis of cellulose as obtained from GC-MS chromatogram as area% (continue)

Methoxy										
31	4.12	2-Butene, 1,1-dimethoxy-	$C_6H_{12}O_2$	-	0.23	-	0.20	0.22	0.18	-
32	5.72	1,1- Dimethoxycyclopentane	$C_7H_{14}O_2$	-	0.25	0.31	0.16	-	-	-
33	5.96	Ethane, 1,1,1-trimethoxy-	$C_5H_{12}O_3$	0.50	1.21	1.67	1.08	0.86	1.75	1.74

Appendix 4: Fourier transform infrared spectrum (FTIR) results from catalytic intermediate pyrolysis of cellulose

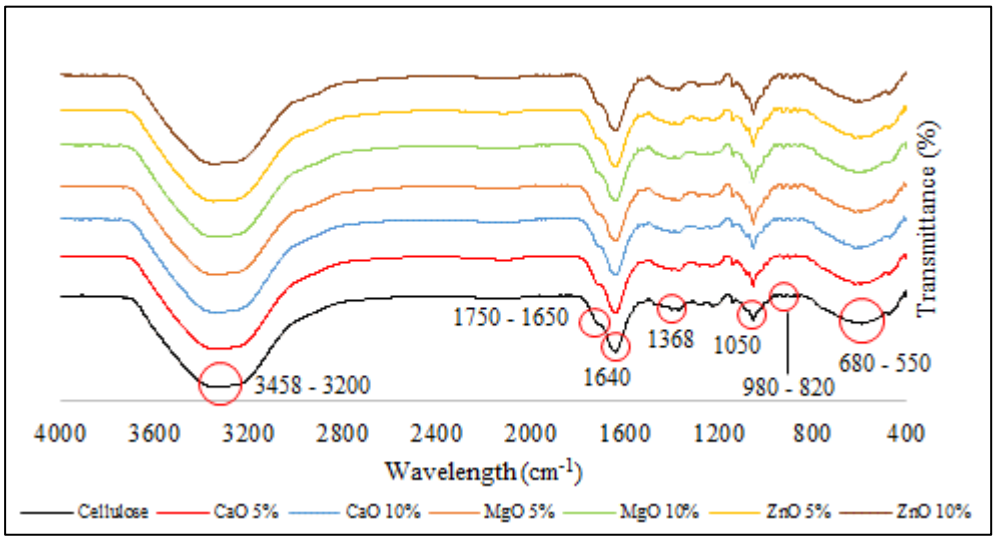

Figure A.28: FTIR spectra of cellulose-derived bio-oils, with and without the presence of oxides

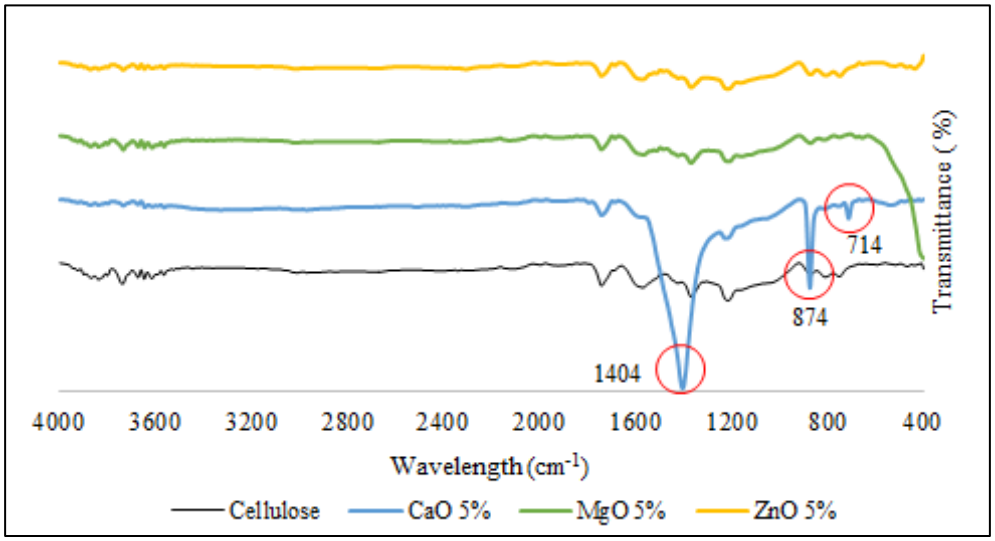

Figure A.29: FTIR spectra of cellulose-derived solid residue, with and without the presence of 5 wt.% oxides

Appendix 5: Fourier transform infrared spectrum results from catalytic intermediate pyrolysis of empty fruit bunch fibre (EFBF)

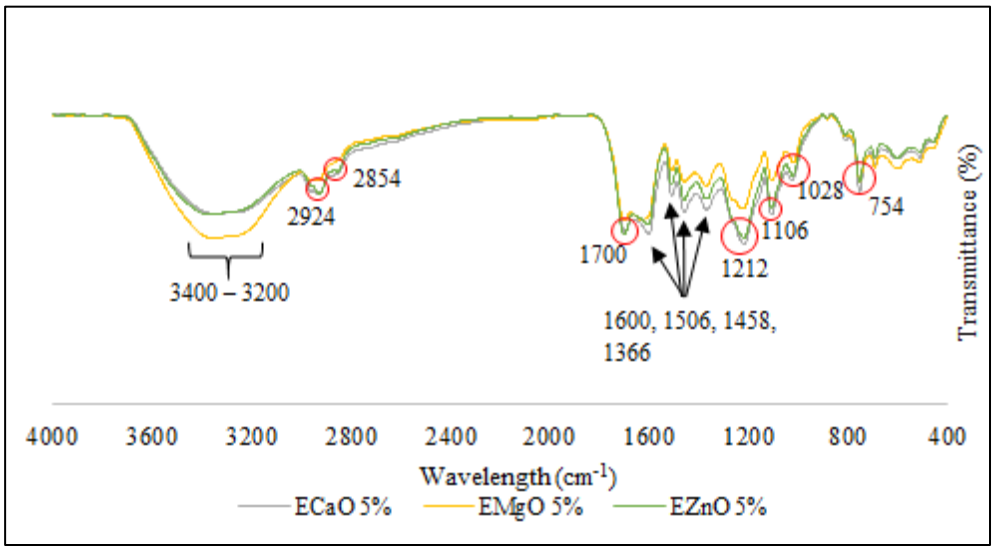

Figure A.30: FTIR spectra of EFBF-derived bio-oil in the presence of 5 wt.% oxides

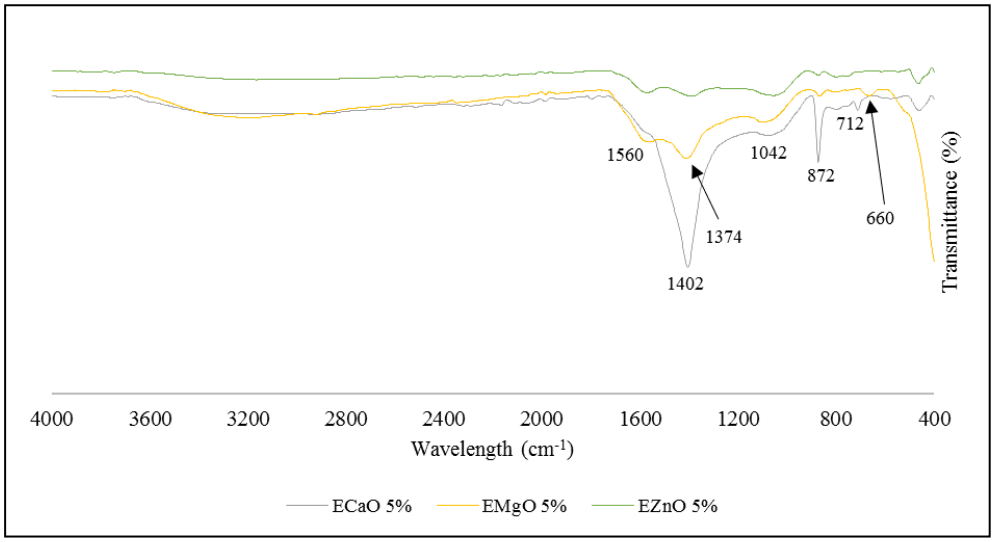

Figure A.31: FTIR spectra of EFBF-derived solid residue in the presence of 5 wt.% oxides

Appendix 6: Detailed results from GC-MS for catalytic intermediate pyrolysis of EFBF

Table A.26: Main products from catalytic intermediate pyrolysis of EFBF as obtained from GC-MS chromatogram as area%

No.	RT (min)	Compounds	Formula	EFBF	CaO 5%	CaO 10%	MgO 5%	MgO 10%	ZnO 5%	ZnO 10%
Acid										
1	3.03	Acetic acid	$C_2H_4O_2$	3.98	0.39	6.99	13.03	14.11	12.71	4.73
2	4.55	Propanoic acid	$C_3H_6O_2$	0.64	0.27	1.24	1.54	1.66	1.18	0.58
3	5.68	Hexadecenoic acid	$C_{16}H_{30}O_2$	0.22						
4	6.05	Hexanoic acid	$C_{16}H_{12}O_2$				0.21	0.21		
5	16.45	Dodecanoic acid	$C_{12}H_{24}O_2$	1.01						
Ester										
6	4.63	Acetic acid, butyl ester	$C_6H_{12}O_2$			0.44		0.43	0.21	0.26

Table A.26: Main products from catalytic intermediate pyrolysis of EFBF as obtained from GC-MS chromatogram as area% (continue)

Furan										
7	6.11	Furfural	$C_5H_4O_2$	1.07	0.31	3.69	3.63	3.78	2.72	1.15
8	6.92	3-Furanmethanol	$C_5H_6O_2$	0.62	0.27	1.58	1.41	1.59	1.37	1.11
9	7.25	2-Furanethanol, á-methoxy-(S)-	$C_7H_{10}O_3$		0.35			0.39		
10	7.34	Ethanone, 1-(2-furanyl)-	$C_6H_6O_2$			0.63		0.50	0.47	0.84
11	8.8	2(5H)-Furanone	$C_4H_4O_2$	0.24	0.48	1.42	1.81	1.50	1.17	0.55
Ketone										
12	3.24	2,3-Pentanedione	$C_5H_8O_2$				0.37	0.39	0.27	
13	5	Cyclopentanone	C_5H_8O		0.14	0.93	0.43	0.51	0.33	0.32
14	7.04	2-Cyclopenten-1-one, 2-methyl-	C_6H_8O	0.45	0.27	1.59	1.17	1.29	0.94	0.91

Table A.26: Main products from catalytic intermediate pyrolysis of EFBF as obtained from GC-MS chromatogram as area% (continue)

15	8.5	2-Butanone, 3,3-dimethyl-	$C_5H_8O_2$			0.23	0.22	0.23	0.19	
16	8.53	2-Cyclopenten-1-one, 2,3-dimethyl-	$C_7H_{10}O$			0.34		0.33	0.45	0.31
17	8.63	2-Cyclopenten-1-one, 3-methyl-	C_6H_8O			0.80	0.66	0.58		0.27
18	9.5	1,2-Cyclopentanedione, 3-methyl-	$C_6H_8O_2$	0.83	0.27	2.02	1.90	1.92	1.77	5.03
19	10.36	2-Cyclopenten-1-one, 3-ethyl-	$C_7H_{10}O$			0.27	0.27	0.29		
Other oxygenate										
20	3.29	2,2-Dimethoxybutane	$C_6H_{14}O_2$			0.22	0.22	0.41		
21	3.48	2-Propanone, 1-hydroxy-	$C_3H_6O_2$	0.43	0.14	1.53	0.92	0.98	1.08	0.35

Table A.26: Main products from catalytic intermediate pyrolysis of EFBF as obtained from GC-MS chromatogram as area% (continue)

22	5.09	1-Hydroxy-2-butanone	$C_4H_8O_2$	0.68	0.41	3.08	2.34	2.66	2.14	0.74
23	10.78	2-Cyclopenten-1-one, 3-methyl-2-hydroxy-	$C_6H_8O_2$					0.25	0.28	0.21
Phenol										
24	10.2	Phenol	C_6H_6O	5.09	1.57	10.29	11.88	11.52	11.71	5.01
25	10.2	Phenol, 2-methoxy-	$C_7H_8O_2$	0.86	0.28	1.5	1.77	1.67	1.76	0.79
26	10.69	phenol, 3-methyl-	C_7H_8O	0.38	0.27	0.51	0.62	0.66	0.59	0.37
27	11.21	p-Cresol	C_7H_8O	0.49	0.19	0.61	0.85	0.77	0.89	0.48
28	11.68	Phenol, 2-methoxy-3-methyl-	$C_8H_{10}O_2$				0.3			
29	11.69	2-Methoxy-5-methylphenol	$C_8H_{10}O_2$	0.38	0.52	0.2			0.39	0.33

Table A.26: Main products from catalytic intermediate pyrolysis of EFBF as obtained from GC-MS chromatogram as area% (continue)

30	11.79	Phenol, 2-ethyl-	$C_8H_{10}O$				0.24			
31	11.87	Phenol, 2,3-dimethyl-	$C_8H_{10}O$		0.51	0.26	0.52	0.28	0.29	0.37
32	12.81	Phenol, 4-ethyl-2-methoxy-	$C_9H_{12}O_2$	0.4			0.45	0.46	0.7	0.31
33	13.53	2-Methoxy-4-vinylphenol	$C_9H_{10}O_2$	0.33			0.59	0.69	0.61	0.48
34	14.14	Catechol	$C_6H_6O_2$	0.35	0.32	0.34	0.26	0.25	0.49	0.41
35	14.23	Phenol, 2,6-dimethoxy-	$C_8H_{10}O_3$	1.17	0.86	2.79	2.51	2.2	3.15	1.15
36	15.2	Phenol, 2-methoxy-6-(1-propenyl)-	$C_{10}H_{12}O_2$	0.22			0.27	0.23	0.46	0.31
37	15.57	Hydroquinone	$C_6H_6O_2$			0.41	0.27	0.36	0.49	0.22
38	16.04	1,4-Benzenediol, 2-methyl-	$C_7H_8O_2$	0.56			0.22	0.43	0.33	0.25

Table A.26: Main products from catalytic intermediate pyrolysis of EFBF as obtained from GC-MS chromatogram as area% (continue)

39	19.69	Phenol, 2,6-dimethoxy-4-(2-propenyl)-	$C_{11}H_{14}O_3$	0.26		0.22	0.25	0.19	0.81	
Sugar										
40	13.26	1,4:3,6-Dianhydro-à-d-glucopyranose	$C_6H_8O_4$			0.51	0.34	0.27	0.40	0.28
41	18.04	á-D-Glucopyranose, 4-O-á-D-galactopyranosyl-	$C_{12}H_{22}O_{11}$		0.24	0.29				
42	19.07	a-D-Glucopyranose, 1,6-anhydro-	$C_6H_{10}O_5$	0.44						
Hydrocarbon										
43	3.59	Cyclobutene, 2-propenylidene-	C_7H_8			0.77	0.38	0.42	0.51	0.18

Table A.26: Main products from catalytic intermediate pyrolysis of EFBF as obtained from GC-MS chromatogram as area% (continue)

44	5.27	p-Xylene	C_8H_{10}				0.24	0.25		
45	14.9	Dodecane, 2,6,10-trimethyl-	$C_{15}H_{32}$	0.22						

Appendix 7: FTIR spectra of aged EFBF bio-oil (liquid and solid fractions)

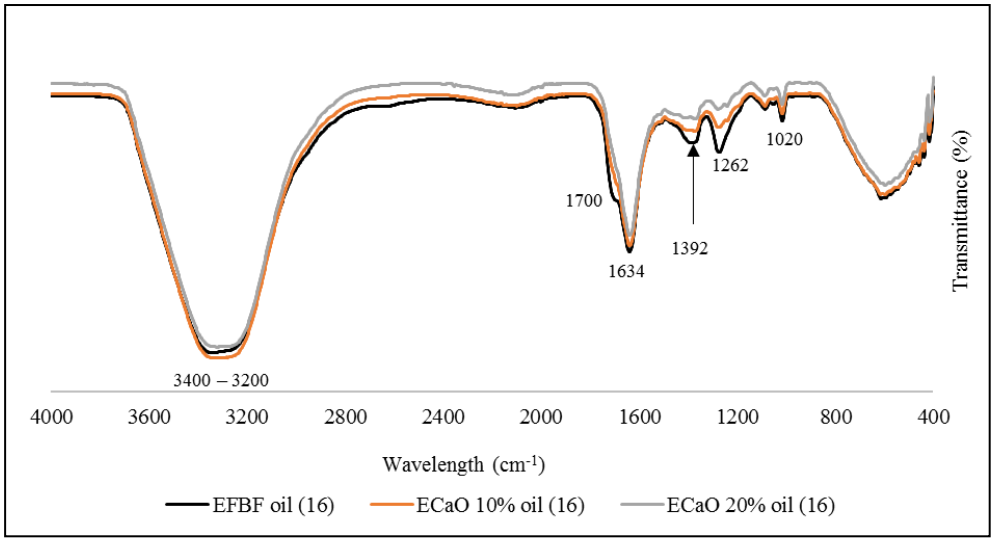

Figure A.32: FTIR spectra of 16 h aged bio-oil (liquid fraction)

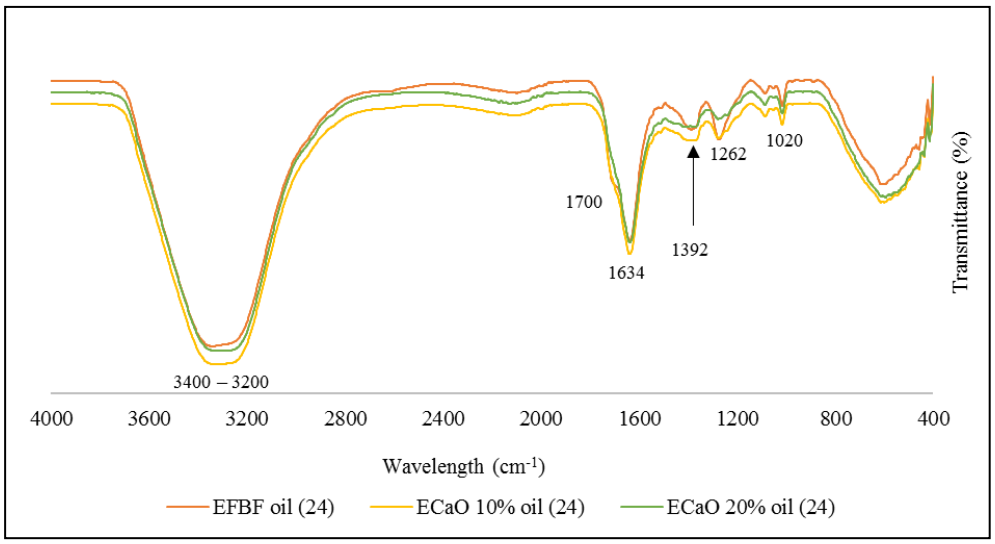

Figure A.33: FTIR spectra of 24 h aged bio-oil (liquid fraction)

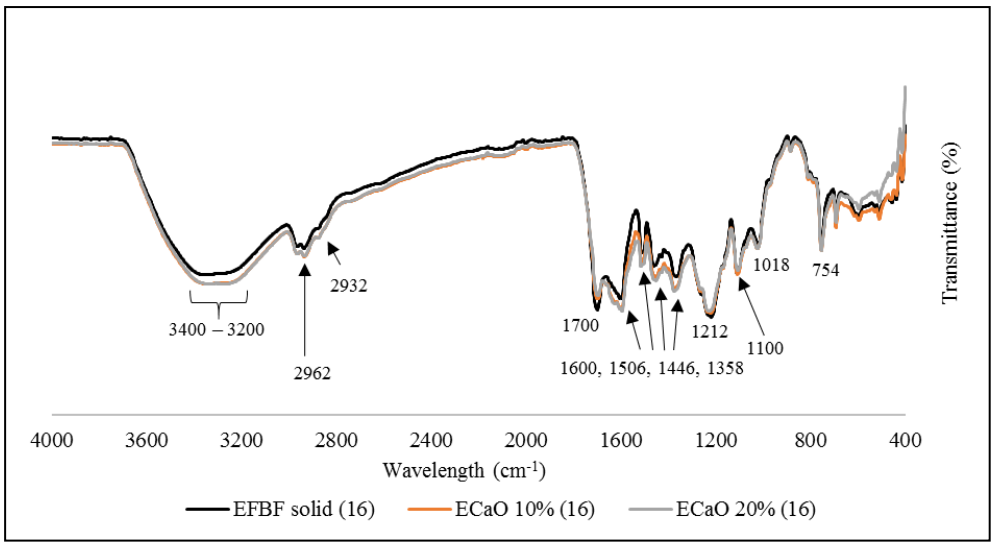

Figure A.34: FTIR spectra of 16 h aged bio-oil (solid fraction)

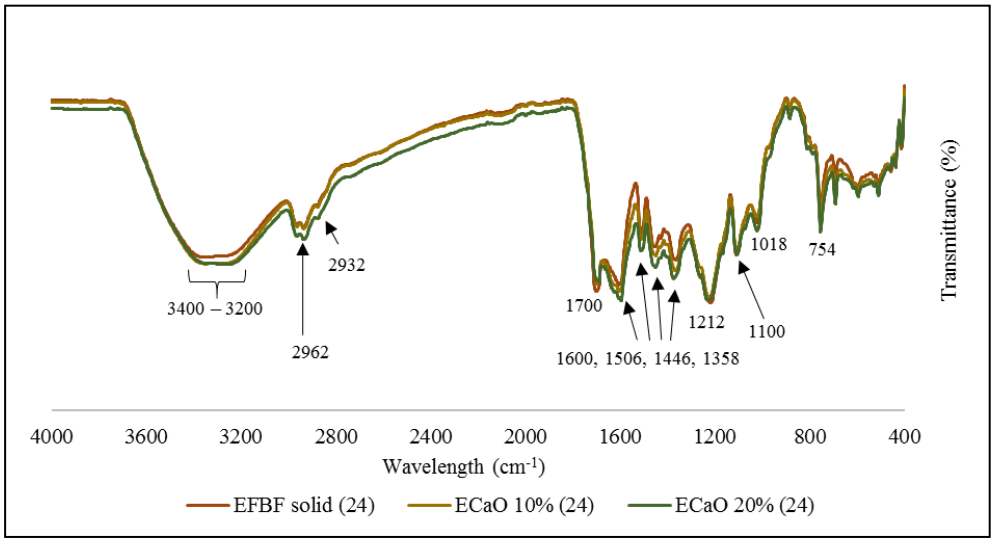

Figure A.35: FTIR spectra of 24 h aged bio-oil (solid fraction)